Non-structural carbohydrates and leaf ecophysiology in tropical and temperate forests



Nicolas Raab

Oriel College

University of Oxford

Thesis submitted to the University of Oxford in fulfilment of the requirements for the degree of

Doctor of Philosophy

Michaelmas 2019

"Hay momentos para recitar poesías
y hay momentos para boxear"

Roberto Bolaño

Acknowledgements

I would like firstly to thank my supervisor Yadvinder Malhi, mainly for teaching me that you can be a rockstar in science and always have a smile. Thank you for your continued support throughout the dissertation-writing process. Also I would like to thank Allie Shenkin for his help along the entire process, from planning field work to polishing the manuscripts.

I would like also to thank the Chilean National Commission for Scientific and Technological Research (CONICYT) for providing me with a doctorate scholarship. Also, I would like to thank Oriel College for supporting my fieldwork in Ghana.

I am also very grateful for my lab, for always finding the time to catch up with a pint whenever it was needed. A big thank you to Alex Morel, to show me how to get into the Bodleian (in the very last term of my DPhil), to Jesús, David, the Cecilias, Erika, Sami, and everyone that has come and gone throughout all of these years. To the people of my DPhil cohort, especially to Agne, Christine, Anabelle and Emma for so many laughs, tears, dance-offs and nights out.

I am thankful for all the people who have hosted me abroad. To Jordi, his lab and all the community in Catalunya. To Robert Turgeon for hosting me in Cornell. To Stephen, Theresa and the guys from the Kwaeemma campaign in Ghana for showing me your amazing culture and helping me when I needed it the most.

Thank to everyone who has been my family away from home: to Nico, Tam and Fran, my expat Chilean family. Anna, Iliana and Arran for turning a shared flat into a home. To Luana, Sergio and Asmita for being the Duchy of Latin America in the UK.

To Justine, and her family, that have always supported me and invited me for a cup of tea, a walk or a night out when I needed it the most. Thank you for checking every word in here.

Thanks to José Luis for being the best Ulises Lima that I could have ever wanted, and to Dina for many tea breaks (maybe too many) when they were most needed and for teaching me how to lift.

And last but not least, I could not have gone through all of this process without the continuous support of my family back home: to my Mom, Dad and Jérôme. A big hug to Mona and Lili, my two grandmothers that passed away whilst I was doing my DPhil.

In memoriam of Nicolás W. Franck

Non-structural carbohydrates and leaf ecophysiology in tropical and temperate forests

Nicolas Raab, Oriel College, Oxford, Michaelmas 2019

Thesis Abstract

Increasing atmospheric CO_2 concentration has led to an increment in forest biomass because of both an inhibition in photorespiration rates, and an increase in photosynthesis main substrate, atmospheric CO_2. Whether this trend can be sustained by biomes, thus helping to regulate anthropogenic CO_2 emissions, or whether this trend will reach a threshold as soil nutrient and soil moisture limitations become controlling factors that limit growth, remains unclear. Non-structural carbohydrates (NSC) have proven to play a major role in downregulating leaf gas exchange by intervening in the Calvin-Benson-Bassham cycle. When sink activity in the plant becomes limited, an increase in NSC concentration in the phloem occurs at a sink level, thus jeopardising the source-sink gradient needed for carbohydrates mass-flow across the phloem. Photoassimilate translocation is hampered, thus accumulating in the blade, and downregulating plant leaf gas exchange. Empirical evidence of NSC downregulation is needed to be integrated with Dynamic Global Vegetation Models in order to improve land-atmosphere exchange predications under climate change scenarios.

The aim of this thesis is to improve the understanding of the role of NSCs on ecosystem productivity. From empirical observations at a leaf level, to modelling at a plot level, this thesis explores leaf NSC concentration across species, sites and time, and how does it affect photosynthesis. I collected data from contrasting sites: a tropical drought gradient in Ghana, encompassing a dry deciduous forest, a moist deciduous transition forest, and a wet evergreen forest, and an ancient temperate woodland in the UK.

In the first empirical chapter of this thesis (**Chapter 3**), I explore the effect of NSC on net photosynthesis at a leaf level. I added sucrose to leaves and studied the effect on photosynthesis, before and after treatment, in six species (three tropical evergreen species, and three temperate deciduous European species). I also correlated the ob-

served decrease in photosynthesis with key leaf traits related to fast translocation of resources from the leaf to the plant, such as investment in leaf vein infrastructure, petiole diameter, and specific leaf area. These key traits showed a negative relation with photosynthetic downregulation mediated by NSC, meaning that species on the fast side of the leaf economics spectrum would benefit more from increasing atmospheric CO_2 concentrations.

In the second empirical chapter (**Chapter 4**), I develop an open source tool to improve the time of analysis of pressure-volume curves, used to determine leaf hydraulic traits. The tool also presents an add-on which allows to uniform the choice between different users when discerning points between the *turgor loss region* and the *linear region*. When emulating different criteria for the selection of the points belonging to each one of these two regions, derived leaf hydraulic traits remain fairly constant. Altogether, the tool reduces the time of curves analysis from 10-15 minutes, to less than 1 minute, and standardises user's choice when determining points belonging to the *turgor loss region* or *linear region* of the curve.

Chapter 5 looks at the seasonal distribution of leaf osmotic potential at full turgor (a hydraulic trait derived from the open source tool for pressure-volume curves presented in **Chapter 4**) across a tropical drought gradient in Ghana. Leaf osmotic adjustment, defined as the capacity of the leaf to accumulate solutes in order to lower its water potential when facing water stress without compromising cell turgor, is a key acclimation mechanism to maintain physiological functioning under low soil moisture. In aerial organs, such as leaves, osmotic adjustment is heavily dependent on the accumulation of NSC. Whether NSC accumulation in the leaf is the result of a passive process resulting from the lack of sink demand given water stress, or is an active mechanism of the plant to cope with water shortage, has been debated. I studied seasonal osmotic adjustment across three contrasting sites across the gradient. Osmotic adjustment was correlated with key leaf traits that provide for fast NSC translocation and avoid photosynthetic downregulation mediated by photoassimilates (from results obtained from **Chapter 3**). Finally, I found that leaf photosynthesis at light saturation was correlated with leaf osmotic potential at full turgor. The evidence found was not enough to sustain the hypothesis that increase in leaf NSC concentration observed during the drought season is solely associated with a decrease in sink activity. The accumulation of solutes in the leaf remains as an active strategy of plant acclimation to water stress.

In the last empirical chapter of this thesis (**Chapter 6**), I try to predict leaf NSC concentration using leaf reflectance in the 400 to 2500 nm spectrum obtained with a field leaf spectrophotometer, thus leading to an opportunity to monitor leaf NSC dynamics *in vivo* in the field. Using several leaves from four temperate European deciduous species, I looked at correlating leaf optical footprint with leaf total NSC, and its fractions (monosaccharides, sucrose, soluble and non-soluble fractions). The relationships found were poor, except for *Fagus sylvatica*. Previous research that found a positive relationship between leaf NSC concentration, and leaf optical footprint obtained with a leaf field spectrophotometer, might be confounded by the strong correlations between leaf NSC concentration and other, more directly detectable, leaf traits such as leaf nitrogen concentration and specific leaf area.

This thesis demonstrates the importance of the role of NSC in leaf and tree physiology. The upscaling of these mechanisms would pave the way to a new generation of Dynamic Global Vegetation Models, with a better understanding of the feedbacks between increasing CO_2 concentration and terrestrial ecosystem productivity.

Contents

1 Introduction **1**

1.1 Research background 1

1.2 Contribution to the State of the Art 5

1.3 Research Aims 6

1.4 Thesis Structure and Chapter Summary 7

2 Literature Review **9**

2.1 Is plant carbon assimilation pushed from the atmosphere, or is it pulled by the plant? 9

2.2 Non-structural carbohydrates dynamics in natural vegetation 11

2.2.1 Non-structural carbohydrates expected values across biomes . . . 11

2.2.2 Seasonality of non-structural carbohydrate concentration 12

2.2.3 Storage allocation of non-structural carbohydrates 13

2.3 Translocation of non-structural carbohydrates from the leaf 14

2.3.1 Understanding phloem translocation: the pressure-flow model for phloem transport 14

2.3.2 Phloem loading 17

2.3.3 Leaf vein infrastructure in support of leaf photosynthesis 19

2.3.4 Non-structural carbohydrate translocation from the leaf 20

2.4 Non-structural carbohydrates and photosynthetic feedback inhibition . . 21

2.5 Leaf hydraulic traits 23

2.6 Leaf chemistry determination with field spectroscopy 24

3 Photosynthetic downregulation in response to non-structural carbohydrates (NSC) in natural forest ecosystems **27**

3.1 Introduction 30

3.2 Materials and Methods 33

3.2.1 Site and species description 33

3.2.2 Non-structural carbohydrates manipulation trial 34

3.2.3 Trait measurement 37

3.2.4 Vein density 37

3.2.5 Soluble sugar measurements . . . 37
3.2.6 Measuring non-structural carbohydrates translocation across the leaf . . . 38
3.2.7 Statistical analysis . . . 39
3.3 Results . . . 40
3.3.1 Downregulation in photosynthesis . . . 40
3.3.2 Leaf traits, vein density and photosynthesis downregulation . . . 43
3.3.3 Leaf traits, vein density and non-structural carbohydrates translocation . . . 45
3.3.4 Predicting photosynthetic downregulation with leaf traits . . . 46
3.4 Discussion . . . 48
3.4.1 Photosynthetic downregulation mediated by soluble non-structural carbohydrates . . . 48
3.4.2 Non-structural carbohydrates, photosynthetic downregulation and leaf traits . . . 49
3.4.3 Predicting NSC downregulation from leaf traits . . . 52
3.5 Conclusions . . . 53
3.6 Supplemental Material . . . 54

4 Open-source tool for the analysis of leaf pressure-volume relations 55
Symbols . . . 58
4.1 Introduction . . . 58
4.2 Theory . . . 59
4.3 Definition of hydraulic traits derived from pressure-volume curves . . . 61
4.4 General description of the open-source PV analyser . . . 64
4.5 User manual . . . 67
4.6 Example data . . . 68
4.7 Conclusions . . . 70
4.8 Appendix . . . 71

5 Seasonal changes in leaf osmotic adjustment across a tropical drought gradient 75
5.1 Introduction . . . 78
5.2 Materials and Methods . . . 81
5.2.1 Sites description . . . 81
5.2.2 Sampling campaigns . . . 84
5.2.3 Pressure-volume curves . . . 86

5.2.4 Seasonal campaigns 87
5.2.5 Osmotic adjustment 87
5.2.6 Species selection and statistical analysis 88
5.3 Results 89
5.3.1 Osmotic adjustment and its along-gradient and seasonal variation 89
5.3.2 Interspecific consistence in maximum osmotic potential at full turgor ($\Delta\Pi_o$) 91
5.3.3 Maximum osmotic adjustment ($\Delta\Pi_o$) and leaf traits 93
5.3.4 Predicting photosynthesis from osmotic leaf traits 95
5.4 Discussion 97
5.4.1 Osmotic adjustment across the plots 97
5.4.2 Within plot species differences in acclimation to drought 98
5.4.3 Osmotic adjustment during the drought season in tropical plots . 99
5.4.4 Osmotic potential and leaf gas exchange at light saturation . . . 100
5.5 Conclusions 101

6 Are leaf non-structural carbohydrates (NSC) directly detectable with field spectroscopy? 103

6.1 Introduction 106
6.2 Materials and Methods 109
6.2.1 Site description and sample collection 109
6.2.2 Spectral measurements 109
6.2.3 Non-structural carbohydrate measurements 110
6.2.4 Data filtering, chemometrics, and statistical analysis 110
6.2.4.1 Partial least square regression 110
6.2.4.2 Assessing model performance 112
6.3 Results 112
6.3.1 Leaf reflectance and non-structural carbohydrates across species 112
6.3.2 Predicting non-structural carbohydrates concentration across species 113
6.3.3 Inter-specific effects on non-structural carbohydrate prediction . 116
6.3.4 Spectral Weights 118
6.4 Discussion 119
6.4.1 Temperate woodland non-structural carbohydrates dynamics in leaves 119
6.4.2 Leaf chemometric determination through optical properties . . . 120

6.4.3 Causes of relatively poor non-structural carbohydrates predictability from spectral measurements 122
6.5 Conclusions 126
6.6 Supplemental Material 128

7 Synthesis and conclusions **131**
7.1 Summary and key findings 131
7.1.1 Photosynthetic downregulation mediated by non-structural carbohydrates 132
7.1.2 Non-structural carbohydrate dynamics throughout the wet-dry season 133
7.1.3 Leaf non-structural carbohydrates prediction with field leaf spectroscopy 134
7.2 Concluding Remarks 134
7.3 Further Work 135

List of Figures

2.1 Schematic representation of Münch Theory of mass flow transport. Sugars are loaded into the phloem from mesophyll cells through companion cells, thus making osmotic potential (Ψ_o) more negative, thus lowering cell's overall water potential (Ψ_w). Water is transferred from the xylem (higher Ψ_w) to the phloem (lower Ψ_w) increasing pressure potential (Ψ_p) which moves the sugars downstream. After sucrose is unloaded by sink cells phloem's cell Ψ_w increases and water is reverted towards the xylem. In order to maintain a turgor gradient across the phloem, companion cells need to actively load the phloem through pumps (apoplastic loading) or generate high photosynthetic rates in order to maintain a mesophyll to phloem sugar gradient (symplastic loading). 15

2.2 Diagram of phloem loading. Panel A shows apopasltic phloem loading where sucrose symporters actively pump sugars from the mesophyll (M) into the companion cell (CC) to then be exported into the phloem sieve element (SE). Panel C shows symplastic phloem loading where sugars are transferred from M to CC *via* plasmodesmata that link both cells. In order to keep the sugar gradient for NSC translocation, leaves need to maintain high photosynthetic rates. Panel B depicts a third mechanism that can be found both in symplastic and apoplastic loading species: once sucrose molecules are transferred to CC, a third molecule of galactose is attached to the sucrose molecule, thus making the molecule too big to go back through the plasmodesmata. Lower rows represent photoassimilate concentrations from radiolabelled carbon. In apoplastic loading, most of the sugars are concentrated in the veins (D), whilst in symplastic loading (F), sucrose is equally distributed across mesophyll cells in order to generate the above-mentioned sugar gradient needed for phloem loading (taken from Turgeon (2010)). 18

2.3 Leaf reflectance of a fresh (thick line) and a dry (thin line) *Quercus* leaf. Absorption bands for different leaf compounds are shown accordingly (taken from Kokaly et al. (2003)). 25

3.1 Top left, a diagram representing leaves used for the six different treatments (control, water, sucrose, at 10 and 30 minutes each), and other five healthy leaves collected for vein density analysis. Bottom left, a diagram of the leaf showing where water and sucrose treatments where applied, and where photosynthesis was measured. Bottom right, shows the section of the leaf used for the vein density analysis: primary and secondary veins were avoided. 36

3.2 Soluble non-structural carbohydrate (Sol. NSC) concentration in the six treatments: Control (C), Water (W), and Sucrose (S) at two different times: 10 and 30 minutes. Concentrations are expressed as grams per leaf square meter ($\mathrm{g\,m^{-2}}$). Tropical species are shown in the upper row, whilst temperate species are shown in the lower one. Different letters represent soluble NSC concentrations statistically different from each other (T-test; $\alpha = 0.10$). 41

3.3 Sucrose (Suc) feeding effect on leaf net photosynthesis at pre-treatment (Pre-Treat), 10 and 30 minutes (min). Net photosynthesis is expressed as a percentage of pre-treatment leaf gas exchange. Results are shown for the control, water and sucrose (Suc) treatments in six different species. Top row shows tropical species: *Duguetia staudtii*, *Ongokea gore*, and *Uapaca guineensis*. Bottom row shows temperate species: *Acer pseudoplatanus*, *Fagus sylvatica*, and *Quercus robur*. Mean for each treatment is shown together with ± 1 standard error. Letters represent statistical differences between treatments (T-test; $\alpha = 0.10$). 42

3.4 Pearson correlation between measured variables. Leaf photosynthetic decrease (Pn Decrease) was defined as the percentage (%) of Pn between pre and post sucrose feeding at 10 minutes, minus the corresponding Pn % decrease for the water treatment in order to account solely for soluble non-structural effect (Soluble NSC) on photosynthetic downregulation. . 44

3.5 Correlation between translocation of soluble non-structural carbohydrates (Sol. NSC), vein density and leaf traits. ΔSol. NSC was measured as the difference between leaf NSC concentration after sucrose addition and natural leaf NSC concentration assumed as NSC concentrations found in the control treatment. Only significant ($\mathrm{P_{value}} < 0.05$) relationships are shown. 45

3.6 Interaction between specific leaf area (SLA) and vein density taken from the most parsimonious model (Model 1; Table 3.4) predicting photosynthetic downregulation with leaf traits. Shaded areas represent predicted errors. Photosynthetic (Pn) decrease was defined as defined as the percentage (%) of Pn between pre and post sucrose feeding at 10 min, minus the corresponding Pn % decrease for the water treatment in order to account solely for soluble non-structural effect on photosynthetic downregulation. On the left panel, maximum and minimum observed SLA were kept fixed, together with average observed petiole diameter in order to predict Pn decrease. Likewise, on the right panel, average SLA was used to predict Pn decrease sensibility to petiole diameter. 47

3.7 Soluble non-structural carbohydrate concentration in the six treatments: Control (C), Water (W), and Sucrose (S) at two different times: 10 and 30 minutes. Concentrations are expressed as percentage of leaf dry weight (DW) mater content (%). Tropical species are shown in the upper row, whilst temperate species are shown in the lower one. Letters represent soluble NSC concentrations statistically different from each other (T-test; $\alpha = 0.10$). 54

4.1 Two regions are observed: a turgor loss region where leaf water potential decreases together with water loss, and a linear region, where water loss does not entail a drop on water potential. 60

4.2 Höfler diagram of a leaf pressure-volume (PV) curve showing changes in leaf water potential (Ψ_{leaf}), turgor pressure (Ψ_{p}), and osmotic potential (Ψ_{o}) following changes in leaf relative water content (RWC). The three curves were obtained as follow: passed the turgor loss point (TLP), Ψ_{p} by definition is equal to 0, therefore $\Psi_0 = \Psi_{\text{o}}$. In the turgor loss region, Ψ_{o} is assumed to follow the linear tendency calculated in Fig. 4.1, then Ψ_{o} can be transformed to its reciprocal and opposed sign in order to go from $\frac{-1}{\Psi}$ to Ψ. Ψ_{p} can be calculated as $\Psi_{\text{p}} = \Psi_{\text{leaf}} - \Psi_{\text{o}}$. 63

4.3 Graphical user interface of the open source software for pressure-volume (PV) leaf curves analysis. Each panel presents the same PV curve with different root mean square error threshold. A more conservative thresholds (A) advice the removal of points from the linear regions, whilst more liberal thresholds (C) include more points to the linear region, changing the turgor loss point each time. 66

4.4 Distribution of osmotic potential (Π_o), leaf water potential at turgor loss point (Ψ_{TLP}), leaf modulus of elasticity (ε) and relative water content at turgor loss point (RWC_{TLP}) obtained after analysing 162 volume-pressure curves from three sites in Ghana. We used a 0.5; 1 and 5 root mean square error (RMSE) thresholds in order to show what is the sensitivity of the obtained parameters to users choice. A and B were fitted using a Gaussian distribution, C was fitted with a Poisson distribution, and D was fitted using a skewed normal distribution. Obtained parameters do not vary largely for different RMSE threshold, meaning that user's subjectivity is not detrimental on leaf pressure-volume curves analysis. 69

5.1 Mean annual precipitation and cumulative water deficit (CWD) distribution along the year for the three study sites from North to South (driest to wettest): Kogyae (KOG), Bobiri (BOB), and Ankasa (ANK). 82

5.2 Diagram of an example leaf pressure-volume curve. The inverse of leaf water potential ($\frac{-1}{\Psi}$) is plotted against the complement to leaf relative water content (100 − RWC; %). Osmotic pressure at full turgor (Π_o) is derived from the extrapolation of the linear regression of points within the linear region of the curve (points defined after the turgor loss point (TLP)) to the Ψ_{leaf} axis. Figure taken from Raab et al., submitted *b*. . . 86

5.3 Osmotic Adjustment per tree in the three study sites. From North to South: Kogyae (KOG), Bobiri (BOB) and Ankasa (ANK). Osmotic adjustment along the season was defined as the most negative osmotic potential at full turgor (Π_o) observed at a tree level within the season ($max(\Pi_o)$), minus the Π_o obtained for each measurement. Coloured lines represent observations for the same tree throughout the year whilst the black line represents campaigns' osmotic adjustments averages. . . . 90

5.4 Per plot distribution of maximum osmotic potential difference per tree ($\Delta\Pi_o$) between different seasons, leaf vein density, and specific leaf area (SLA). Letters symbolise statistical difference given by a T-test at an α value of 0.05. 93

5.5 Specific leaf area (SLA) from the model explaining most of the observed variation (Table 5.5)when predicting maximum osmotic potential at full turgor between different seasons ($\Delta\Pi_o$) at a species level. 95

5.6 Effect of leaf nitrogen concentration (Π_o) on leaf net photosynthesis at light saturation (A_{sat}). Predictors were taken from the most parsimonious model (Model 1; Table 5.7). 97

6.1 Leaf reflectance of *Acer pseudoplatanus*, *Fagus sylvatica*, *Quercus robur* ($n = 60$ each), and *Fraxinus excelsior* ($n = 40$) for each wavelength (λ). Solid lines represent the average reflectance of each species whilst the coloured area represents ± 1 standard deviation from the mean. 113

6.2 Box plot of leaf non-structural carbohydrates (NSC) partitioning for *Acer pseudoplatanus*, *Fagus sylvatica*, *Fraxinus excelsior* and *Quercus robur*. Monosaccharides correspond to both glucose and fructose, soluble sugars are both monosaccharides and sucrose concentrations. Total NSC correspond to the addition of soluble sugars and starch. Samples were collected between August and September 2016. Concentrations are expressed as % of leaf dry weight content. 114

6.3 Observed and predicted values across *Acer pseudoplatanus*, *Fagus sylvatica*, *Fraxinus excelsior* and *Quercus robur* by partial least square regression using full cross validation procedure. Each panel represents a different fraction of the total non-structural carbohydrates fraction (NSC). The solid line represents a 1 to 1 relationship whilst dashed lines represent the regression for each species. 115

6.4 Observed against predicted concentrations, as percentage (%) of leaf dry matter content, by partial least square regression per species, using a full cross validation. Each panel represents a non-structural carbohydrates (NSC) fraction, or total NSC for each species sampled. Dashed lines correspond to the linear regression whilst solid lines represent a 1 to 1 relationship. 117

6.5 Spectral weights for the soluble sugars fraction and total NSC. The solid line represents the mean of 50 iterations with 70% of the data set, the coloured area represents ± 1 standard deviation from the mean. The dashed lines represent maximum and minimum weights observed for the 50 iterations. The further the trend deviates from zero, the higher is the contribution of a specific spectral region to NSC prediction. 119

6.6 Pairwise comparison at wavelength level between different species reflectance. Comparison was done using two-sample T-test. P_{Value} shows the probability that both samples have the same mean. Probability below 0.05 (α Value) indicates that samples are statistically different at a given wavelength. 128

Chapter1

Introduction

1.1 Research background

The imbalance between increasing anthropogenic CO_2 emissions and limited planetary carbon sink capacity has led to an augmentation of Earth's radiative forcing, thus paving the way for an overall increase in global temperatures and extreme events such as drought and storms. In order to meet international goals following the Paris Agreement on climate change, and therefore to limit the global average temperature increase below 2 °C and pursue efforts to limit temperature increase by 1.5 °C compared to pre-industrial global average temperatures (UNFCCC, 2015), the planetary carbon budget needs to become carbon neutral by mid-century (IPCC, 2018). Hence, understanding the planet's carbon sinks under increasing atmospheric CO_2 concentrations (C_a), higher temperatures, and lower soil moisture, is of paramount importance.

Averaged over the 2008-2017 period, Earth's terrestrial ecosystems held a carbon stock of 450 Pg_C to 650 Pg_C comprised of vegetation biomass, with an estimated yearly carbon input of $+120\,Pg_C\,yr^{-1}$ through photosynthesis, and a carbon loss of $-119\,Pg_C\,yr^{-1}$ (autotrophic respiration: $60\,Pg_C\,yr^{-1}$ + heterotrophic respiration: $55\,Pg_C\,yr^{-1}$ + combustion: $4\,Pg_C\,yr^{-1}$) yielding a net balance of $-1\,Pg_C\,yr^{-1}$, equivalent to around 10% of fossil fuels CO_2 emissions ($+9.4\,Pg_C\,yr^{-1}$). Land biosphere CO_2 uptake accounts for around 25% of anthropogenic emissions (Quéré et al., 2018).

Even if land's sink capacity is sensitive to climatic variability, such as El Niño Southern Oscillation (ENSO) (Fang et al., 2017), research has found that during the 1990-2000 decade, the terrestrial carbon sink has shown an increasing trend, because of increased atmospheric CO_2 (C_a) absorption capacity by vegetation (Sarmiento et al., 2010). Even if this trend could be partially explained by a much more benign climate for vegetation growth during this period of time, especially in cold regions, land ecosystems' positive response to increasing C_a has played a key role in limiting the rate of rise of atmospheric CO_2 concentrations in recent decades.

Carbon fertilization occurs because an increase in C_a has a positive effect on leaf photosynthesis without increasing leaf respiration. Current C_a levels (just over 410 ppm; NOAA (2019)) are less than half the concentrations at which photosynthesis becomes CO_2 saturated (around 1000 ppm for C3 plants, Körner (2006)), indicating that plants could still benefit from increasing C_a.

Furthermore, Ribulose-1,5-biphosphate carboxylase oxygenase (RuBisCO), the enzyme responsible of catalysing the initial step of the Calvin-Benson-Bassham (CBB) cycle by reducing a molecule of CO_2 into a molecule of Ribulose-1,5-biphosphate (Miziorko and Lorimer, 1983) comes with some pitfalls. RuBisCO can also fix a molecule of O_2 in a molecule of Ribulose-1,5-biphosphate (RuBP) in a process called photorespiration. This may have appeared as an adaptation to higher C_a, when photosynthesis evolved in bacteria 3.4 billion years ago (Flexas et al., 2012), a pathway to dissipate the excess of UV radiation given the lack of an ozone layer (Willis and McElwain, 2002), or as an optimization of its own 3-dimensional architecture (Griffiths, 2006). Molecular O_2 fixation occurs in 1 out of 4 RuBisCO reactions at current C_a concentrations. Carbon dioxide is a competitive inhibitor of RuBisCO oxygenase activity, therefore an increase in C_a would reduce photorespiration, thus ultimately improving photosynthetic efficiency.

Crop scientists have long sought to convert this potential surplus of carbon fixation into economic yield. However, carbon allocation is a complex process depending on several genes and is constrained by physical limitation, such as maximum height which still permits water lift from the soil to the canopy (Sala et al., 2012). Free-Air Concentration Enriched (FACE) experiments in crops have failed to show that increased C_a will offset yield losses associated with expected future climate change scenarios resulting from lower precipitations and higher temperatures (Long et al., 2006).

Natural ecosystems are no exception. Early work in FACE experiments showed an increase in forest growth associated to high C_a (e.g., Ainsworth et al., 2003; Nowak et al., 2004; Zotz et al., 2005). However, forest growth is not only limited by C_a. Soil nutrient availability, soil moisture, and temperature, are also drivers of plant growth, and hence carbon demand (Fatichi et al., 2014; Hayat et al., 2017). An increase in forest growth supported by high C_a is only likely to be sustained as long as soil moisture and fertility can support biomass growth (Norby et al., 2010).

Therefore, are trees carbon limited? If so, ecosystems would have leeway to increase their carbon uptake driven by increasing C_a associated with anthropogenic emissions, therefore increasing the terrestrial carbon sink capacity. A compendium of several forest growth studies across contrasting biomes has suggested that forest growth is no longer limited by carbon and that there are other factors constraining net ecosystem productivity (NEP) (Bader et al., 2013; Ellsworth et al., 2017; Fleischer et al., 2019; Girardin et al., 2016; Körner, 2003; Norby et al., 2010; Terrer et al., 2019). Non-structural carbohydrates (NSC), mainly soluble sugars and starch (Hartmann and Trumbore, 2016), were targeted as the main signal coordinating plant internal carbon sinks (organ respiration, organ growth and storage) with plant's carbon sources (leaves). When NSCs are synthesised in leaves, they need to be translocated through the phloem in order to supply carbon demand in non-photosynthetic organs. If this demand is less than supply rate, an NSC source-sink imbalance occurs, affecting NSC translocation downstream the phloem. This imbalance can result in increased leaf NSC concentrations, which in turn can trigger photosynthetic downregulation to reduce supply rates to match demand. Leaves may be often at their highest possible leaf NSC concentration threshold when comparing leaf NSC concentration across time or similar biomes with similar characteristics (Körner, 2003), indicating that plants are no longer carbon limited and other abiotic factors might be constraining growth, thus leaving little potential for increased productivity under rising C_a. Resolving this question of sink limitation is therefore crucial for understanding feedbacks between vegetation carbon uptake and global change.

Across a *Pinus cembra* altitudinal gradient, Hoch et al. (2002) found a rise in NSC concentration in different organs with increasing altitude, indicating that when tree growth, and hence carbon demand, becomes limited by temperature, the above-mentioned source-sink imbalance occurs. NSC start accumulating in leaves as they are unable

to be transported *via* phloem. Tropical vegetation has shown higher NSC concentration during the dry season when compared to the wet season (Würth et al., 2005). Similar to the altitudinal gradient, this suggests that when tree growth is limited by water supply, a source-sink imbalance is formed, thus triggering leaf NSC accumulation.

Nevertheless, NSCs not only serve to meet metabolic demand and carbon construction costs across the plant. They also have other important physiological roles regarding plant acclimation to environmental stresses, such as osmotic adjustment. Plant cells accumulate solutes in order to make their osmotical potential more negative, thus lowering their water potential without affecting cell's turgor. Soluble NSCs, together with other compounds such as acids, amino acids, and cations, are actively accumulated in organs like leaves as an acclimation strategy in order to endure with abiotic stresses. During periods of soil moisture shortage, active NSC accumulation in leaves has helped plants to lower their water potential in order to maintain the soil-plant-atmosphere water continuum (e.g., Bowman and Roberts, 1985; Subbarao et al., 2000). On the other hand, NSC accumulation has also been observed in high altitudes trees (e.g., Rada et al., 1985). Accumulations of solutes can grant supercooling features to leaves, meaning that soft tissue can withstand sub-zero temperatures without freezing. Therefore, the question of whether NSC accumulation in leaves is always derived from a passive process resulting from a lack of sink demand or is indeed an active strategy to acclimate to abiotic stresses, rises.

Non-structural carbohydrates dynamics in natural vegetation are key to understanding the future pathway of the terrestrial carbon sink, and therefore the prospects for achieving carbon neutrality by mid-century. Furthermore, understanding the role of NSC dynamics in photosynthesis regulation would allow a better understanding of the future ecosystem productivity under climate change scenarios.

Experimental research regarding plant's carbon imbalance and its further effect on leaf carbon assimilation has mostly been limited to *Arabidopsis thaliana* and crops. Therefore, most of what we know about these relationships between plant's carbon sources and sink organs is restricted to annual species. Experimental research in trees and natural vegetation is infrequent. When studying these imbalances in long-lived species, differences arise. The main one is that trees are much more complex organisms with much more specialised organs for carbon allocation as storage, whereas annual species such as *Arabidopsis* store mostly of their NSCs in the leaf to be rapidly mobilised

to seeds to maximise chance of reproduction. Carbon partitioning in trees entails complex architecture, organ topology and long-distance transport. Therefore, empirical research is needed to better understand feedbacks between natural vegetation and global change.

1.2 Contribution to the State of the Art

In order to simulate the effect of increasing C_a on terrestrial carbon balance, researchers have employed Dynamic Global Vegetation Models (DGVM). DVGMs predict an increase in net ecosystem productivity by the end of the century (e.g., Cramer et al., 2001; Huntingford et al., 2013), mainly attributed to increasing C_a. DGVMs rely on photosynthetic equations derived from RuBisCO kinetics to simulate canopy-atmosphere exchange (e.g., Collatz et al., 1990; Farquhar et al., 1980); an increase in C_a in these models translates to higher CO_2:O_2 ratios and concomitantly reduced photorespiration rates, resulting in an increased in ecosystems biomass storage (Eckardt, 2005; Somerville and Ogren, 1982).

The empirical data needed to understand the effects of carbon fertilization on NEP in natural vegetation is still lacking. The current research aims to better understand leaf and forest carbon exchange under an atmosphere with higher C_a, which will allow a next generation of DVGMs to model feedback inhibitions and expand the understanding of photosynthesis from the chloroplast to the organism level.

1.3 Research Aims

The present doctoral thesis has three overall questions, asked in the context of tropical and temperate broadleaf tree species:

1. First Paper

    (a) Is there evidence that high NSC concentrations cause a downregulation of leaf photosynthesis?

2. Second Paper

    (a) Are leaf hydraulic traits, derived from pressure-volume curves, dependant on the user's decisions when analysing these curves or are intrinsic to the curve itself?

3. Third Paper

    (a) Is osmotic regulation in leaves a passive process resulting from the lack of sink activity during periods of water stress, or is it an active process where leaves accumulate NSCs in order to maintain a soil-plat-atmosphere hydraulic gradient.

    (b) Are seasonal changes in leaf photosynthesis linked to seasonal changes in NSC concentration given by osmotic potential at full turgor?

4. Fourth Paper

    (a) Is it possible to measure *in vivo* leaf NSC concentrations using field leaf spectrometry?

1.4 Thesis Structure and Chapter Summary

The first paper of the thesis explores NSC photosynthetic downregulation in natural vegetation. By manipulating natural leaf NSC concentration in leaves of three tropical species from a lowland rainforest in Ankasa: *Duguetia staudtii*, *Ongokea gore*, *Uapaca guineensis*; and three species from a temperate European woodland in Oxford, UK: *Acer pseudoplatanus* (sycamore), *Fagus sylvatica* (beech), and *Quercus robur* (European oak) I explore the relationship between leaf NSC concentration and the observed decrease in net leaf photosynthesis.

I also looked at the importance of different leaf traits such as: specific leaf area (SLA), leaf vein density, leaf thickness, and petiole diameter, in predicting the degree of NSC photosynthetic downregulation.

The second paper of this thesis consists of a methodological section where I design an open-source tool for the analysis of leaf pressure-volume (PV) curves. PV curves are derived from relationships between leaf water potential (Ψ_{leaf}) and leaf water content. These relationships are paired at different intervals of leaf water content, thus providing hydraulic associated leaf traits, such as leaf water potential at turgor loss point (Ψ_{TLP}), which sheds light on trees ecophysiological adaptations to drought, leaf osmotic potential at leaf full turgor pressure (Π_{o}) which in turns regulates Ψ_{TLP}. Π_{o} allows ecophysiological acclimation to drought since the leaf can reach a lower Ψ_{leaf} without jeopardising leaf cell turgor. Π_{o} in aerial organs has shown to rely on the accumulation of NSC.

The existing tools (mainly Microsoft Excel spreadsheets) are time consuming. Moreover, they are heavily dependant on user criteria to select the different points that belong to the different regions of the curve. I offer an open-source tool that shortens the analysis from 20 minutes, to 1 to 2 minutes and standardises user choice.

The third chapter uses the outputs from PV curves taken across three plots in a drought gradient in Ghana during the wet and dry seasons. Using the open-source tool from paper 2, we derived Π_{o} from several species. After studying the effect of NSC in leaves of tropical species in paper 1, we aimed to upscale NSC effect on downregulation by pairing Π_{o} with seasonal leaf gas exchange measurements.

The fourth paper explores the properties of field leaf spectroscopy in predicting NSC concentrations. If true, leaf NSC dynamics could be monitored *in vivo*, together with photosynthesis. This would allow researchers to couple changes in leaf gas exchange with variations in leaf NSC concentration in the field. Nowadays, NSC can only be determined in the laboratory, which entails destructive sampling, thus restricting a continuous monitoring along the day, and/or throughout the wet-dry season, which is not the case with leaf photosynthesis.

I paired field leaf spectroscopy from four European temperate species (*A. pseudoplatanus*, *F. sylvatica*, *Q. robur* and *Fraxinus excelsior* (ash)) with leaf NSC fractions and total NSC concentrations. Given the low inter-specific diversity of our pool (only four species) I explore if similar research done with higher inter-specific diversity was indeed measuring leaf NSC concentration or just predicting leaf traits that have proven to have optical properties and correlate well with leaf photosynthetic capacity, therefore NSC leaf concentration, such as leaf nitrogen content and SLA.

Chapter2

Literature Review

2.1 Is plant carbon assimilation pushed from the atmosphere, or is it pulled by the plant?

Following Farquhar's model of photosynthesis (Collatz et al., 1990; Farquhar et al., 1980), plant carbon assimilation heavily depends on C_a. The model is based on enzymatic kinetics in the chloroplast and at the beginning was never intended to represent whole canopy gas exchange. The Farquhar photosynthesis model simulates leaf net photosyntesis as the result of the most limiting rate process between RuBisCO kinetics (A_c) and RuBP regeneration (A_j), the last being dependent on the radiation intercepted by the leaf:

$$A_n = min\{A_c; A_j\} - R_d \tag{2.1}$$

Where A_n is leaf net carbon, and R_d is leaf's dark respiration rate, all terms in $\mu mol_{CO_2}\, m^{-2}\, s^{-1}$. A_c relies on RuBisCO maximum carboxylation rate (Vc_{max}), depending on enzymatic kinetics and the concentration of dissolved CO_2 in the chloroplast stroma (Farquhar et al., 1980). Thus, Farquhar's model depends on atmospheric supply, *via* stomata, of carbon to the leaf in order to predict A_n. An increase in C_a would lead to an increase in leaf photosynthesis. However, complex interactions do occur at an organism level, leading to feedback mechanisms that hamper the plant's positive response to elevated C_a (Arp, 1991; Díaz et al., 1993).

A series of monographs have arisen during the past years (e.g., Fatichi et al., 2014; Körner, 2013; Matthews et al., 2017) pointing out the need to update photosynthesis models if indeed these are looking to predict forest carbon assimilation under climate change scenarios. Some models have aimed to determine plant growth in terms of carbon demand by sinks, rather than in terms of carbon supply by photosynthesis. Hayat et al. (2017) modelled plant growth based on meristem growth, looking to optimise light interception (by growing taller and avoiding nearby competitors) and limited by maximal size of the tree. Under this framework, plant growth in not the result of photosynthesis but is constrained by abiotic factors driving cambial and meristem cell division, which ultimately represents carbon demand by tissue growth.

Since tissue growth (cell division + cell expansion) is usually more sensitive to environmental variables (e.g., soil moisture, temperature, soil fertility) than photosynthesis (Fatichi et al., 2014), a source-imbalance is usually generated when conditions are sub-optimal. When this imbalance is triggered, plants respond in three different levels depending on the timescale over which the imbalance persists: *a*) in the short term, NSCs accumulate in the leaf triggering photosynthetic downregulation, thus affecting source activity; *b*) in the midterm, the excess of NSC are allocated to storage, increasing the plant's NSC concentration across different organs; and *c*) in the long term, sink activity ends regulating source activity through a complex phytohormonal balance that regulates genes associated with the photosynthetic machinery and leaf deployment (Fatichi et al., 2014).

Next, I describe NSC dynamics across contrasting ecosystems in order to better understand what the main drivers of NSC concentration in different tissues are, but ultimately focusing on leaf NSC concentration.

2.2 Non-structural carbohydrates dynamics in natural vegetation

2.2.1 Non-structural carbohydrates expected values across biomes

Non-structural carbohydrates are divided between a soluble sugar fraction (glucose and fructose mainly) as end products of the Calvin-Benson-Bassham (CBB) cycle and a non-soluble fraction composed of starch. The CBB metabolic cycle consists of three stages: *i*) a carboxylation phase where a molecule of CO_2 is fixed in an organic molecule of RuBP to then split into two molecules of 3-phosphoglycerate (triose phosphate); *ii*) a reduction phase in the chloroplast where the two molecules of 3-phosphoglycerate are reduced into two molecules of glyceraldehyde-3-phosphate, one molecule will be further combined with another molecule of glyceraldehyde-3-phosphate in the cytosol to finally yield fructose 1,6-bisphosphate (hexose); and *iii*) a regeneration phase where the remaining glyceraldehyde-3-phosphate is combined with other triose phosphate to regenerate the molecule of RuBP used at the beginning of the cycle. Soluble sugars obtained from the CBB cycle are used for metabolic needs, such as respiration and tissue growth. However when these demands are satisfy within an organ, conversion of soluble sugars to starch is triggered in order to be used as a form of energy storage (Dietze et al., 2014). The sum of both fractions, referred to as total NSC, represents roughly 10% of tissues dry weight (Martínez-Vilalta et al., 2016).

Martínez-Vilalta et al. (2016) in their compendia on NSC across biomes, found higher soluble NSC in leaves (14.4% ± 1%; mean ± standard deviation) when compared to stem (7.0% ± 0.7%) and belowground concentrations (10.6% ± 0.8%). This is consistent with the fact that soluble NSCs are the result of the photosynthetic pathway generated in the leaves as source organs, whereas stem and roots are mostly used for storage purposes. In contrast, starch concentration within leaves, stem, and roots, were similar. During the day, when photosynthesis rates are higher than translocation rates, a portion of end-products of the CBB cycle is stored as starch, to then be hydrolysed and re-routed across the plant when photosynthesis production diminishes. Starch content was lower than soluble NSC in leaves (6.4% ± 0.6%), stem (3.3% ± 0.5%), and roots (7.1.3% ± 0.7%).

When NSC concentrations were categorised by different biomes (boreal, temperate, Mediterranean and tropical), different habitats did not explain much of the observed variability around NSC concentration in different organs.

Altogether, leaves tend to be the organs with the largest NSC pool, and soluble NSCs are the largest contributors to total NSC concentration across different tissues. NSC concentrations across several studies indicate little effect of biomes in explaining observed NSC concentration variability, meaning that NSC concentrations are site-specific, vary seasonally, and depend on genetic traits that drive trees' photosynthetic, as well as NSC storage, capacities.

2.2.2 Seasonality of non-structural carbohydrate concentration

As abovementioned, NSC concentration varies according to periods of photosynthetic surplus and deficit. Even if is hard to understand NSC concentration's variability in terms of biomes, seasonal variability plays a major role in explaining NSC concentration differences. Martínez-Vilalta et al. (2016) found that NSC concentration in plants only exhibited differences between seasons in boreal and temperate biomes. Nevertheless, Würth et al. (2005) in their compendium of NSC dynamics in tropical vegetation did find higher leaf NSC concentration during the dry season when sink activity is expected to be constrained by soil moisture.

In temperate ecosystems, Hoch et al. (2003) found that maximum leaf NSC in a mixed forest stand in Switzerland (47°33′ N; 7°36′ E; 500 m.a.s.l.) occurred in June, two months and a half after bud break, constantly decreasing until October with the onset of leaf senescence. Total NSC concentrations in leaves reached by *Acer*, *F. sylvatica*, *Quercus*, the same genus, and the same species in the case of *F. sylvatica*, that were sampled in this thesis, exhibited similar total NSC concentration to the ones that we found for the month of August when samples were collected.

Similar studies in tropical vegetation are less frequent. Würth et al. (2005) described NSC dynamics in Panama using the Smithsonian plots (8°58′ N; 79°34′ W, 15-20 m.a.s.l.). Researchers found that across 17 species total NSC averaged 6.2% of leaf dry weight, ranging from 5 to 10%. Differently to Martínez-Vilalta et al. (2016), stem instead of leaves, was the organ representing plants total NSC largest concentration

(9.1%), meanwhile roots averaged (7.4%). As previously mentioned, seasonal differences were indeed found. During the dry season, when tissue growth becomes limited by plant's water potential, total NSC concentration increased across all organs mainly led by an increase in starch concentration whilst soluble NSC concentration remained fairly constant.

This is consistent with findings from Poorter and Kitajima (2007). When comparing contrasting dry (16°1′ S; 61°4′ W) and wet tropical forest (15°47′ S; 62°55′ W) in Bolivia, they found similar concentrations to the ones found in this thesis. Furthermore, wet tropical trees presented larger total NSC concentrations, these being dominated by starch, rather than soluble NSC content.

2.2.3 Storage allocation of non-structural carbohydrates

Non-structural carbohydrates storage occurs on two-time scales: diurnal and long-term (inter-seasonally and -annually). These reserves might be used in the future to help the plant cope with environmental stresses like drought, shading, herbivory, pathogen attack and fire (e.g., Cardoso et al., 2016; Chapin et al., 1990; Doughty et al., 2015; O'Brien et al., 2014; Richardson et al., 2013). NSC stored in organs such roots and stem has proven to be highly dynamic, thus providing metabolic demand when carbon assimilation through photosynthesis becomes diminished. Observations have shown that these reserves on average are 10 years old (Richardson et al., 2013).

Although it is not completely clear if NSC allocation into storage is: *a*) a passive process, meaning that allocation to storage only occurs when other factors constrain a plant's growth, thus diverting carbon from assimilation to storage. *b*) is quasi-active: storage allocation occurs when growth is regulated by the plant in order to allocate surplus NSCs to storage. Meanwhile, a third option, *c*) active allocation to storage, follows when the plant actively invests NSC in storage rather than in growth (Dietze et al., 2014; Palacio et al., 2014).

Even if this thesis does not directly examine NSC allocation as storage, these dynamics are important to understand when addressing the other hypotheses underlying this. I test the hypothesis that plants are no longer carbon-limited, therefore there is

no leeway to increase land's carbon sinks. Körner (2013) advocates for this hypothesis after observing that NSC concentrations in different plant tissues around the globe are hitting an upper threshold, based on the idea that NSC allocation into storage is a passive process that only occurs after carbon demand for new growth is limited by other environmental factors. If carbon allocation to storage is indeed an active process, his hypothesis risks being wrong, and other observations should be used to determine if indeed plants are no longer carbon-limited.

2.3 Translocation of non-structural carbohydrates from the leaf

NSC translocation from the leaf to the rest of the plant is important to maintain low NSC concentrations in the blade and therefore avoid photosynthetic downregulation. In the following section I will present key physiological features of the main drivers of this phenomenon.

2.3.1 Understanding phloem translocation: the pressure-flow model for phloem transport

Long-distance transport in the plant occurs in two tissues, usually studied by separate research communities but intrinsically entwined within the plant vascular tissue. Water transport from soil to the leaf happens in a dimension ruled by rigid biophysical and mathematical rules, ultimately representing xylem's dead status. In contrast, phloem transport occurs across living cells, being less studied because apparently of its much more complex biological nature. Nevertheless, both tissues coexist together, and their interdependence is much greater than biophysicists and molecular biologists would like to admit.

The main driver of water movement through xylem is the negative hydrostatic pressure (or tension) at the top of the canopy which *"pulls"* the water trough the xylem because of the cohesive properties of water molecules. Thus, water lifting is energetically cost-free for the plant. In contrast, mass flow in the phloem is driven by difference in

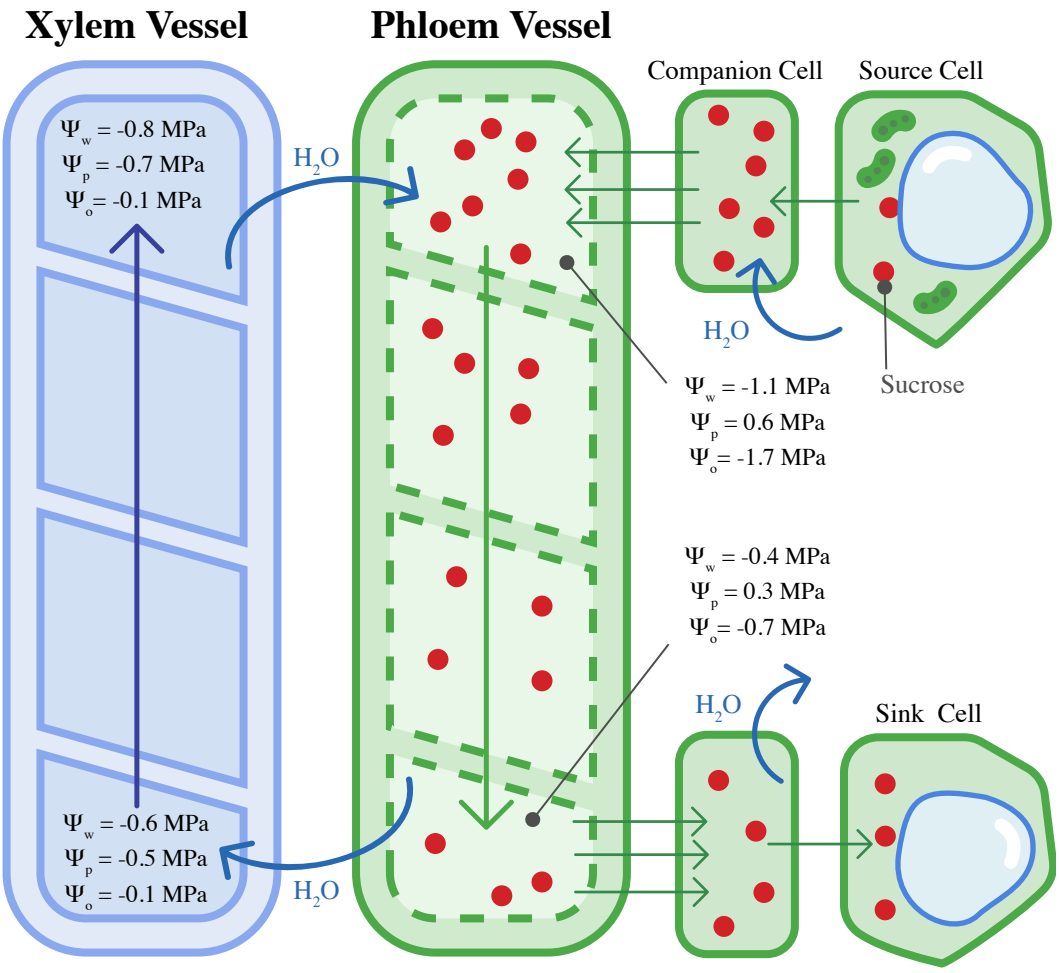


Figure 2.1: Schematic representation of Münch Theory of mass flow transport. Sugars are loaded into the phloem from mesophyll cells through companion cells, thus making osmotic potential (Ψ_o) more negative, thus lowering cell's overall water potential (Ψ_w). Water is transferred from the xylem (higher Ψ_w) to the phloem (lower Ψ_w) increasing pressure potential (Ψ_p) which moves the sugars downstream. After sucrose is unloaded by sink cells phloem's cell Ψ_w increases and water is reverted towards the xylem. In order to maintain a turgor gradient across the phloem, companion cells need to actively load the phloem through pumps (apoplastic loading) or generate high photosynthetic rates in order to maintain a mesophyll to phloem sugar gradient (symplastic loading).

turgor pressure between source and sink tissues along the phloem. This turgor pressure difference provides the gradient to transport carbohydrates along the sieve tubes pathway (Van Bel, 2003). This model of phloem transport is currently known as the pressure-flow model for phloem transport, developed by Ernst Münch in 1930 (Münch, 1930).

Turgor pressure is generated in the phloem in leaves when photoassimilates are loaded from their place of synthesis in the mesophyll, into an array of sieve elements/companion cells next to minor veins (Fig. 2.1). Since the sieve element of the phloem will be loaded with sucrose from the leaf mesophyll, its osmotic potential (Ψ_o) will be lower (more negative), thus lowering overall cell water potential (Ψ_w) and moving water from a nearby xylem vessel in which Ψ_w is higher. As water potential in the phloem increases, turgor is generated, increasing pressure potential (Ψ_p) and triggering the expansion of the cell, thus generating a turgor pressure gradient along the sieve elements, providing the work needed to transfer the NSC *via* bulk flow. Since phloem transport occurs throughout a chain of sieve elements involving sieve plates between them, rather than a single cell connecting both source and sink organs, Ψ_o and Ψ_p does not equilibrate along the phloem. This gradient allows the movement of NSC along the phloem. At the end of the path, where sink cells unload the photoassimilates from phloem, the process is reversed. Ψ_o in the phloem becomes less negative, thus increasing cell Ψ_w, water movement is now reversed and the phloem transfers water to the xylem, thus decreasing Ψ_p at the sink level. This provides the energy to mobilize NSC from leaves to sink organs along the phloem.

Nevertheless, some difficulties regarding the pressure-flow model for phloem transport arise. Mainly *i*) the resistance resulting from long-distance transport in trees increases, therefore Ψ_p gradients for long distance transport in trees needs to be incredibly high (Hölttä et al., 2014; Mencuccini and Hölttä, 2010; Minchin and Lacointe, 2005; Savage et al., 2017); *ii*) bidirectional transport in the phloem and *iii*) energy requirements for phloem transport. Nevertheless, these doubts have been overcome by empirical observations of the phloem structure. Sieve plates separating sieve elements along the phloem are free of proteins and other obstructions, lowering resistance along the phloem and allowing movements at a lower Ψ_p differences between source and sink. Secondly, bidirectional nature of phloem flow, contrary to water movement in the xylem which only occurs from soil to the canopy, can occur but never in the same sieve element at the same time. Therefore, phloem transport in two opposite directions can occur at the same time but in parallel sieve conduits. Finally, NSC transport in the phloem has a low energy requirement. Given the large amount of NSCs translocated along the phloem in order to sustain plant metabolic and growth demand, an energy demanding system such as active pumping of sugars along the sieve elements would represent an energy cost too high for the plant. However, energy requirements for NSC translocation are low. Pressure gradients are sufficient for photoassimilates transport *via* mass flow.

Energy expenditure is indeed needed to repair and maintain phloem infrastructure and to reload any sugars leaked into the apoplast and to regulate sieve elements turgor. However, phloem movement is solely driven by Ψ_p gradients which in turn does not involve an active expenditure of energy for the plant.

In most, but not all plant species, sucrose is the most commonly translocated sugar across the phloem (Taiz and Zeiger, 2006). Because NSCs are translocated from leaves to sink cells through the phloem which consists of living cells, sugars must be translocated in a nonreducing form. Thus, only specialised enzymes that hydrolyse sucrose into glucose and fructose, synthesised in sink cells, can unload the photoassimilates coming from the leaf (Giaquinta, 1978), otherwise phloem's living tissue would use the NSCs synthesised in the leaf for its own metabolic needs.

2.3.2 Phloem loading

What is the energetic cost of moving photoassimilates across the plant? Even if NSC translocation in the phloem is driven by water transfer from the xylem vessels to phloem vessels, a sugar gradient in the phloem must be generated in order to trigger sideway water movement. Companion cells play a pivotal role on this. There are mainly two kind of mechanisms to load sucrose into phloem (Gamalei, 2007; Turgeon, 2010). Symplastic loading is characterised by passively loading sucrose into the phloem, thus needing the accumulation of soluble sugars in the leaf to generate a mesophyll-phloem osmotic gradient. Its counterpart, apoplastic loading, relies on active phloem loading by investing in sucrose pumps that can defy this gradient. In general, trees tend to present the former mechanism, whilst herbaceous species present the latter (Comtet et al., 2017; Savage et al., 2016).

Symplastic loading is depicted in panel C, Fig. 2.2. Sucrose is transferred from mesophyll cells (M) into companion cells (CC) through plasmodesmata (Latin *plasmo*: formation; cell + Greek *desma*: bond; chain) between both cells, hence a sugar gradient across both cells must be generated by high photosynthetic rates. On the other hand, apoplastic loading (Fig. 2.2 A) is where sucrose symporters actively pump sugars

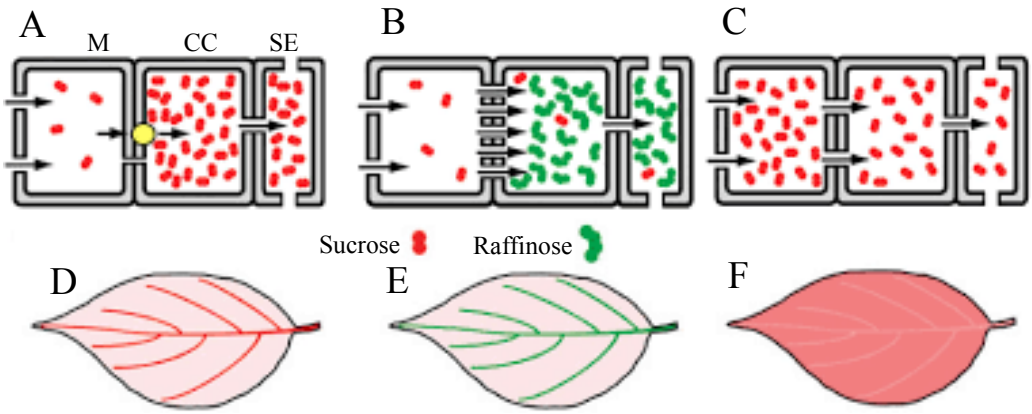


Figure 2.2: Diagram of phloem loading. Panel A shows apopasltic phloem loading where sucrose symporters actively pump sugars from the mesophyll (M) into the companion cell (CC) to then be exported into the phloem sieve element (SE). Panel C shows symplastic phloem loading where sugars are transferred from M to CC *via* plasmodesmata that link both cells. In order to keep the sugar gradient for NSC translocation, leaves need to maintain high photosynthetic rates. Panel B depicts a third mechanism that can be found both in symplastic and apoplastic loading species: once sucrose molecules are transferred to CC, a third molecule of galactose is attached to the sucrose molecule, thus making the molecule too big to go back through the plasmodesmata. Lower rows represent photoassimilate concentrations from radiolabelled carbon. In apoplastic loading, most of the sugars are concentrated in the veins (D), whilst in symplastic loading (F), sucrose is equally distributed across mesophyll cells in order to generate the above-mentioned sugar gradient needed for phloem loading (taken from Turgeon (2010)).

from the mesophyll, thus allowing plants to maintain lower photoassimilates in leaves whilst generating a high concentration in the phloem sieve element (SE), which ultimately allows long distance transport. Apoplastic loading is better suited to withstand photosynthetic downregulation onset by higher C_a since it can override high leaf soluble sugars concentration to transport NSC across the plant (Ainsworth and Lemonnier, 2018; Körner et al., 1995). As depicted in the lower panels in Fig. 2.2, apoplastic loaders concentrate sucrose in minor veins (Fig. 2.2 D) whilst symplastic loaders need to build up a sucrose gradient across the entire mesophyll in order to load sucrose in already sucrose rich companion cells (Fig. 2.2 F).

2.3.3 Leaf vein infrastructure in support of leaf photosynthesis

Vein infrastructure has four main roles in the leaf: *a*) structural support of the blade which enables the leaf to act as a solar panel, harvesting photons from the sun; *b*) transport of phytohormones and other information signals between the leaf and other organs; *c*) water and nutrient distribution in order to sustain stomatal opening and photosynthetic activity; and *d*) translocation of photoassimilates from the leaf to other organs in order to supply non-photosynthetic tissues for NSC metabolic and growth demands (Adams et al., 2018).

Vein infrastructure has been largely studied from the point of view of leaf hydraulics (e.g., Blonder et al., 2017; Sack and Holbrook, 2006; Scoffoni et al., 2016). These papers examine the role of veins from the point of view of xylem, acting as a piping system rapidly supplying leaves with water from roots in order to maintain leaf turgor pressure and keep stomata open for CO_2 gas exchange, thus sustaining high photosynthetic rates, and high overall plant growth rates.

William W. Adams III and Barbara Demmig-Adams, have dedicated a good part of their research to investigate the role of phloem and leaf vein infrastructure in sustaining leaf high photosynthetic rates (e.g., Adams et al., 2013; Amiard et al., 2005; Muller et al., 2014a,b). After studying mostly annual species grown in greenhouse conditions, they have found that photosynthetic rates in species presenting symplastic phloem loading greatly benefited from higher investment in leaf infrastructure together with cross-sectional area of the sieve elements. Indeed, a linear relationship between vein density times the number of cells per area and photosynthetic capacity was found (Adams et al., 2013; Muller et al., 2014b) indicating the importance of increasing phloem density in order to rapidly export NSCs from the mesophyll, thus avoiding photosynthetic downregulation. A higher investment in leaf vein infrastructure has shown to improve leaf photosynthetic capacity by combining two different factors: *a*) more intuitively improving the mesophyll to phloem contact area, and *b*) greater number of companion cells, given an increase in cross-sectional area.

Similarly, Hölttä et al. (2009) also theorise that a higher investment in vein infrastructure would facilitate phloem transport. The pressure-flow model for phloem transport described above, needs of cross water transport between xylem and phloem conduits. A more negative xylem hydrostatic pressure in the leaf would lead to a higher osmotic concentration in the phloem in order to draw water from the xylem into the sieve element, which in turn increases phloem viscosity, thus hampering phloematic transport. Hence, higher investment in vein infrastructure would increase xylem conductance (Scoffoni et al., 2016), which in turn would maintain a high xylem water potential for a given transpiration rate. Therefore, phloem sieve elements would not have to accumulate a high photoassimilate concentrations to decrease its Ψ_o and increase their hydrostatic pressure (Hölttä et al., 2009).

2.3.4 Non-structural carbohydrate translocation from the leaf

Experimental observations of translocation rates have proven to be faster than expected. Peuke et al. (2001), using nuclear magnetic resonance spectrometry in *Ricinus communis* (castor oil shrub,) found translocation rates of $90\,\mathrm{cm\,h^{-1}}$. Accordingly, Tixier et al. (2018) found the presence of ^{13}C in twigs only 2 hours after being assimilated in *Prunus dulcis* (almond tree), while Keel et al. (2007) when investigating translocation rates in temperate natural vegetation using the same ^{13}C labelling technique found similar translocation rates. *Quercus*, *Tilia* and *F. sylvatica* exhibited the presence of recently assimilated carbon in twigs within 2 to 9 h (Keel et al., 2007).

However, NSC translocation across phloem will also depend on the sink activity of the plant. During periods of low sink activity, as previously discussed, or when sink demand has been restricted because of fruit thinning, it has been observed that translocation slows down (Kallarackal and Milburn, 1984), thus increasing leaf NSC concentration and triggering a cascade of signals that onset photosynthetic downregulation. Next, we present photosynthetic downregulation mechanisms that occur in the leaf once NSC translocation has been hampered.

2.4 Non-structural carbohydrates and photosynthetic feedback inhibition

At a physiological level, when leaf NSCs reaches a threshold concentration, an accumulation of end product of the CBB cycle on the chloroplast controls the cycling of inorganic phosphate (Pi) necessary for the regeneration of RuBP, which fixes the molecule of CO_2 coming from the atmosphere, into an organic molecule (Paul and Foyer, 2001; Pieters et al., 2001; Sharkey et al., 1986). In the long run, an excess of NSC in the leaf can be responsible for regulating genes associated with the photosynthetic machinery (Moore et al., 1999; Paul and Foyer, 2001). However, periods of high sink demand are characterised by synthesis of cytokinins in roots which in turn enhances source activity by coding for genes related to photosynthesis and promoting new leaf deployment (Lobo et al., 2015). Thus, high NSC concentrations in leaves do not only serve as an indicator that carbon demand is limited by growth requirements, but are also an active signal that modulates ecosystem productivity.

Non-structural carbohydrates concentration in the leaf can not only regulate leaf photosynthesis at the CBB cycle level but can also regulate whole leaf gas exchange. Wong et al. (1979) found that leaf stomatal conductance depended on irradiance, thus paving the road for an optimization theory for leaf gas exchange. As irradiance, or C_a, can limit or boost leaf photosynthetic rates, stomatal opening reacts to these stimuli in order to maximise carbon gain in terms of water loss through transpiration. Therefore, when irradiance levels are low, thus limiting leaf photosynthesis, stomatal conductance is controlled in order to avoid unnecessary water loss (Ball et al., 1987; Cowan and Farquhar, 1977; Medlyn et al., 2011). Similarly, increasing C_a has been shown to reduce stomatal conductance and increase ecosystem water use efficiency since the same mesophyll internal CO_2 concentration can be achieved at a lower stomatal conductance (Keenan et al., 2013).

The theoretical canopy gas exchange models mentioned above predict leaf stomatal conductance dynamics by relying on C_a to model carbon assimilation rates which in turn regulate stomatal conductance. Nevertheless, experimental observations have determined that while photosynthesis indeed shows a rapid response to irradiance, stomatal conductance does not respond in the same way, showing reaction times up to one order of magnitude slower than photosynthesis acclimation (Lawson et al., 2012). Therefore,

if it is not C_a directly regulating stomatal conductance, what is the signal to open or close stomata? Leaf NSC concentration has been targeted as the indicator of photosynthesis leading to stomatal regulation (Matthews et al., 2017; Santelia and Lawson, 2016) and hence leaf transpiration.

Optimisation models seek to optimise photosynthesis in terms of losses and constrains to the system. At the leaf level, photosynthesis has been expressed as a function of carbon gain whilst minimising water loss (e.g., Cowan and Farquhar, 1977; Medlyn et al., 2011). When scaling up to the plant level, other restrictions apply. Feedbacks between photosynthetic and hydraulic traits are crucial in order to optimise carbon gain and avoid xylem embolism, thus optimising water delivery to the leaf in order to allow stomatal opening without compromising xylem integrity (Mencuccini and Christoffersen, 2019). Nevertheless, novel approaches regarding phloem translocation have emerged. Huang et al. (2018), rather than only maximising carbon input trough photosynthesis, argue that the true objective of the plant in terms of evolutionary fitness is to maximise the energy flow through the system (Lotka, 1922) in order to satisfy energetic demands for maintenance and growth across the plant, thus conceding phloem physiology a major role in carbon acquisition. Based on the holistic views of Münch (Münch, 1930) and Hölttä et al. (2014) regarding the inter-relationship of xylem and phloem, Huang et al. (2018) present a model where photosynthetic, hydraulic and NSC-transport traits are coordinated in order to maximise chemical energy (in form of sugars) transport across the plant. Stomatal conductance is therefore constrained to optimise hyrdrostatic pressure in order to maximise lateral movement from the xylem to the phloem to generate the needed turgor to translocate NSCs along the sieve elements in the phloem. Altogether, Huang et al. (2018) presents an optimization model that seeks to maximise carbon gain through stomata opening without jeopardising high (less negative) Ψ_w in the xylem needed to produce high hydrostatic pressure in the phloem in order to translocate photoassimilates from source to sink organs.

Therefore, NSC leaf dynamics and translocation do not only affect the leaf itself but can also control water transpiration and canopy gas exchange. These fluxes can be studied *in vivo* and in real time whilst the determination of leaf NSC concentration requires cutting the leaf off and the analysis can only be done in the laboratory.

Nevertheless, leaf NSC concentrations are not only the result of a sink-source imbalance. The next section examines pressure-volume (PV) curves and how hydraulic leaf traits can be derived from them. A key leaf hydraulic trait for plant acclimation to drought is leaf osmotic potential at full turgor (Π_o) which enables decreasing leaf Ψ_w, without affecting cell's turgor pressure. Evidence shows that Π_o is heavily dependent on leaf NSC accumulation, showcasing leaf NSC active accumulation as a mean of acclimation to drought.

2.5 Leaf hydraulic traits

Leaf PV curves result from relationships between leaf water potential (Ψ_{leaf}) and leaf water content. Number of key leaf hydraulic traits can be obtained from these relationships indicating different degrees of plants adaptations, and acclimations to seasonal changes in soil moisture. In **Chapter 4** (Paper 2), I develop an open-source tool to analyse leaf PV curves. Next, I will focus on leaf hydraulic traits followed by how these traits are related to leaf NSC concentration.

Imbalances between water supply, provided from soil moisture, and atmospheric water demand result in changes in the water status of plants. Leaves account for roughly the 30% of plant's total resistance to water movement through the soil-plant-atmosphere water continuum (Sack and Holbrook, 2006). Changes in leaf water potential (Ψ_{leaf}) regulate stomatal opening, and hence leaf photosynthesis. Leaf water potential at turgor loss point (Ψ_{TLP}) reveals the point at which passed the cell is unable to rehydrate. The Ψ_{TLP} has been acknowledge as one of the key traits that indicates plant adaptation to drought (Bartlett et al., 2012). The lower the cell water potential at the turgor loss point, the better adapted the plant is to moisture shortage.

Leaf water potential at turgor loss point is also dependent on other leaf hydraulic leaf traits. The modulus of elasticity (ε) describes how Ψ_{leaf} changes following leaf water loss before reaching Ψ_{TLP}. A steep decline of Ψ_{leaf} for a given amount of water loss would indicate a high elasticity modulus, meaning low elasticity of the cell wall. Since changes in Ψ_{leaf} would occur at a higher rate, Ψ_{TLP} would be reached sooner, meanwhile, species exhibiting lower ε, such as sclerophyllous vegetation, would reach Ψ_{TLP} later.

Another key feature regulating Ψ_{TLP} is osmotic regulation. Solute concentration decreases the free energy of water inside the cell. Drought-tolerant species exhibit an accumulation of solutes in the leaf during drought, thus maintaining turgor pressure despite a decrease in Ψ_{leaf}. When water potential in soil decreases following drought, leaves need to reach a lower Ψ_{leaf} in order to maintain the soil-plant-atmosphere continuum and transfer water from already low water potential vessels in the xylem. Osmotic adjustment is often associated with compounds accumulation of carbohydrates (i.e., NSCs), cations and anions, organic acids, and amino acids (Sanders and Arndt, 2012).

Accumulation of NSCs in the leaf can occur by limiting sucrose export through phloem and/or cleaving starch long chains into soluble carbohydrates. Hence NSC dynamics can not only regulate processes occurring in the leaf, as earlier parts of this literature review have shown, but can also be a physiological tool in order to acclimate the whole individual to drought conditions. **Chapter 5** (Paper 3) studies osmotic adjustment and its effect on leaf photosynthesis across a drought gradient in Ghana by using the PV curve tool developed in **Chapter 4**.

2.6 Leaf chemistry determination with field spectroscopy

I have previously shown throughout this literature review that NSC regulate both CO_2 and water exchange between the leaf and its surrounding atmosphere by means of regulating stomatal conductance (Matthews et al., 2017). These fluxes can be studied *in vivo* and in real time whilst the determination of leaf NSC concentration requires cutting the leaf off and the analysis can only be done in the laboratory. A non-destructive approach to assessing NSC concentrations would be immensely helpful in both observational and scaling studies. The next section describes advances in leaf spectroscopy and explores how this technique could be of use in the field to determine real time NSC leaf concentration and diurnal dynamics.

Chapter 6 (Paper 4) explores the use of field leaf spectroscopy in the determination of total, and leaf NSCs fractions (i.e., glucose-fructose, sucrose and starch). Here we presented previous experience in leaf field spectroscopy in the determination of several leaf chemical traits.

The clearest interaction between leaves and light is colour. Leaves owe their colour to chlorophyll since this pigment within the photosynthetic active spectrum (400 to 700 nm) absorbs photons on the blue and red bands, whilst reflecting more photons in the 500 nm (green) region. Nevertheless, other pigments (i.e., carotenoids which grant the colour orange to leaves in autumn, or anthocyanins which makes for wine to be red), less abundant in the leaf, and other molecules also interact with light at a level that our eyes cannot perceive. High resolution leaf spectroscopy aims to determine leaf reflectance (from 0 to 1) in several spectral regions within the visible and infrared spectrum.

Spectroscopy of ground and dried leaf samples has been successful in correlating spectral signatures with concentrations of leaf chemical compound such as chlorophyll, cellulose, lignin, proteins, sugars, and oil (Curran, 1989). In turn, these compounds also have a major influence in shaping overall leaf stoichiometry, such as nitrogen concentration (heavily dependent on leaf chlorophyll content), and specific leaf area (dependent on cellulose and lignin concentrations). Researchers have looked at the spectral footprint of leaves across a variety of species and biomes, looking to describe leaf traits distribution at a regional scale (e.g., Asner et al., 2009; Doughty et al., 2017; Townsend et al., 2008).

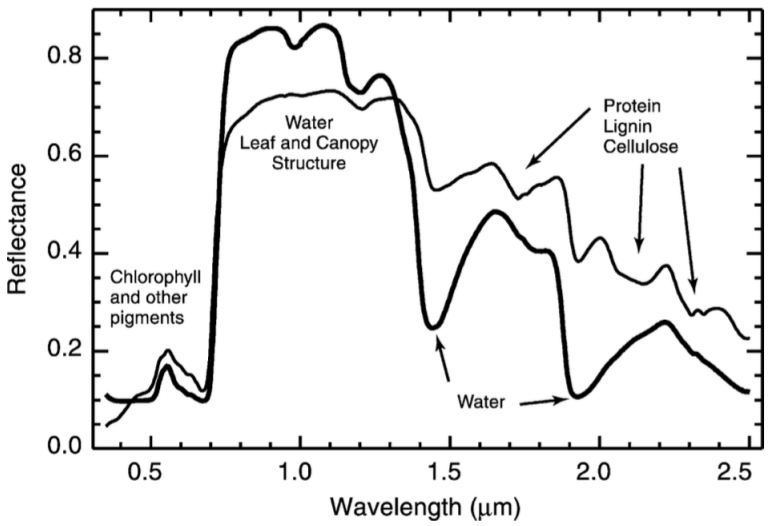


Figure 2.3: Leaf reflectance of a fresh (thick line) and a dry (thin line) *Quercus* leaf. Absorption bands for different leaf compounds are shown accordingly (taken from Kokaly et al. (2003)).

Figure 2.3 shows how different compounds in the leaf present different peaks and valleys of reflectance given the interaction between light and these compounds. For instance, leaf reflectance in the 1500 nm and 2000 nm range correlates with water absorption in these bands, thus given particular information on the water status of the leaf. Water stressed leaves present less absorption in these bands (Fig. 2.3). Other leaf compounds, such as chlorophyll, protein, and lignin and cellulose concentrations are depicted in other spectral bands.

Since leaf spectroscopy has been successful in correlating leaf spectral footprint with several leaf compounds, it has also been studied to determine leaf NSC fractions and total NSC concentrations. Several researchers have succeeded in determining leaf NSC concentration using spectroscopy in crops (e.g., Batten et al., 1993; Dreccer et al., 2014; Yendrek et al., 2017). Furthermore, Asner and Martin (2015) were able to predict total leaf NSC concentration across several tropical and sub-tropical biomes. Nevertheless, it is not clear whether in fact these studies directly managed to measure leaf NSC concentration from NSC concentrations *per se*, or if they are indirectly estimated by across-species correlations between NSC concentrations and other leaf traits that are good predictors for leaf photosynthetic capacity, hence leaf NSC concentration.

In this literature review I have covered the basics concepts to undergo the next four empirical chapters.

Chapter3

Photosynthetic downregulation in response to non-structural carbohydrates (NSC) in natural forest ecosystems

"...the great prodigality of Paris, her marvelous fête, her Beaujon folly, her orgy, her full-handed outpouring of gold, her pageant, her luxury, her magnificence, is her sewer."

Victor Hugo, *Les Misérables*

The first empirical chapter of this thesis examines the relationship between non-structural carbohydrates and photosynthesis at a leaf level between several species in a tropical wet forest (Ghana), and temperate ancient woodland in the UK.

Based on the premises that an increase in atmospheric CO_2 concentrations given anthropogenic emissions would lead to an imbalance between non-structural carbohydrates synthesis *via* photosynthesis and their use because of nutrient availability and soil moisture limitations in natural ecosystems, I assess the effects of leaf sugar concentrations on photosynthesis, thus aiming to quantify photosynthetic downregulation in wild vegetation.

Furthermore, I analyse the role of leaf traits and leaf's phloem investment on regulating the extent to which some species could benefit from the so called carbon fertilization effect.

I designed the experiments, conducted the fieldwork, did the analysis and wrote the manuscript with the support of AS and YM. SAB and LA supported me during fieldwork in Ghana. JMV supported me with laboratory NSC analysis and helped with the manuscript preparation. JAG helped me with the statistical analysis. The manuscript is ready for submission and I expect to submit it to *New Phytologist*.

Photosynthetic downregulation in response to non-structural carbohydrates (NSC) in natural forest ecosystems

Nicolas Raab[1*], Alexander Shenkin[1], Jordi Martínez-Vilalta[2,3], Jesús Aguirre-Gutiérrez [1], Stephen Adu-Bredu[4], Lidya Afriyie[4], Yadvinder Malhi[1]

[1]Environmental Change Institute, School of Geography and the Environment, University of Oxford, Oxford, OX1 3QY, UK.[2]CREAF, Cerdanyola del Vallès, E-08193, Barcelona, Spain. [3]Universitat Autònoma de Barcelona, Cerdanyola del Vallès, E-08193, Barcelona, Spain. [4]Forestry Research Institute of Ghana, Council for Scientific and Industrial Research, Kumasi, PO Box UP 63 KNUST, Ghana.[*]Corresponding Author: nicolas.raab@ouce.ox.ac.uk

Abstract

Increasing atmospheric CO_2 concentration (C_a) has been thought to increase ecosystem net productivity, thus offsetting anthropogenic impact in the atmosphere. Nevertheless, plant carbon demand has been proven to be more sensitive to abiotic factors (soil fertility, temperature, soil moisture) than leaf photosynthesis. When an imbalance between non-structural carbohydrates (NSC) synthesis and demand occurs, phloem translocation is hampered, leading to an increase in NSC concentration in the leaf. Leaf's NSC concentration has proven to downregulate photosynthesis, affecting net ecosystem exchange and therefore hindering a carbon fertilization effect on forest productivity. Here, we quantified photosynthetic downregulation in natural vegetation by manipulating leaves' natural NSC concentration in the short term in six species in two contrasting ecosystems: a wet tropical forest in Ghana and a temperate woodland in the UK. We found that leaves that presented higher investment in vein density together with species that were on the fast region on the leaf economic spectrum where less susceptible to photosynthetic downregulation mediated by NSC, whereas slow species with low investment in vein infrastructure would benefit less from the positive effects of elevated C_a in plant's productivity.

3.1 Introduction

The role of photorespiration in C3 plants has been the subject of multiple hypotheses. Whether serving as a mechanism of photochemical energy dissipation (Kozaki and Takeba, 1996), or as a result of past higher ambient CO_2 concentration (C_a), photorespiration is a process whereby a molecule of O_2, instead of CO_2, is fixed by RuBisCO. This occurs in one out of four RuBisCO reactions, and thereby reduces net leaf net CO_2 exchange and overall plant and ecosystem productivity.

Early research from free-air CO_2 enrichment (FACE) experiments has supported the hypothesis that increased C_a would result in higher CO_2 uptake given a decrease in O_2 fixation by RuBisCO, thus translating into increased biomass stocks (e.g., Ainsworth et al., 2003; Nowak et al., 2004; Sholtis et al., 2004; Zotz et al., 2005). Photosynthesis enhancement was observed under high C_a, revealing that grasslands and forests were carbon-limited. Nevertheless, extended observations have shown that this initial enhancement is not sustained over time (Bader et al., 2013; Ellsworth et al., 2017; Fleischer et al., 2019; Girardin et al., 2016; Norby et al., 2010; Terrer et al., 2019) because of nutrient and water limitation to biomass growth.

While nutrient supplies may ultimately constrain how much ecosystems are able to respond to elevated C_a, physiological mechanisms also play a role in how much plants are able to take advantage of it. Specifically, while leaves produce carbohydrates at higher rates under elevated C_a, they must be able to export these carbohydrates quickly in order to avoid photosynthetic feedback inhibition. When leaf NSC concentration reaches a threshold, a series of feedback inhibition mechanisms are triggered in the chloroplast (Paul and Foyer, 2001; Paul and Pellny, 2003), thus ultimately affecting leaf gas exchange.

Experiments have manipulated natural NSC concentrations in leaves to better understand metabolic and gene downregulation in photosynthesis mediated by NSC concentration (Jones et al., 1996). Azcón-Bieto (1983) studied NSC effects on photosynthetic downregulation in wheat. Instead of increasing leaf NSC concertation by inducing long-term source-sink imbalance (e.g., by thinning sink organs such as ears), which incurs changes in plant's nutrient and hormonal balances, he chilled leaf bases to restrict NSC translocation and found a negative correlation between leaf NSC concentration and

leaf overall photosynthesis. However, this kind of research on natural ecosystems is still lacking.

Researchers have studied the effect of leaf veins on photosynthesis (e.g., Brodribb et al., 2007; Scoffoni et al., 2016) focusing on the role of veins as plant infrastructure designed to supply water for leaf gas exchange. However, veins not only function as a "piping system" supplying water (*via* xylem) but also as a "collecting network" translocating soluble non-structural carbohydrates (NSC) across the plant (*via* phloem).

Trees load NSC from companion cell into phloem sieve elements *via* symplast (Savage et al., 2017), which relies on plasmodesmata to channel photoassimilates being synthesised in the mesophyll into the phloem sieve elements (Turgeon, 2010). Symplastic annual species grown in laboratory conditions have shown that when grown under a high-light environment, they show higher vein density than plants grown under low light conditions. High light conditions did not show an increase in plasmodesmatal frequency per companion cell, however leaf total plasmotesmatal density did increase, thus facilitating NSC loading and translocation in order to maintain higher photosynthetic rates by avoiding NSC photosyntheic feedback inhibition (Adams et al., 2013; Amiard et al., 2005; Muller et al., 2014a; Polutchko et al., 2018) .

When companion cells load NSCs in into the phloem its overall water potential becomes more negative. This decrease in water potential triggers lateral water movement from the xylem, which is at a higher water potential, thus increasing turgor pressure in the phloem cell. As soon as NSC are unloaded at sink level the process is reversed, thus reducing turgor pressure and generating a turgor gradient along the phloem following Münch theory (Münch, 1930; Savage et al., 2016). Higher investment in vein infrastructure would improve leaf hydraulic conductivity (Scoffoni et al., 2016), allowing the xylem to maintain higher water potentials at a given transpiration rate compared to leaves with low vein density. At a lower xylem water potential, the phloem would have to reach higher NSC concentrations (more negative osmotic potential) in order to allow water transfer from the xylem and generate the turgor gradient needed for photoassimilates translocation (Hölttä et al., 2009). Therefore, higher investment in vein infrastructure would facilitate lateral water movement and NSC translocation, not only by enabling higher plasmodesmatal density, but also by decreasing the NSC concentration in the phloem needed for turgor generation.

Leaf traits have been largely used to categorise species within the leaf economic spectrum (LES) (Díaz et al., 2016; Niinemets and Sack, 2006; Wright et al., 2004). By means of natural selection, leaf traits have shown coordination within an axis raging from species producing leaf area at a low carbon cost (high specific leaf area; SLA) with short lifespan and higher photosynthetic rate in order to rapidly recover carbon investment, and species producing leaves with a lower SLA (higher carbon investment per unit of leaf area), longer lifespan and lower photosynthetic rates. This categorisation has prioritised features to acquire resources (namely photoassimilates) through higher nutrient allocation in high SLA leaves in order to achieve higher photosynthetic rates and allowing the tree to rapidly recover their carbon costs during their short lifespan.

Given the importance of NSC translocation in sustaining high photosynthesis rates, a plant's success is not solely based on its capacity to rapidly assimilate CO_2 from the atmosphere, but also on its capacity to quickly mobilise these resources to other organs, thus alleviating leaves from high NSC concentrations and avoiding photosynthetic feedback.

To better understand the effect of rising C_a on natural vegetation we designed an *in-situ* experiment to test NSC downregulation of mature individuals of six tree species across two contrasting biomes: a tropical West African forest and a temperate European woodland. By manipulating short-term natural sucrose content in leaves we explored the following hypotheses:

- **Hypothesis 1:** Addition of NSC to leaves results in a downregulation of photosynthesis because of NSC effect on photosynthetic inhibition.

- **Hypothesis 2:** Across species, the degree of downregulation following NSC addition is related to leaf morphological traits (e.g., SLA), as a proxy of leaf's strategy to recover the carbon cost of deploying leaf area, thus proving coordination between traits that have been selected to improve plant's resource acquisition and physiological traits facilitating rapid NSC translocation to sustain given photosynthetic rates.

- **Hypothesis 3:** Higher investment in leaf vein infrastructure will result in higher NSC translocation along the leaf, and lower downregulation by NSC because of the importance of overall leaf hydraulic traits and leaf plasmodesmata frequency on carbohydrates' transfer from the blade.

3.2 Materials and Methods

3.2.1 Site and species description

Field work was conducted in permanent forest monitoring plots from the Global Ecosystem Monitoring network (GEM; `http://gem.tropicalforests.ox.ac.uk`). Tree growth and carbon fluxes in GEM plots are monitored at monthly frequencies (Marthews et al., 2014), with the aim of better understanding forest carbon dynamics under a changing climate.

Tropical evergreen species were sampled from a moist lowland rainforest situated in Ankasa National Park (5°16′ N; 2°4′ W; 114 m.a.s.l.; plot code ANK-03), Ghana, in the Upper Guineo-Congolian rainforest region in February and March 2015. The mean annual temperature is 25.0 °C and the total mean annual precipitation is 2050 mm (Moore et al., 2017). We chose three relatively common species in the plot (*Duguetia stuadtii*, *Ongokea gore*, and *Uapaca guineensis*) that were also accessible by tree climbers.

Temperate work was conducted in Wytham Woods (51°46′ N; 1°20′ W; 160 m.a.s.l.; plot code WYT-13), a mature broadleaf woodland located in Oxfordshire, UK, during July and August 2015. Bud break begins end of March, canopy full deployment is observed late April-early May and canopy senescence (50% of the canopy changing colour) occurs end of October. Mean annual temperature is 10.1 °C with an average total annual precipitation of 730 mm (Thomas et al., 2010). Leaf NSC photosynthesis downregulation was studied in three European common species: *Acer pseudoplatanus* (sycamore), *Fagus sylvatica* (beech), and *Quercus robur* (European oak). Individual trees were selected because of being in reach from an on-site canopy walkway. Species representation in terms of their basal area for both sites is shown in Table 3.1.

Table 3.1: Species representation per plot given their percentage of woody basal area. Table shows number (N.) of trees, mean diameter at breast height (DBH) together with ± standard deviations, and percentage (%) wood basal area representation for each plot.

	N. of Trees	Mean DBH (m)	Basel Area (m^2ha^{-1})	% Wood Basal Area
Ankasa Plot (ANK-03)	501	0.22 ± 0.139	25.9	100
D. staudtii	9	0.42 ± 0.146	0.15	0.58
O. gore	9	0.28 ± 0.161	0.72	2.78
U.guineensis	14	0.45 ± 0.285	3.1	12
Wytham Plot (WYT-13)	724	0.21 ± 0.122	32.9	100
A. pseudoplatanus	552	0.13 ± 0.101	11.2	34
F. sylvatica	27	0.19 ± 0.658	0.47	1.43
Q. robur	38	0.59 ± 0.122	10.9	33

3.2.2 Non-structural carbohydrates manipulation trial

Six branches of each species were collected from at least three different individuals except for *F. sylvatica*, where we had access to only one individual. Details for the number of individuals sampled for each species can be found in Table 3.2. In Ankasa, top-of-canopy branches were collected by a tree climber before 8:00 am. As soon as the branch reached the ground, an under water cut was performed and a plastic bag with water was tightened 5 cm above the cut, after which a black bag was internally sprinkled with water and placed over the branch to avoid leaf transpiration and to raise branch and leaf water potential. Bagged branches were kept under shade until noon and then transported to the field laboratory. At the laboratory, branches were put in a bucket with water, a second cut under water was performed, and the black bag was removed. After waiting 30 minutes (min) to stabilise branch water status and acclimate branches to daylight (Verryckt et al., 2020), leaf net photosynthesis (Pn) was measured with a leaf gas exchange analyser (Li-6400XT, LI-COR, Lincoln, NA, USA). Leaf chamber temperature was set at 30 °C, and photosynthetic active radiation (PAR) at 1200 µmol m^{-2} s^{-1}, to avoid heat damage and photoinhibition in tropical leaves (Doughty, 2011). Leaf chamber CO_2 concentration was set at 2000 μmol_{CO_2} mol^{-1} to ensure maximal Pn.

Table 3.2: Trees and number of individuals sampled for each species. Note that tree tags numbers in Wythams Woods are larger than the number of trees found in WYT-13 plot because this plot is a sub-plot of an 18 ha larger plot.

Site	Species	Tree Tag Sampled	No Branches Sampled
Ankasa Plot (ANK-03)	*D. staudtii*	T026	3
		T027	1
		T509	2
	O. gore	T222	2
		T293	2
		T466	2
	U.guineensis	T098	1
		T401	1
		T464	4
Wytham Plot (WYT-13)	*A. pseudoplatanus*	T41140	2
		T41155	2
		T41503	2
	F. sylvatica	T12326	6
	Q. robur	T41158	2
		T41171	1
		T41451	3

Before starting any treatment, photosynthesis was measured. Leaves exhibiting Pn between 10 and 25 $\mu mol_{CO_2}\, m^{-2}\, s^{-1}$ were selected and gas exchange recorded once photosynthesis was stable. Then, we adapted six treatments: control (C), water (W), and sucrose (S) (soluble NSC) from Franck et al. (2006), each one at 10 or 30 min. For W and S treatments, an area of 2 cm^2, located 2 cm above the area where photosynthesis was measured, was gently scrubbed with a softwood sand paper to remove the cuticle of the leaf. The scrubbed area was then immediately wet with water (W treatment), or a solution of 0.7 M of sucrose (S treatment) using a paintbrush. The sucrose solution emulates natural phloem concentrations (Franck et al., 2006). In both W and S treatments water or sucrose solution was constantly added with the paintbrush to maintain the area where cuticle was removed fully hydrated. Leaves of the C treatment were neither scrubbed nor wet. Pn was measured 2 cm below the area where the treatment was applied. Fig. 3.1 shows a diagram displaying the leaves used for each of the six treatments, together with a representation of where the treatment was applied and where photosynthesis was measured. Given that pre-treatment Pn largely ranged between 10 and 25 $\mu mol_{CO_2}\, m^{-2}\, s^{-1}$ within the branch, we express treatment photosynthesis (10 and 30 min) as a percentage of pre-treatment (0 min) CO_2 gas exchange. Once the photosynthesis measurement was completed, the leaf was dried with blotting paper to remove excess water and sucrose and was clipped at the petiole-twig interception.

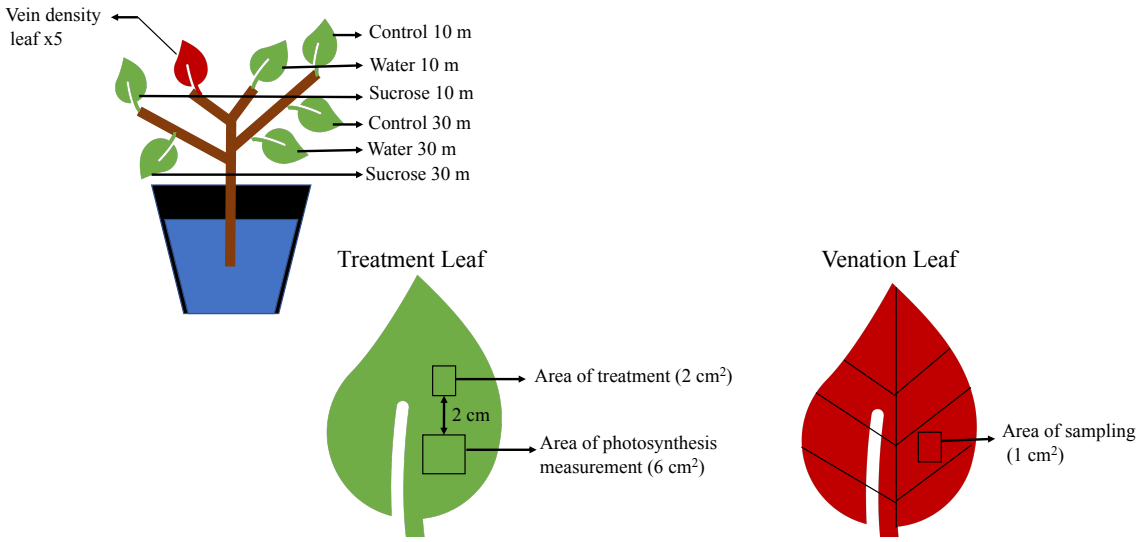


Figure 3.1: Top left, a diagram representing leaves used for the six different treatments (control, water, sucrose, at 10 and 30 minutes each), and other five healthy leaves collected for vein density analysis. Bottom left, a diagram of the leaf showing where water and sucrose treatments where applied, and where photosynthesis was measured. Bottom right, shows the section of the leaf used for the vein density analysis: primary and secondary veins were avoided.

To stop enzymatic activity for later sugar measurements, leaves were immediately microwaved for around 180 s (depending on species sensitivity to microwaving to avoid NSC burning after testing a few leaves and visual examination) at 800 W (Quentin et al., 2015; Richter et al., 2009). Finally, leaves were oven dried at 65 °C until weight difference was no longer observed. Leaves were dried-stored prior to NSC analysis.

In the Wytham Woods site, top-of-canopy branches were collected at 6:00 pm *via* a canopy walkway. After pruning, branches were wet cut in a bucket with water, covered with a black bag sprinkled with water, and left overnight in order to allow branch full re-hydration. The next morning at 9:00 am, the same experimental procedure as in Ankasa was performed with the leaf chamber temperature set to 23 °C for optimal temperate species performance (Sendall et al., 2014).

3.2.3 Trait measurement

Petiole diameter was measured by averaging three measurements made with an electronic calliper after leaf collection and before microwaving. Similarly, leaf thickness was obtained by averaging three measurements with the same calliper while avoiding major veins. Leaves were then scanned with a flatbed scanner, resulting images were then processed using a Matlab R2015b (Natwick, MA, USA) to calculate leaf area from number of pixels given a fix reference of known area. Final weight after leaf oven-drying, in combination with leaf area from scans, was used to obtain leaf specific leaf area (SLA; $m^2\,kg^{-1}$).

In addition to sampled leaves, an additional five healthy leaves per branch were collected at random, bagged, and oven-dried for later vein density analysis.

3.2.4 Vein density

One cm^2 section, avoiding primary and secondary veins and prioritising the area between secondary veins (Fig. 3.1), was obtained from oven-dried leaves and used for analysis. Samples were chemically cleared with bleach and stained with saffranine following Pérez-Harguindeguy et al. (2013). Vein density was measured by photographing dyed slices using a trans-illumination microscope (Olympus SZX-12, Olympus, Tokyo, Japan) attached to digital camera (Canon T1i, Tokyo, Japan). Images were taken with a 179 pixels mm^{-1} resolution. Veins of a region of interest were traced using a computer pen and pad, and the resulting paths were divided by the area of interest using an image processing algorithm (Blonder et al., 2017) to yield vein density ($mm\,mm^{-2}$).

3.2.5 Soluble sugar measurements

Soluble NSC concentrations were determined in the area where photosynthesis was measured by enzymatic wet assay adapted from Hoch et al. (2002). Approximately 10 mg of leaf dried ground powder, obtained mostly from the area where photosynthesis was measured and its surroundings, were mixed with 1.6 ml of distilled water, vortexed for 10 s and steamed for 1 h. Vials were mixed again and 0.7 ml were extracted

on a new vial and centrifuged for 15 min. 20 µL aliquots were extracted and mixed with invertase, (Invertase from baker's yeast (*S. cerevisiae*), Sigma-Aldrich), for sucrose hydrolysis into monosaccharides, and mixed with isomerase (Phosphoglucose isomerase from baker's yeast (*S. cerevisiae*), Sigma-Aldrich) for fructose conversion into glucose, hexokinase (Glucose assay reagent, Sigma-Aldrich), and glucose-6-phosphate dehydrogenase (Glucose assay reagent, Sigma-Aldrich) on a 96 well microplate. Soluble sugars NSC content was derived from difference in light absorption between NAD^+ and NADH at 340 nm using a microplate absorbance reader (Sunrise Absorbance Reader, Tecan, Mannedorf, Switzerland) and subtracted from enzymatic blank and water absorption measurements. Soluble NSC concentration was obtained as g of soluble NSC per g of dry leaf content (%).

In order to correlate leaf soluble NSC ($g\,g^{-1}$) with Pn ($\mu mol\,m^{-2}\,s^{-1}$), percentage of soluble NSC was combined with SLA to yield soluble NSC concentration per leaf area (Sol. NSC; $g\,m^{-2}$).

3.2.6 Measuring non-structural carbohydrates translocation across the leaf

NSC translocation along the leaf was calculated as the difference in percentage of soluble NSC (ΔSol. NSC) between the S treatment and C for both 10 and 30 min treatments, resulting in:

$$\Delta\text{Sol. NSC} = [\text{Sol. NSC}]_S - [\text{Sol. NSC}]_W \tag{3.1}$$

Where $[\text{Sol. NSC}]_S$ and $[\text{Sol. NSC}]_W$ are soluble NSC concentrations expressed as a % of leaf dry weight of leaves from the S and W treatments respectively. Since leaves from the W were not treated with any form of NSC and their cuticle was gently scrubbed, as with leaves for the S treatment, NSC concentrations in W were assumed as the leaf natural concentration whilst NSC concentration in the S treatment were assumed as the NSC resulting from the translocation across the 2 cm from where the cuticle was removed to the area where both NSC and Pn were measured. ΔSol. NSC was then correlated to vein density and the other traits measured (SLA, petiole diameter and leaf thickness) for both 10 and 30 min treatments.

3.2.7 Statistical analysis

Statistical differences between treatments was calculated using a T-test at a significance level (α) of 0.10. Correlation between the different leaf traits was assessed using Pearson correlation coefficient (PCC).

In order to test whether photosynthetic downregulation triggered by NSC can be predicted from leaf traits and vein density, we tested a series of linear mixed effects models using the species identity as a random effect. Predicting variables and their interaction were selected based on ecophysiological knowledge on how they interact with photosynthesis and NSC downregulation.

Since photosynthetic decrease in the 30 min interval was similar for the C, W and S treatments, only the photosynthetic decrease in the 10 min interval was considered as explained variables. Decrease in photosynthesis was defined as the difference between the percentage of Pn decrease in the sucrose treatment at 10 min (S_{10}) and the percentage of Pn decrease of the water treatment at 10 min (W_{10}), resulting in:

$$\text{Pn decrease} = 100 - \frac{\text{Pn}_{S_{t=0}} - \text{Pn}_{S_{t=10}}}{\text{Pn}_{S_{t=0}}} \times 100 - 100 - \frac{\text{Pn}_{W_{t=0}} - \text{Pn}_{W_{t=10}}}{\text{Pn}_{W_{t=0}}} \times 100 \quad (3.2)$$

Where $\text{Pn}_{W_{t=0}}$ and $\text{Pn}_{S_{t=0}}$ are the pre-treatment Pn measurements for W and S at 10 minutes respectively. This metric was chosen in order to account only for the effect of NSC on leaf gas exchange while excluding the effect of damaging the leaf when removing the cuticle. Model goodness of fit was assessed with the adjusted coefficient of determination (R^2_{adj}), and the most parsimonious models were chosen based on the Akaike Information Criterion (AIC).

3.3 Results

3.3.1 Downregulation in photosynthesis

The sucrose feeding trial succeeded in translocating soluble NSC across the 2 cm distance between the area of sugar-feeding and where photosynthesis was measured in one tropical species (*D. staudtii*) and two temperate species (*A. pseudoplatanus* and *Q. robur*; Fig. 3.2).

In most cases, except for *F. sylvatica*, a significant decrease in Pn was observed across all treatments, including *C*, where leaves remained untouched (Fig. 3.3). The largest differences between treatments were observed at 10 min, whilst at 30 min leaf Pn decreased similarly in all species except for *Q. robur*, which had the largest difference between *S*, *C*, and *W* treatments in both time intervals (10 and 30 min).

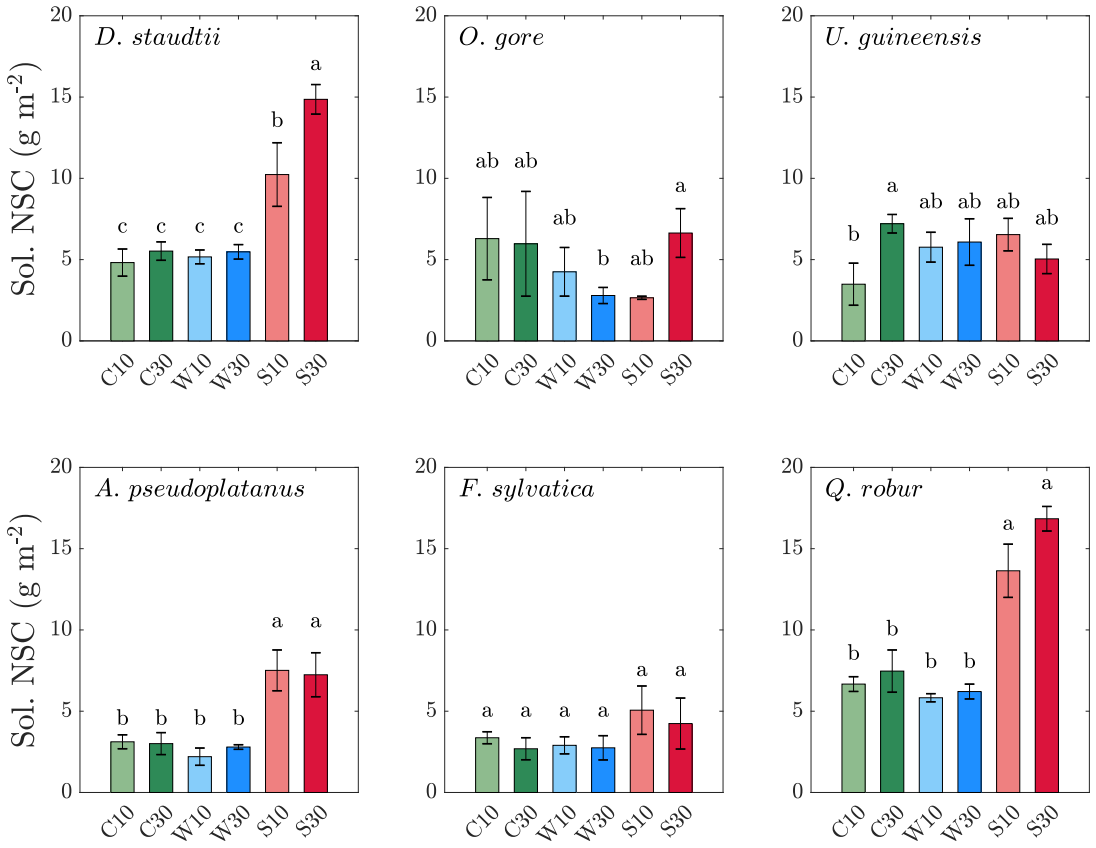


Figure 3.2: Soluble non-structural carbohydrate (Sol. NSC) concentration in the six treatments: Control (C), Water (W), and Sucrose (S) at two different times: 10 and 30 minutes. Concentrations are expressed as grams per leaf square meter ($\mathrm{g\,m^{-2}}$). Tropical species are shown in the upper row, whilst temperate species are shown in the lower one. Different letters represent soluble NSC concentrations statistically different from each other (T-test; $\alpha = 0.10$).

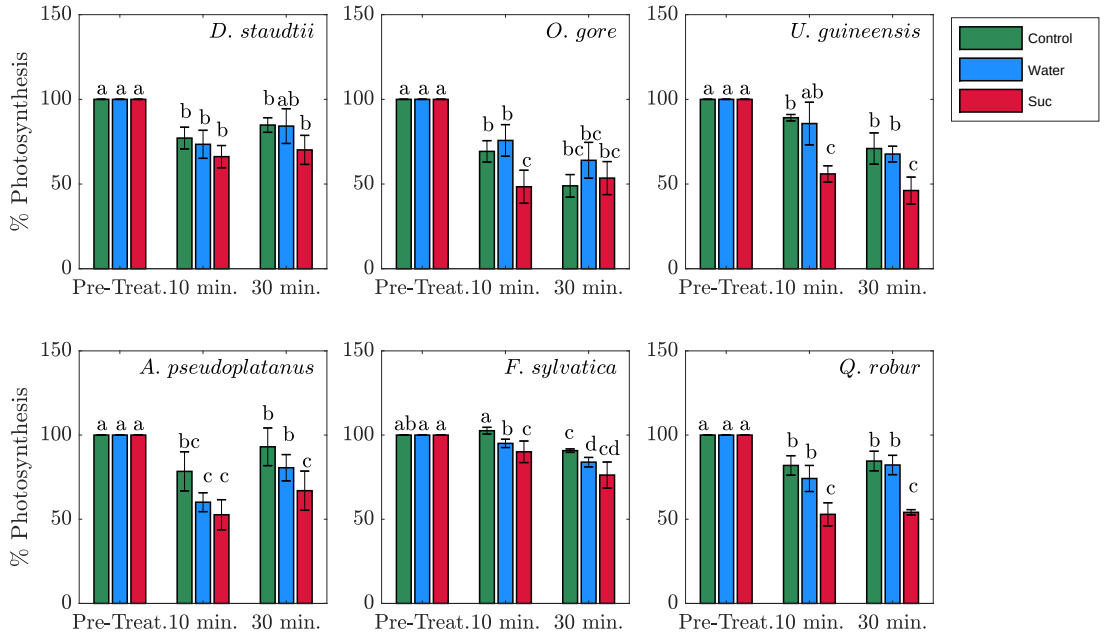


Figure 3.3: Sucrose (Suc) feeding effect on leaf net photosynthesis at pre-treatment (Pre-Treat), 10 and 30 minutes (min). Net photosynthesis is expressed as a percentage of pre-treatment leaf gas exchange. Results are shown for the control, water and sucrose (Suc) treatments in six different species. Top row shows tropical species: *Duguetia staudtii*, *Ongokea gore*, and *Uapaca guineensis*. Bottom row shows temperate species: *Acer pseudoplatanus*, *Fagus sylvatica*, and *Quercus robur*. Mean for each treatment is shown together with ±1 standard error. Letters represent statistical differences between treatments (T-test; $\alpha = 0.10$).

F. sylvatica exhibited especially small differences between treatments at both 10 and 30 min, and a mild increase in Pn (2% with respect to pre-treatment leaf gas exchange) at 10 min and a slight decrease (∼10%) at the 30 min interval which was not statistically different from pre-treatment gas exchange. Sucrose treatment at 10 min in *D. staudtii*, and *A. pseudoplatanus* show no statistical difference from *C* treatment, thus indicating that NSC addition did not trigger any downregulation mechanism in these species.

Table 3.3: Species traits and leaf vein density averages together with their ± standard deviations. Specific leaf area (SLA), petiole diameter and leaf thickness average corresponds to the 36 leaf samples for each species, meanwhile vein density averages are the results of 6 observations per species.

Species	SLA ($m^2\,kg^{-1}$)	Petiole Diameter (mm)	Leaf Thickness (mm)	Vein Density ($mm\,mm^{-2}$)
Duguetia staudtii	10.32 ± 1.6	2.61 ± 0.2	0.4 ± 0.4	15.6 ± 0.8
Ongokea gore	10.34 ± 1.5	2.13 ± 0.4	0.3 ± 0.1	13.8 ± 0.4
Uapaca guineensis	7.3 ± 1.0	2.53 ± 0.6	0.4 ± 0.5	10.7 ± 2.8
Acer pseudoplatanus	14.51 ± 2.0	2.2 ± 0.2	0.3 ± 0.06	11.6 ± 0.2
Fagus sylvatica	18.10 ± 3.2	1.1 ± 0.1	0.09 ± 0.02	16.1 ± 0.8
Quercus robbur	10.52 ± 1.2	1.7 ± 0.2	0.2 ± 0.03	14.2 ± 1.8

3.3.2 Leaf traits, vein density and photosynthesis downregulation

Table 3.3 summarises leaf traits at species level. Higher investment in leaf venation translated into a lower photosynthetic decrease mediated by NSC photosynthetic downregulation (Fig. 3.4) (0.38 PCC). Similarly, conservative species, with low SLA according to the leaf economic spectrum (LES; Wright et al. (2004)), proved to be more sensitive to photosynthetic downregulation mediated by soluble NSC than fast-growing species (Fig. 3.4; PCC: -0.45; Fig. 5). Correlation between leaf photosynthetic downregulation and ΔSol. NSC concentration was low (Fig. 3.4; PCC = -0.14).

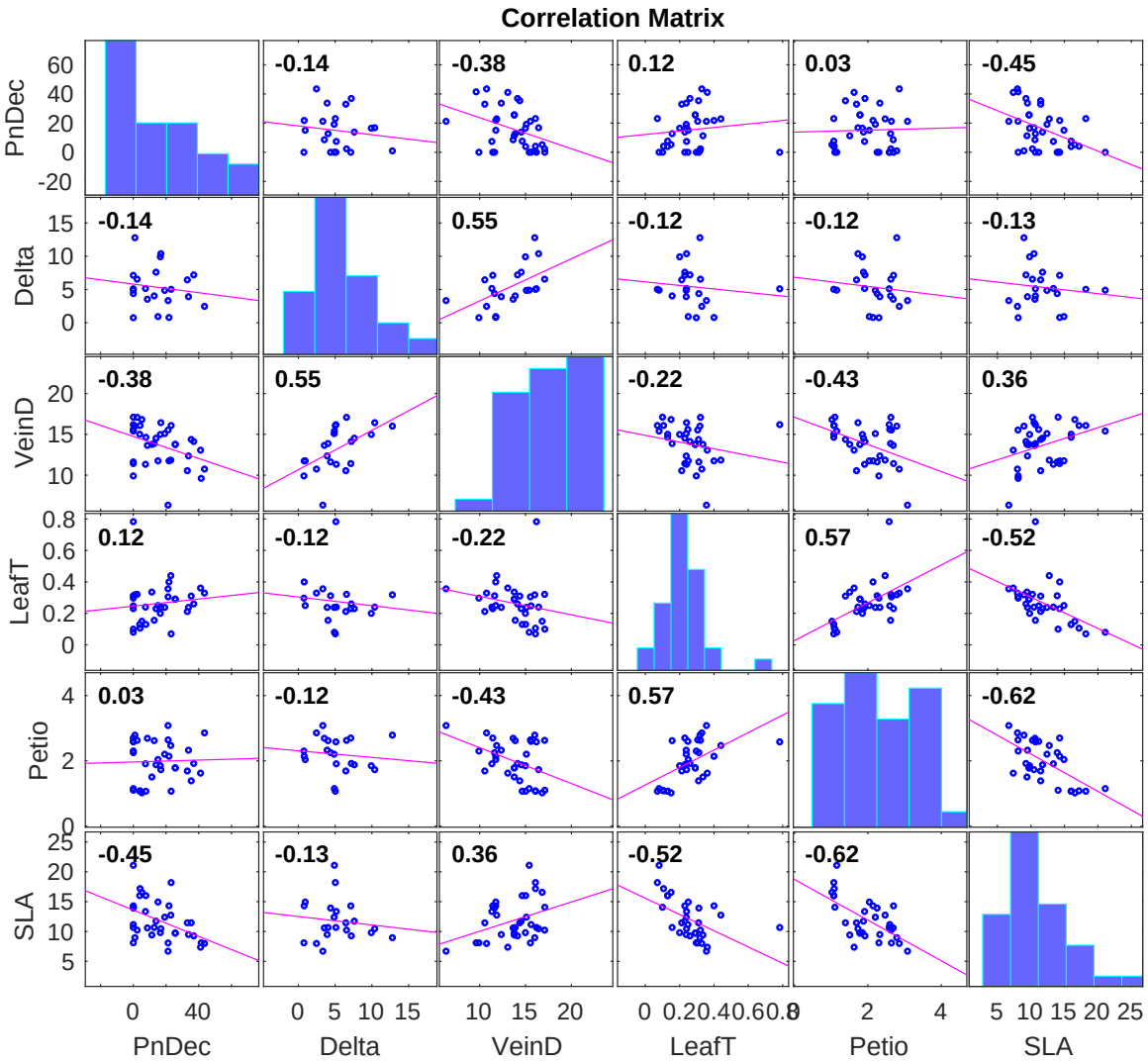


Figure 3.4: Pearson correlation between measured variables. Leaf photosynthetic decrease (Pn Decrease) was defined as the percentage (%) of Pn between pre and post sucrose feeding at 10 minutes, minus the corresponding Pn % decrease for the water treatment in order to account solely for soluble non-structural effect (Soluble NSC) on photosynthetic downregulation.

3.3.3 Leaf traits, vein density and non-structural carbohydrates translocation

Correlation between ΔSol. NSC was only significant with vein density in both the 10 and 30 min treatment (Fig. 3.5), higher leaf investment in vein infrastructure resulted in lower NSC translocation rates when comparing natural NSC leaf concentrations (W treatment) and sucrose addition (S treatment) since at higher vein density, ΔSol. NSC was higher. (Fig. 3.5). Correlations between other leaf traits and NSC translocation were non-significant ($P_{value} < 0.05$).

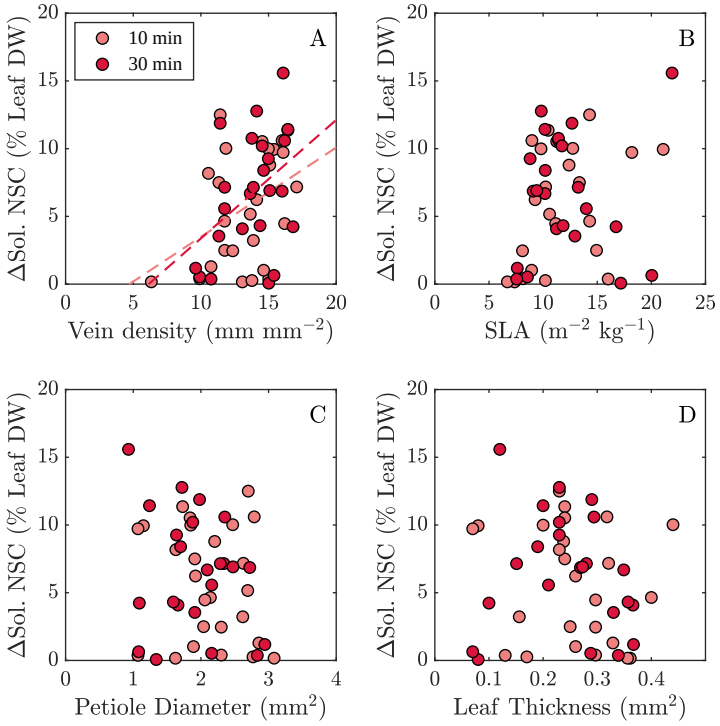


Figure 3.5: Correlation between translocation of soluble non-structural carbohydrates (Sol. NSC), vein density and leaf traits. ΔSol. NSC was measured as the difference between leaf NSC concentration after sucrose addition and natural leaf NSC concentration assumed as NSC concentrations found in the control treatment. Only significant ($P_{value} < 0.05$) relationships are shown.

3.3.4 Predicting photosynthetic downregulation with leaf traits

The best performance was achieved by the model that considered leaf investment in vein infrastructure (VeinDensity), SLA, petiole diameter (PetioleDiameter), and SLA and vein density interaction, together with species as random factor (AIC = 277.79; R^2_{adj} = 0.27; Table **??**). Vein density was the most important variable contributing with 31.6% to the model's explained variance (Table 3.5), followed by the interaction between SLA and VeinDensity (24.4%), PetioleDiam (22.9%), and SLA (21.1%).

Table 3.4: Model performance for different variable combination, aiming to predict leaf photosynthetic decrease. Leaf photosynthetic decrease (PnDecrease) was defined as the percentage (%) of Pn between pre and post sucrose feeding at 10 minutes, minus the corresponding Pn % decrease for the water treatment in order to account solely for soluble non-structural effect (Soluble NSC) on photosynthetic downregulation. Model performance was asses using both the Akaike Information Criterion (AIC) and the adjusted coefficient of determination (R^2_{adj}). Models are sorted by their ranking determined by their AIC score.

	Model	ΔAIC	ΔR^2_{adj}
1	PnDecrease ∼ VeinDensity+SLA+SLA×VeinDensity+PetioleDiameter+(1|Species)	0 (277.8)	0 (0.27)
2	PnDecrease ∼ VeinDensity+SLA+SLA×VeinDensity+ SolNSC×VeinDensity+PetioleDiameter+LeafThicness+(1|Species)	+5.63	−0.07
3	PnDecrease ∼ VeinDensity+SLA+(1|Species)	+5.98	+0.01
4	PnDecrease ∼ VeinDensity+(1|Species)	+0.98	+0.04
5	PnDecrease ∼ VeinDensity+SLA+SolNSC+(1|Species)	+0.87	−0.06
6	PnDecrease ∼ VeinDensity+SLA+SLA×VeinDensity+(1|Species)	+0.01	0.00
7	PnDecrease ∼ VeinDensity+SLA+SLA×VeinDensity+SolNSC×VeinDensity+(1|Species)	+3.84	−0.05

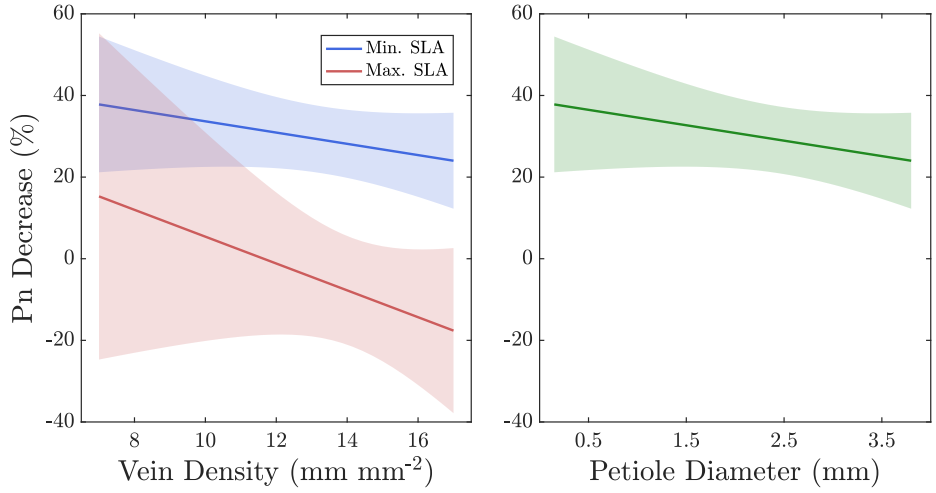


Figure 3.6: Interaction between specific leaf area (SLA) and vein density taken from the most parsimonious model (Model 1; Table 3.4) predicting photosynthetic downregulation with leaf traits. Shaded areas represent predicted errors. Photosynthetic (Pn) decrease was defined as defined as the percentage (%) of Pn between pre and post sucrose feeding at 10 min, minus the corresponding Pn % decrease for the water treatment in order to account solely for soluble non-structural effect on photosynthetic downregulation. On the left panel, maximum and minimum observed SLA were kept fixed, together with average observed petiole diameter in order to predict Pn decrease. Likewise, on the right panel, average SLA was used to predict Pn decrease sensibility to petiole diameter.

On the other hand, the simplest model (predicting photosynthetic downregulation only from vein density and accounting for species as a random effect) explained a quarter of the Pn decrease variability (AIC = 290.38; $R^2_{adj} = 0.25$; Table 3.4). When adding leaf ΔSol. NSC concentration (SolNSC), model's performance decreased, AIC = 283.42, and $R^2_{adj} = 0.20$ for the model accounting only for leaf vein investment and soluble NSC interaction. When accounting for both leaf soluble NSC concentration and leaf investment interaction, and vein investment and SLA interaction, model's performance was even lower (Table 3.4). Species with a higher investment in vein infrastructure were prone to show less photosynthetic downregulation (Fig. 3.4).

Table 3.5: Relative importance of explanatory variable for the the best ranked model (Model 1; Table 3.4) in terms of their Akaike Information Criterion

Variables	Relative Importance (%)
VeinDensity	31.6
SLA×VeinDensity	24.4
PetioleDiameter	22.9
SLA	21.1

3.4 Discussion

3.4.1 Photosynthetic downregulation mediated by soluble non-structural carbohydrates

Levels of photosynthetic downregulation mediated by NSC was different within the cohort of species that we sampled, indicating different physiological adaptations in order to acclimate at higher photosynthetic rates for each species. Ten min after treatment, sucrose feeding triggered a decrease in leaf gas exchange in the six species sampled: both in tropical and temperate sites. Notably, *O. gore* and *U. guineensis* in the tropics, and *Q. robur* in higher latitudes, achieved large differences between C and W treatments. On the other hand, sucrose-feeding photosynthesis reduction was the same in *D. staudtii* in Ankasa, and *A. pseudoplatanus* and *F. sylvatica* in Wytham, when compared to W treatment, thus indicating a lower degree of NSC downregulation in these species. Fast NSC translocation has been reported, where in a matter of hours photoassimilates from the leaf have reached woody tissue in the branch (Keel et al., 2007).

Considering fast NSC translocation across the blade reported in the literature and rapid photosynthetic downregulation mediated by sugars (Moore et al., 1999; Paul and Foyer, 2001), the 10 min treatment serves as a robust test to understand interaction between soluble NSC concentration and leaf gas exchange. Meanwhile, low translocation rates might be expected in leaves that already exhibit high NSC concentrations, thus impeding the generation of a sugar gradient for their translocation. Moreover, our results show that higher investment in leaf vein infrastructure improved NSC translocation across the blade.

By manipulating natural concentrations of sucrose, we might have affected the Calvin-Benson-Bassham (CCB) cycle, together with the recycling of inorganic phosphate (Pi) by accumulation of end-product (Paul and Foyer, 2001; Paul and Pellny, 2003; Sharkey et al., 1986). Short term control over photosynthesis has proven to depend on leaves' Pi availability. By affecting the CCB cycle, regeneration of Ribulose 1,5-bisphosphate is impeded because of photosynthetic downregulation, thus Pi is kidnapped in intermediary compounds within the CBB cycle, which in turns affects the availability of the cell to reduce CO_2 in the mesophyll. On the longer term, sucrose feeding trials have shown to affect both enzymatic and gene expression. Lobo et al. (2015) found downregulation

in RuBisCO abundance and a decrease in electron transport rates, indicating the leaf's need to maintain cell redox balance. We are unlikely to have affected these mechanisms, however the S treatment might have interfered the Pi cycling within the CBB cycle, thus affecting leaf gas exchange (Azcón-Bieto, 1983).

3.4.2 Non-structural carbohydrates, photosynthetic downregulation and leaf traits

Vein density was the variable that most contributed to the model with the best performance to predict photosynthetic downregulation. Species which exhibit symplastic phloem loading, see Turgeon (2010) for a complete description of different mechanisms, such as all arboreal species (Savage et al., 2017), have shown to greatly benefit from investment in vein infrastructure (Adams et al., 2013; Amiard et al., 2005; Muller et al., 2014a; Polutchko et al., 2018). Species with symplastic phloem loading present high plasmodesmata frequency, cellular channels that link the parenchyma with the companion cell, which in turn load the sugar into the sieve elements of the phloem passively for later transport and allocation in within the plant (Turgeon and Wolf, 2009). This mechanism relies on an osmotic gradient, where mesophyll cells in the leaf must build up a higher sucrose concentration in order to allow transport towards already sucrose rich sieve cells. An increase in vein density would translate in a higher mesophyll cell-to-sieve element ratio, thus facilitating sucrose loading, given an increased in conductance.

Accordingly, the second most contributing variable to our model was the interaction between vein density and SLA. High SLA relates to a *"live fast, die young"* strategy which entails plants' investment in low density leaves, short tissue life span and most importantly in our case: *"high rates of resource acquisition and flux at organ and individual scales"* (Reich, 2014). Species presenting higher SLA must have developed: *a*) high tolerance to high leaf NSC concentrations in order to avoid photosynthetic downregulation, and *b*) an efficient way to translocate photoassimilates from source to sink organs in order to sustain rapid growth rates (Savage et al., 2016; Turgeon, 2010). *F. sylvatica* exhibited the highest SLA and lowest NSC photosynthetic downregulation (Fig. 3.3). *A. pseudoplatanus*, a fast-growing species (Morecroft and Roberts, 1999), showed the second largest SLA, whilst difference in Pn decrease at 10 min between C and S was minimal (thus indicating low Pn downregulation). On the other hand, leaves of *Q. robur* presented the lowest SLA compared to the other species sampled in

the temperate forest, and high photosynthetic downregulation. Furthermore, a similar behaviour was observed in the tropics, *U. guineensis* exhibited the lowest SLA in the lowes latitude site and highest photosynthetic downregulation. Unfortunately, existing literature does not say much about growing habits of the three tropical species sampled in our experiment. Nevertheless, our results show a consistent trend between SLA and photosynthetic downregulation. Similarly, species presenting wider petioles were better at coping with induced photosynthetic decrease, indicating the importance of minor veins in regulating photosynthetic downregulation.

Photosynthetic downregulation did not correlate as well with leaf NSC content as was expected (Fig. 3.4). This might be because the amount of sucrose applied in the *S* treatment was above a certain threshold of sensitivity for Pn downregulation. Würth et al. (2005) found that during dry season in tropical vegetation, when tree sinks are limited because of low soil moisture (hence foliar NSC is expected to be high), leaf NSC concentration averaged 7.2%. In terms of percentage of dry matter content, *D. staudtii* in the *S* treatment at 10 min averaged 11%, whilst *O. gore* and *U. guineensis* averaged 4 and 5% respectively (Supplemental Material 3.7). NSC concentrations achieved in *D. staudtii* were above natural expected values, thus avoiding a spectrum of concentrations which could trigger different levels of Pn downregulation. *O. gore* and *U. guineensis* showed NSC concentrations closer to natural values, although comparison of concentration across labs must be taken with caution (Quentin et al., 2015). This should allow a mixture of Pn responses to different NSC concentrations, albeit our results show the contrary. Regarding high latitude vegetation, (Körner, 2003) found that trees grown under high C_a, thus exhibiting photosynthetic downregulation, in Switzerland achieved leaf NSC concentrations of 14; 14 and 12% for *Quercus*, *Fagus* and *Acer* respectively. *Q. robur* in our case also presented values of 14% for the *S* treatment at 10 min. Nevertheless, leaf NSC concentrations achieved in *A. pseudoplatanus* (10%), and *F. sylvatica* (9%) were slightly lower than the ones observed by Körner (2003). Although inter-laboratory comparison must be observed with caution, these results would suggest that leaf Pn in *A. pseudoplatanus* and *F. sylvatica* could still present a positive response to carbon fertilisation effect.

Furthermore, differences in physiological traits regarding phloem anatomy and structure have been found across species. One of the main challenges that phloem translocation imposes in trees is that phloem resistance increases with long-distance transport. Because sieve tube elements in the phloem are living cells but do not have nuclei nor

ribosomes, they rely on companion cells for maintenance and development. If they increase their volume in order to decrease path resistance, they risk jeopardising their volume to surface ratio, which is their way to remain in contact to their companion cells. However, phloem resistance has shown to vary across species (**?**) and within individuals. Changes in sieve tube anatomies and the plates that connect these, do change in order to minimise resistance as transport distance increases. These physiological and anatomical traits were not quantified in this experiment but could help to explain how some species are much more efficient at translocating NSCs in order to maintain a carbohydrate supply to support high growth and maintenance demands and avoid an overstock of NSCs in the leaf.

3.4.3 Predicting NSC downregulation from leaf traits

The inclusion of leaf traits like vein density, SLA and petiole diameter yielded the best model performance (Table 3.4). Within species (intraspecific) differences in SLA have proven to be mostly correlated to photoassimilates acquisition traits, such as net photosynthetic rate, nitrogen and phosphorus concentration (Osnas et al., 2018). However, at an interspecific level, SLA variation has poorly correlated with these traits, and is mostly attributed to leaf toughness and other structural features (Osnas et al., 2018). By adding species as a random variable, we accounted for this effect, thus meaning that interspecific differences in SLA not only translate into traits that improve photosynthesis, but also in coordination of other features that alleviates leaves from NSC downregulation and facilitate rapid NSC translocation across the plant.

The addition of vein density and SLA interaction to the model improved model performance. Vein density on its own has been shown to improve leaf photosynthetic capacity by combining two different factors: *a*) more intuitively improving the mesophyll to phloem contact area, *b*) greater number of plasmodesmata per leaf (Adams et al., 2013; Muller et al., 2014a), and *c* maintain a less negative water potential in the xylem at a given transpiration rate that would benefit sideway water movement to the phloem in order to promote a turgor gradient for NSC translocation. Our study did not look at cell arrangement within minor veins. However, we expect that fast-growing species presenting high SLA not only invest more in veins *per se*, but also in accessory cells to load NSC into the phloem (companion cells), and to translocate them across the vein path (sieve elements). The petiole both transports water to the leaf and translocates photoassimilaetes from the blade to the rest of the time, therefore leaf petiole diameter has been associated to vein leaf infrastructure investment (Sack and Scoffoni, 2013). Leaf petiole diameter addition to the model, indeed improved photosynthetic downregulation prediction.

Our study highlights the importance of leaf traits in predicting photosynthetic downregulation given uprising levels of C_a. Currently, DGVMs rely on equations taken from enzymatic kinetics in the chloroplast, thus obliterating the importance of complex interactions and feedbacks occurring at an organism level (Palacio et al., 2014). Leaf traits collection has garnered increasing relevance in the last five years (Blonder et al., 2017; Kattge et al., 2011; Violle et al., 2007), together with longstanding data regarding

ecosystems carbon dynamics, which ultimately can lead to NSC respiration, growth and storage demands (e.g., Malhi et al., 2009, 2011; Moore et al., 2017).

3.5 Conclusions

Our experiments and analysis allowed us established the effect of NSC concentration on leaf photosynthesis and tree productivity. NSC caused different reduction in photosynthesis in the six species sampled. Species in the fast region of the LES, such as *A. pseudoplatanus* and *F. sylvatica*, presented lower Pn downregulation, thus indicating that leaf traits that are related to higher photosynthetic rates, are coordinated with other physiological mechanisms that facilitate rapid NSC translocation across the phloem to avoid photosynthetic downregulation. On the contrary, species on the slowregion of LES, like *Q. robur* and *U. guineensis*, presented higher levels of NSC downregulation.

Our study suggests that veins cannot be perceived only as supplier of water for stomatal opening, but also as a mean to rapidly translocate photoassimilates across the plant, relieving the blade from high NSC concentrations. Moreover, this study shows that plant's response to increase C_a might differ between fast and slow species within the LES. Integration of features such as leaf traits into dynamic global vegetation models represent a new opportunity for modellers to integrate plant's biology together with biochemical performance in order to better understand the fate of natural vegetation under increasing C_a.

Acknowledgements

NR would like to thank the Chilean Science and Technology Commission (CONICyT) for providing a full scholarship for his doctoral studies, as well to Oriel College for helping with fieldwork and travelling expenses to go to Ghana. YM is supported by the Jackson Foundation Grant. We are also thankful of Marta Ramirez Boixaderas for helping to run NSC assays, and to Teresa Rosas for setting up the NSC protocol.

3.6 Supplemental Material

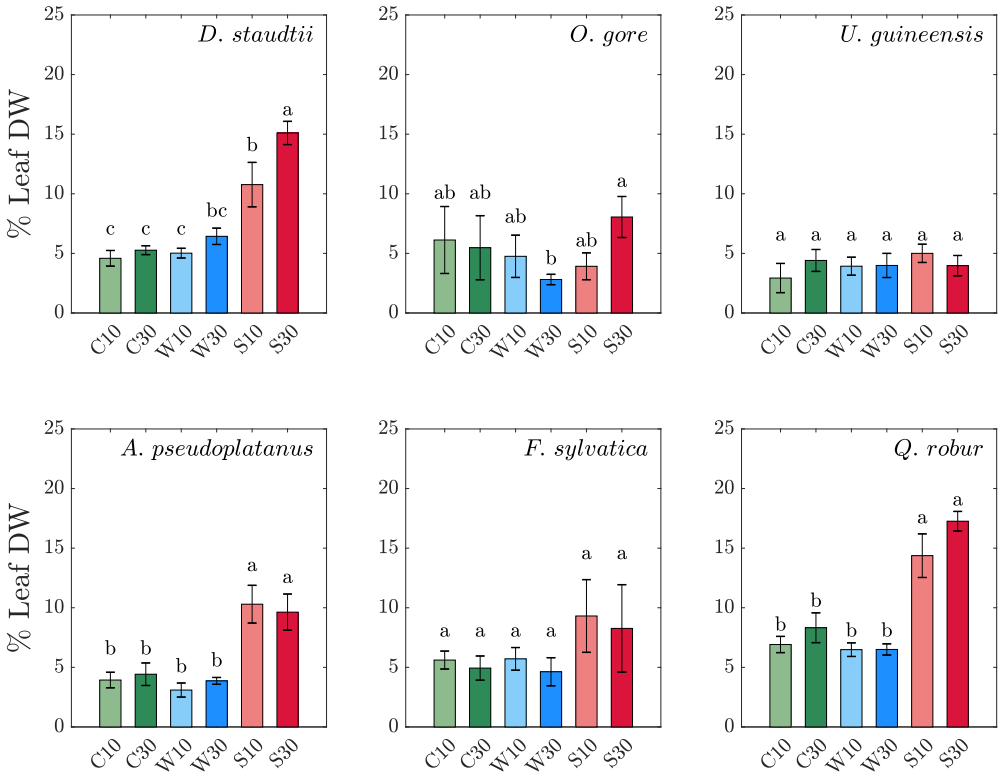


Figure 3.7: Soluble non-structural carbohydrate concentration in the six treatments: Control (C), Water (W), and Sucrose (S) at two different times: 10 and 30 minutes. Concentrations are expressed as percentage of leaf dry weight (DW) mater content (%). Tropical species are shown in the upper row, whilst temperate species are shown in the lower one. Letters represent soluble NSC concentrations statistically different from each other (T-test; $\alpha = 0.10$).

Chapter4

Open-source tool for the analysis of leaf pressure-volume relations

The second empirical chapter of my this thesis is a methodological paper briefly describing leaf hydraulic traits and focusing on their determination derived from leaf pressure-volume curves. I present a novel tool that uses a graphical user interface that would enable researchers to shorten the time of analysis from 15-20 minutes to 1 minute per curve.

This tool allowed me to process a large number of pressure-volume curves focusing mostly on osmotic potential, which in parts is driven by leaf non-structural carbohydrate concentration. Later on, these results will be correlated with photosynthetic measurements taken along a drought gradient North to South Ghana during dry and wet seasons in order to determine the effects of leaf non-structural carbohydrates on acclimation to drought and leaf gas exchange.

I developed the script in Matlab, did the analysis and wrote the manuscript. IO supplied the data for the pressure-volume curves analysis, as well as commenting on the manuscript. YM and GG also commented on the manuscript.

Open-source tool for the analysis of leaf pressure-volume relations

Nicolas Raab[1*], Greg Goldsmith[2], Yadvinder Malhi[1], Imma Oliveras[1]

[1]Environmental Change Institute, School of Geography and the Environment, University of Oxford, Oxford, OX1 3QY, UK.[2]Schmid College of Science and Technology, Chapman University, Orange, CA 92866, USA. [*]Corresponding Author: nicolas.raab@ouce.ox.ac.uk

This manuscript is under preparation. The tool here presented is written in Matlab and I am working on an open-source version for an R package.

Abstract

The study of leaf hydraulic traits is of paramount importance to better understand species dwelling over large moisture gradients. The study of pressure-volume (PV) curves provides several hydraulically-associated leaf traits, however the existing tools for PV curves analysis are cumbersome, time demanding, and non-standardised to user's choice. Here we present an open-source tool for the analysis of PV curves that adds robustness to the analysis and shortens the time from 20 minute to 1 minute per curve. Also, this tool allows to account for user's subjective choice, thus standardising PV curves analysis within the research community. Although user's subjective choice for the analysis of these curves has been a target for its lack of consistency across different studies, we demonstrate that within a reasonable degree of discrepancy between user's choice, means and distribution for leaf hydraulic traits derived from PV curves are not greatly affected.

Symbols

Symbol	Description	Unit
C_{FT}	Leaf Area Specific Capacitance at full turgor	MPa^{-1}
C^*_{FT}	Leaf Area Specific Capacitance at full turgor (Area Based)	$mol\,m^{-2}\,MPa^{-1}$
C_{TLP}	Leaf Area Specific Capacitance at Turgor Loss Point	MPa^{-1}
ε	Total Modulus of Elasticity	MPa
Π_o	Osmotic Potential at Full Turgor	MPa
PV	Pressure-Volume	NA
RWC	Relative Water Content	%
RWC_{TLP}	Relative Water Content at Turgor Loss Point	%
SWC	Saturated Water Content	NA
Ψ_{leaf}	Leaf Water Potential	MPa
Ψ_o	Osmotic Potential	MPa
Ψ_p	Turgor Pressure	MPa
Ψ_{TLP}	Leaf Water Potential at Turgor Loss Point	MPa
TLP	Turgor Loss Point	NA

4.1 Introduction

Leaf water relations are often described by pressure-volume curves (PV), which describe how leaf water potential (Ψ_{leaf}) varies as a function of changes in leaf relative water content (RWC) as the leaf loses water (Tyree and Hammel, 1972; Sinclair and Venables, 1983), providing a number of key hydraulically-associated leaf traits. These include the turgor loss point (TLP), a critical metric describing plants adaptation to drought (Kramer and Boyer, 1995), as well as a suite of chemical (e.g., osmotic potential; Ψ_o), and physical (e.g., cell wall elasticity; ε) traits that contribute to controlling TLP, thus overall leaf water status. These PV traits vary at local, regional and global scales in response to water gradients, demonstrating their broader role in determining plant functioning and species fitness (Baltzer et al., 2008; Bartlett et al., 2012; Galmés et al., 2007).

Currently, the methods used for generating PV curves are tedious and time-consuming, a single leaf taking about 5-6 hours to process (Sack and Pasquet-Kok, 2011). The leaf sampling procedure demands a very strict protocol, in which branches are wet-cut from the tree, taken to the laboratory and kept on a bucket with water overnight in the dark in order to ensure full re-hydration of branches and leaves. Next day, a healthy leaf is selected and cut at the twig-petiole intersection, Ψ_{leaf} and leaf weight are recorded in tandem, then the leaf is bench-dried for 10 minutes and the process is

repeated up to 12 times in order to correlate Ψ_{leaf} with leaf dehydration. Furthermore, current methods (usually Microsoft Excel spreadsheets) for analysing the resulting PV curves are subjective, time-demanding (up to 20 minutes), and not standardised. Here we present a new open-source tool that advances on existing resources (namely Sack and Pasquet-Kok, 2011) to provide for rapid and accurate analysis of PV curves. The software reduces the time of analysis to 1 minute (or even less) per curve and provides new tools for standardising the difference between users' subjective choice.

4.2 Theory

Water movement through the soil-plant-atmosphere water continuum is driven by differences in the free energy of water within these three components. Water free energy is related to its capacity to move (i.e., across cells because of osmosis or to move from the soil to the leaf against gravity), which can be negatively affected (less capacity to perform work) by presence of solutes and negative pressure (suction), or positively affected by temperature, pressure and height (more capacity to perform work). In thermodynamics, water free energy is expressed in $\mathrm{J\,mol^{-1}}$, however in ecophysiology these units are expressed as units of pressure (e.g., MPa, bar, PSI). A leaf that has suffered an important water loss will present a lower pressure by the cell wall (i.e., turgor pressure) and a more negative osmotic potential, thus resulting in a loss of its capacity to perform work, affecting the transpiration flux and photosynthesis.

Leaf PV relations are obtained by plotting the inverse of leaf water potential as a function of changes in leaf relative water content. Two regions are identified in the resulting plot: 1) a non-linear region, or turgor loss region that goes from full turgor (100-RWC(%) $\approx$ 0) to TLP, where Ψ_{leaf} drop is buffered by changes in the turgor pressure potential (Ψ_p) of the cell given a determined amount water loss from the leaf; and 2) a linear region after the TLP where water loss is accompanied by big changes in Ψ_{leaf} since the cell vacuole can no longer buffer changes in Ψ_{leaf} accompanied by water loss (Fig. 4.1). Ψ_{leaf} results from the contribution of the osmotic (Ψ_o) and (Ψ_p) potentials, resulting in:

$$\Psi_{leaf} = \Psi_o + \Psi_p \tag{4.1}$$

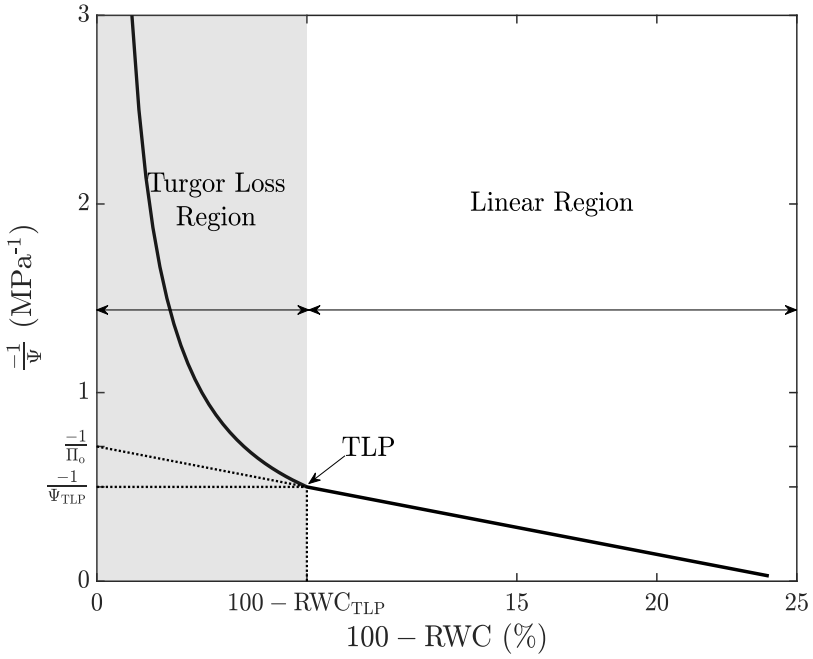


Figure 4.1: Two regions are observed: a turgor loss region where leaf water potential decreases together with water loss, and a linear region, where water loss does not entail a drop on water potential.

All potentials estimated in MPa. The dissolution of solutes into a solution, such as sugars in a cell, reduces the free energy of water within a system, therefore Ψ_o acts decreasing Ψ_{leaf}, thus this term is always associated with negative values. Whereas Ψ_p increases Ψ_{leaf}, by means of a positive pressure of the cell wall against the cell, in response to cell's vacuole expansion, following Newton's third law.

Since plant cells present rather rigid cell walls, cell water losses from transpiration are often accompanied by large losses in Ψ_p in order to maintain a fairly constant cell volume, thus resulting in the turgor loss region. Since the TLP is point at which the cell's vacuole no longer can perform a positive force against the cell wall, changes in cell RWC can no longer be compensated by changes in Ψ_p, thus resulting in $\Psi_{leaf} = \Psi_o$, causing a linear relationship between leaf's water loss and a drop in Ψ_{leaf}.

The analysis of PV relations can be tracked back to 1920 when Karl Höfter, after compiling a series of works performed during the precedent decade, managed to illustrate the relationship between Ψ_o and cell volume (Fig. 4.2) (Richter, 1978). From there, Tyree and Hammel (1972) and Sinclair and Venables (1983) compiled the theoretical work that led to the equations used to determine the different leaf hydraulic traits. However, these equations rely on fitting empirical curves to theoretical equa-

tions, thus imposing a challenge on how to interpret these relationships. Furthermore, the selection of the linear region of the curve is sensitive to the user's choice. With a wider use of computer machines to perform calculations, Schulte et al. (1985) developed an algorithm to avoid user's subjectivity and rely only in set parameters to select the points belonging to the linear region of the curve and therefore calculate the parameters leading to the determination of leaf hydraulic traits.

4.3 Definition of hydraulic traits derived from pressure-volume curves

Leaf water potential at Turgor Loss Point (Ψ_{TLP}, MPa). This is a critical metric describing the point at which key metabolic functions, such as the expansion of new cells, can no longer be maintained (Kramer and Boyer, 1995). It also describes the point when passed re-hydration of the cell is no longer possible, correlating with the permanent wilting point of the plant. The TLP is the most important metric predicting plant response to water stress (Bartlett et al., 2012). Species reaching Ψ_{TLP} at a lower potential (more negative), are better adapted to arid areas, whist species with a less negative Ψ_{TLP}, are related to wet tropical regions. On the other hand, a different strategy to cope with soil moisture shortage could also be associated to a less negative Ψ_{TLP}. By triggering stomatal closure at higher Ψ_{leaf} (less stressed), the plant maintains Ψ_{leaf} by limiting water loss through transpiration, thus avoiding water stress. Interpretation of Ψ_{TLP} is cumbersome and does not fall within the aim of this paper, for a better description of this parameter and its physiological consequences on plant performance, please refer to Bartlett et al. (2012).

The TLP lies between the turgor loss and the linear region. The selection of the points belonging to the linear region is visually done and depends on the user choice, risking being subjective. Therefore, PV curves traits of relevant importance for ecological analysis, such as Ψ_{TLP}, resulting from the extrapolation of the TLP into the y-axis (Fig. 4.2), might vary from user to user, thus imposing difficulties for meta-analysis. Similarly, leaf relative water content at the TLP ($\mathrm{RWC}_{\mathrm{TLP}}$) can be obtained by extrapolating the TLP to the x-axis of the PV curve, replicating the same uncertainty.

Saturated Water Content (SWC, dimensionless). This metric corresponds to the ratio of the water mass at leaf's saturated water content (g), over leaf dry weight (g). Leaf saturated content can be obtained by *a*) assuming that the first leaf weight, after full branch hydration overnight, corresponds to leaf saturated content, or *b*) by plotting leaf water content (leaf fresh weight − leaf dry weight) against Ψ_{leaf} and extrapolating leaf weight when $\Psi_{\text{leaf}} = 0$. The software allows users to choose within these two options to calculate SWC.

Osmotic potential at full turgor (Π_{o}, MPa). Since water moves across the soil-plant-water continuum, from a less negative (soil) to a more negative (atmosphere) water potential (Kramer and Boyer, 1995), it has been observed that during soil moisture shortage (when soil water potential becomes more negative), the solute concentration in the leaf is regulated to maintain the needed potential gradient for water transport, in a process called osmotic adjustment (Sanders and Arndt, 2012). A control on Π_{o} would enable plants to adjust their water potential and Ψ_{leaf} without affecting cell's turgor pressure, hence maintaining the water gradient needed for water transport and cell hydration without jeopardising cell functioning.

Osmotic potential at full turgor is given by the solute concentration of the leaf at full hydration. After TLP, $\Psi_{\text{leaf}} = \Psi_{\text{o}}$, therefore Π_{o} is defined as the projection of Ψ_{o} at full re-hydration given by the *y*-intercept of the regression of the linear region of the curve (Fig. 4.2). The assumptions of a linear relationship between 100−RWC and $\frac{-1}{\Psi}$has been criticised across the literature (e.g., Cortes and Sinclair, 1907; Tyree and Richter, 1981; Urban et al., 1993; Wardlaw, 2005). Water loss along the different measurements can come from an osmotic fraction of the leaf tissue, namely the symplast of each cell, or from the apoplast (extracellular space and the xylem lamina) which does not account for solutes. For the relationship to remain linear, all water loss must come from the symplast. The tool here presented does not account for a correction for apoplastic fraction and assumes that different in water content are related to losses from the symplast and more research is needed on this issue.

Total modulus of elasticity (ε, MPa^{-1}). Within the turgor loss region, the fall in Ψ_{leaf} with decreasing RWC is mainly dominated by a drop in Ψ_{p} because of a decrease in the pressure of the cell wall against the cell. A steeper decline of Ψ_{leaf} indicates a rigid the cell wall; on the other hand, a less steep decline means that the cell wall is more elastic, thus maintaining Ψ_{leaf} despite leaf water loss. Higher ε indicates that TLP

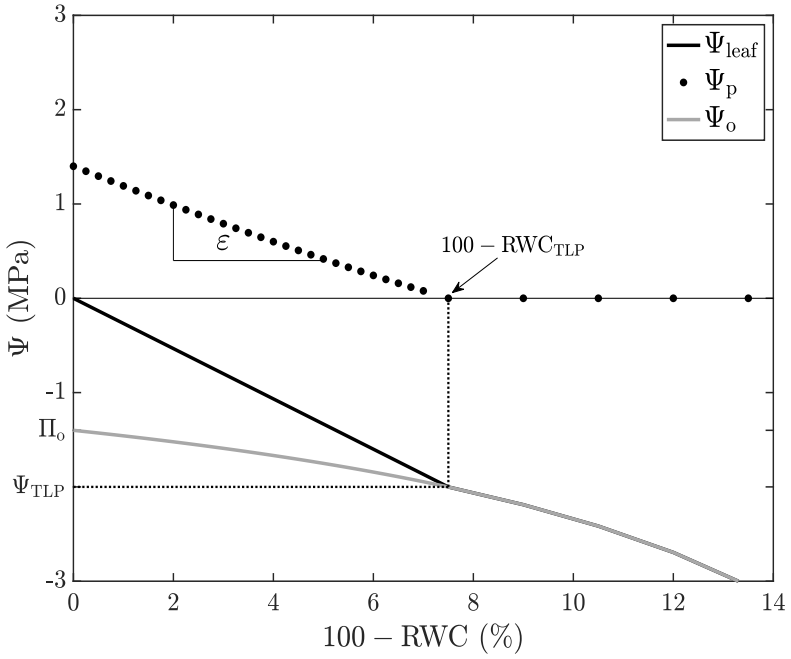


Figure 4.2: Höfler diagram of a leaf pressure-volume (PV) curve showing changes in leaf water potential (Ψ_{leaf}), turgor pressure (Ψ_p), and osmotic potential (Ψ_o) following changes in leaf relative water content (RWC). The three curves were obtained as follow: passed the turgor loss point (TLP), Ψ_p by definition is equal to 0, therefore $\Psi_0 = \Psi_o$. In the turgor loss region, Ψ_o is assumed to follow the linear tendency calculated in Fig. 4.1, then Ψ_o can be transformed to its reciprocal and opposed sign in order to go from $\frac{-1}{\Psi}$ to Ψ. Ψ_p can be calculated as $\Psi_p = \Psi_{leaf} - \Psi_o$.

would be achieved at a less negative Ψ_{leaf}, indicating a lower tolerance to drought, or an avoidance mechanism by conserving water by means of stomatal closure (Bartlett et al., 2012). The ε is obtained after calculating the slope between Ψ_p and RWC in the turgor loss region (Fig. 4.2), including the TLP, giving:

$$\varepsilon = \frac{\Delta \Psi_p}{\Delta \text{RWC}} \tag{4.2}$$

Leaf area specific capacitance at full turgor (C_{FT}, MPa). It relates to the leaf's capacity to store water. A high C_{FT} would enable plants to buffer water to allow stomatal opening and physiological functioning despite high water loss through transpiration. C_{FT} is given by the slope of RWC against Ψ_{leaf} in the turgor loss region, including the TLP. Similarly, we estimate the capacitance of the leaf in the linear region, C_{TLP}, also in MPa^{-1}, by estimating the same slope in the linear region, including TLP. Finally, the software estimates full turgor capacitance in terms of mol of H_2O per leaf area:

$$C^*_{FT} = \frac{C_{FT} \times SWC/18}{LA/1000} \tag{4.3}$$

Where LA is leaf area obtained from scanning the fresh leaf after finishing measuring the PV curve in cm; C^*_{FT} is given in mol m^{-2} MPa^{-1}.

4.4 General description of the open-source PV analyser

We provide an open source tool for the analysis of PV relations in a graphic user interface (GUI) through Matlab (Matlab R2015b, Natick, MA, USA).

The tool allows to set a working folder in GUI with all the data in it and provides a spreadsheet template for raw data input. When a spreadsheet is selected for analysis, the raw data is automatically displayed in an interactive graph that allows the user to: *a*) delete points that might correspond to outliers or faulty measurements that do not fit the expected behaviour of a PV curve (Fig. 4.1), *b*) select the points that fall within the linear region, and *c*) display all the calculated parameters, allowing the user to decide to save the calculated hydraulic traits derived from the PV curve, or to repeat the analysis.

The determination of TLP is highly subjective as it relies on the researcher's choice of the points falling within the linear region, therefore derived TLP values can change from user to user. Some attempts to provide a more objective choice include the choice of those points that maximize the coefficient of determination (r^2). The software presents a standardised statistical tool to provide an objective choice of the points that fall into the flat regions. Schulte et al. (1985) suggested that if the slope between the last selected point (i) and the next one $i^{(th+1)}$ (moving towards increasing RWC, left region of the plot), falls within a determined range or error, the new point should be considered to belong to the linear region of the curve. We have developed an algorithm coupled to the software that calculates the root mean square error (RMSE) between the regression line and the selected points without considering the $i^{(th+1)}$ point, the i^{th} point moves from right lo left of all the points of the curve. If the error of the i^{th} point is larger than the threshold selected by the user (e.g.: 3 RMSEs) the software shows a message letting the user know what points do not meet this standard. Accordingly, the software runs

the same algorithm to the points that were not selected (turgor loss region), advising the user to re-select points that fall on a lower RMSE than the threshold selected, thus falling within the linear region. Figure 4.3 shows the GUI displaying the same PV curve, however, for each panel a different error threshold was selected: 1.5; 5; and 10 RMSEs. By selecting a very conservative threshold (1.5 RMSEs), the software advises to remove one of the points from the linear region (Fig. 4.3 A), with a less conservative threshold (Fig. 4.3 B) the user's choice is right and no warning is displayed, with a more liberal threshold (10 RMSEs), the software advises adding a new point to the linear region of the point. It is important to highlight that the TLP for the same curve changes for each of these thresholds. By offering this mathematical tool, we expect to decrease the subjectivity of choosing the TLP, or at least researchers can state what threshold they used in their analysis, thus making PV curves comparison more robust within different groups.

In order to determine the slopes and intercepts needed to calculate the different leaf hydraulic traits that the software can provide (the Appendix section shows a detailed descriptions of these calculations), we used the *fitlm* function in Matlab (Matlab R2015b, Natick, MA, USA) to fit linear regressions. Although the software allows to assess the user's uncertainty in their choice of the TLP and linear region, as abovementioned, it does not provide standard errors for these parameters.

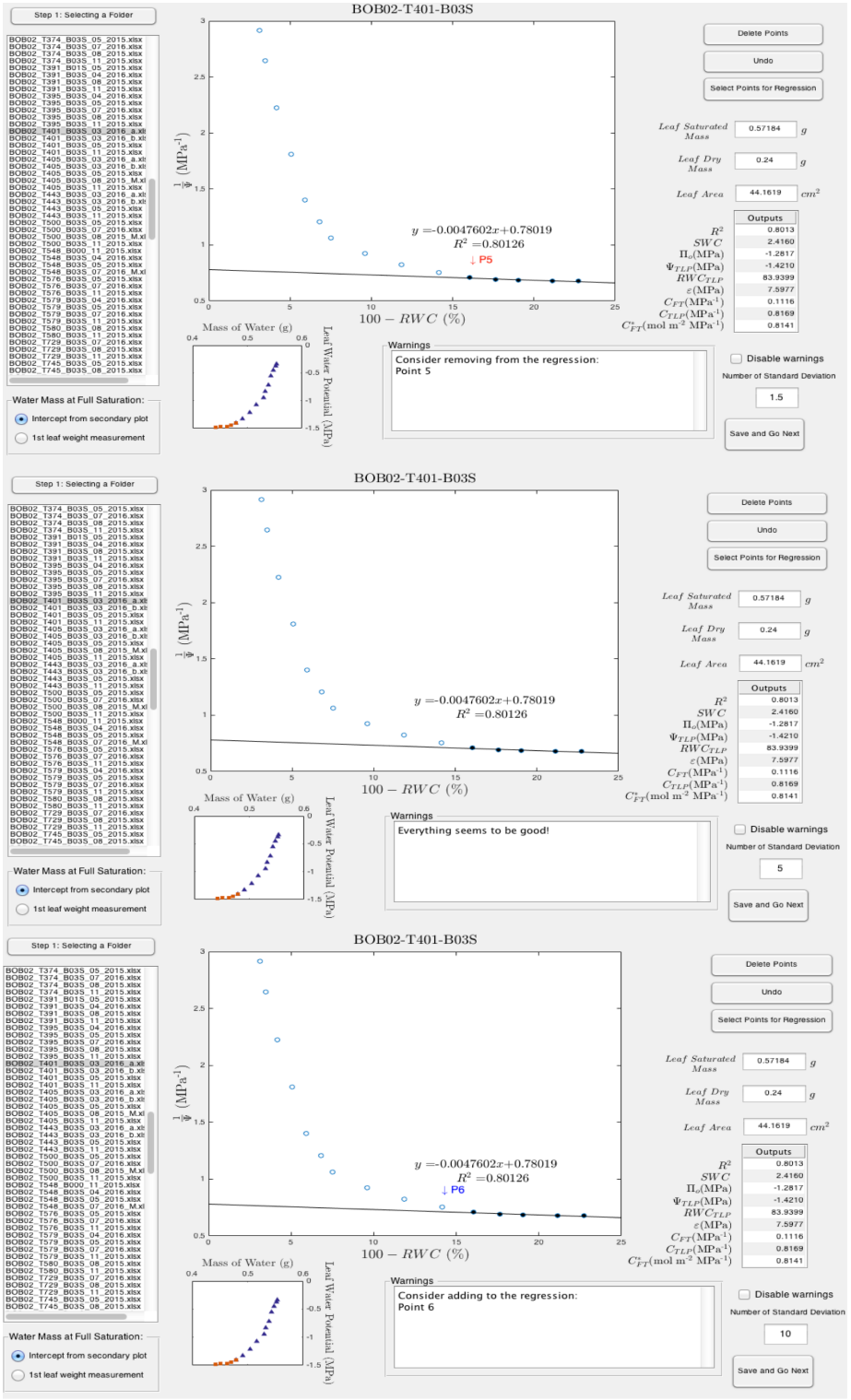


Figure 4.3: Graphical user interface of the open source software for pressure-volume (PV) leaf curves analysis. Each panel presents the same PV curve with different root mean square error threshold. A more conservative thresholds (A) advice the removal of points from the linear regions, whilst more liberal thresholds (C) include more points to the linear region, changing the turgor loss point each time.

4.5 User manual

- *Selection of settings*: As we mentioned above, the tool allows users to choose between obtaining leaf SWC using leaf's first weight after overnight full hydration, or by extrapolating leaf's water mass when $\Psi_{\text{leaf}} = 0$. Before starting the analysis, the user can choose between the two option in the bottom-left corner of the GUI (Fig. 4.3A). The user can also choose how many RMSE to use as an error threshold to add, or delete, points from the linear region of the curve. According to our experience, 3 RMSE gives a correct selection of points falling in the linear region of the curve. The number of standard deviations can be set in the bottom-right corner of the GUI.

- *Selecting a folder*: By pressing on "Selecting a Folder" button on the top-left corner of the GUI, the user can select the folder where the raw data is stored. Together with the script of the software in Github, researcher can find an Excel spreadsheet (Microsoft, USA) to input the raw data. The data of each curve must be added in a different spreadsheet. The software displays all the Excel files contained in the selected folder, allowing the user to double click in any spreadsheet to be further analysed.

- *Deleting outliers*: When analysing real data some points can be considered outliers since they not follow the expected pattern of a turgor loss region followed by a flat region. Our software allows deleting these points by selecting "Delete Points" (right-upper corner Fig. 4.3A) and clicking on them. Given that the software uses all the non-deleted points for calculating the parameters, the user must remove all the points that might not follow the expected PV shape, even if they not belong to the linear region of the curve.

- *Selecting points on the Linear Region*: After cleaning the data from outliers, the user can proceed to select the points belonging to the linear region of the curve using the button "Select Point for Regression" (right-upper corner Fig. 4.3A). After selecting the points, the software shows the parameters of the regression, it's r^2 on the main axis, and the hydraulic traits derived from the PV curve: SWC, Π_o, Ψ_{TLP}, RWC_{TLP}, ε, C_{FT}, C_{TLP}, and C^*_{FT}. If the user would like to try another selection of points falling in the linear region, the user can simply press

the "Undo" button (top-right of the GUI), re-select the curve to be scrutinise within the list, and carry on with the analysis.

- *Saving traits derived from PV curves*: if the user is satisfied with the traits derived from the PV curve, the user can press the "Save and Go Next" button (bottom-right corner of the console). The tool automatically saves the obtained parameters for each curve in a single .csv file. Besides saving the abovementioned traits, the file also contains a record of the points that were deleted, the points belonging to the turgor loss region, the TLP, and the points that conform the linear region. After the traits being automatically saved, the GUI displays the next PV curve on the list to be analysed.

4.6 Example data

We demonstrate the application of the software using data collected in six 1-ha plots along a rainfall gradient in Ghana (for more details, please refer to Moore et al. (2017)). In each plot, the seven most common species were selected and from each species three individuals were collected for PV curve analysis. In each tree, a branch with fully flushed leaves was collected, re-cut under water, and rehydrated overnight whilst covered with a black plastic bag sprinkled with water in the inside. Re-hydration time was standardized at ca. 15 h. PV curves were generated by repeatedly making paired measurements of Ψ_{leaf} and leaf mass following intervals of bench drying ($n = 9 - 12$ points curve^{-1}). Leaves were scanned in order to obtain their area (cm^2) and then oven-dried for 3 days at 60 °C in order to obtain leaf dry mass. We analysed 162 PV curves.

By manipulating the original software, we obtained all the leaf hydraulic traits described above, for different RMSE thresholds (0.5; 1; and 5). By doing so, we aim to show what is the sensitivity of the parameters obtained to the user's choice of the points falling within the linear region of the curve. Figure 4.4 shows a selection of four parameters (Π_o, Ψ_{TLP}, ε, RWC_{TLP}) obtained with different RMSE thresholds. In most cases, the selection of different threshold does not produce much parameters variation. Thus, even if different users might get a different selection of points for the linear region, the distribution of the parameters obtained should not largely vary. Given that most of the calculated parameters are slopes (ε, C_{FT}, CTLP and C^*_{FT}) the inclusion or exclusion

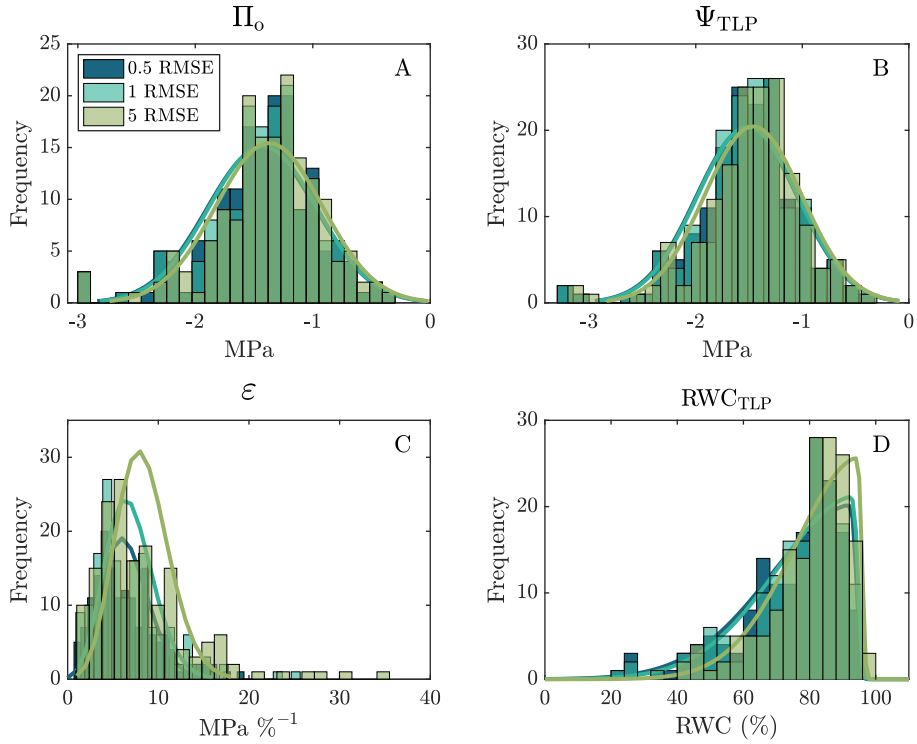


Figure 4.4: Distribution of osmotic potential (Π_o), leaf water potential at turgor loss point (Ψ_{TLP}), leaf modulus of elasticity (ε) and relative water content at turgor loss point (RWC_{TLP}) obtained after analysing 162 volume-pressure curves from three sites in Ghana. We used a 0.5; 1 and 5 root mean square error (RMSE) thresholds in order to show what is the sensitivity of the obtained parameters to users choice. A and B were fitted using a Gaussian distribution, C was fitted with a Poisson distribution, and D was fitted using a skewed normal distribution. Obtained parameters do not vary largely for different RMSE threshold, meaning that user's subjectivity is not detrimental on leaf pressure-volume curves analysis.

of an extra point in the linear region should not affect the determination of these parameters. Similarly, Π_o, obtained from the intercept of the linear region with the y-axis, is less sensitive to user's choice. Nevertheless, the parameter that showed the highest sensitivity to different thresholds of error is RWC_{TLP} (Fig. 4.4 C) given that is the projection of the TLP on the x-axis, thus highly depending on where the user sets the boundary of the left side of the linear region of the PV curve.

4.7 Conclusions

Plant hydraulic traits that have been proven to correlate with water uptake and plant's control over water status are key elements to understand how vegetation has adapted to different soil moistures regimes, encompassing the wet tropics to the most xeric environments of the globe. Our tool allows research teams working on hydraulic traits to optimise their time regarding the analysis of PV curves. Similarly, we have proven that even if the selection of points belonging to the linear region is subjective, within an acceptable range of error, the user's choice should not change the overall distribution of the parameters obtained. Accordingly, our statistical tool should standardise the approach within the ecophysiological community working on these issues.

Acknowledgements

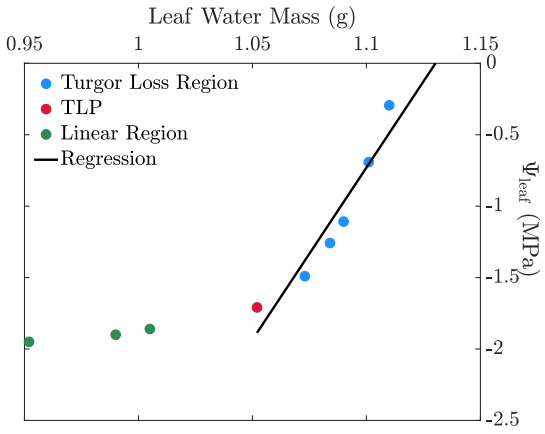
We thank the Chilean National Commission for Scientific and Technological Research (CONICYT) for the corresponding author's doctorate scholarship. The dataset used was funded with ERC GEM Traits (Yadvinder Malhi) and EU- Marie Curie Fellowship TipTropTrans (Imma Oliveras).

4.8 Appendix

The following appendix shows the equations used in the open-source tool to calculate all the leaf hydraulic traits. From the field, or laboratory, it is possible to determine Ψ_{leaf} (MPa) and leaf fresh weight (LFW; g) at different time intervals following natural dehydration. Furthemore, leaf dry weight (LDW) can be obtained after oven-dehydration at 65 °C until weight variation is no longer observed. From there, the tool allows to assume leaf saturated water content (SWC) as the first reading following overnight branch rehydration:

$$\text{SWC} = \text{LFW}_{t=0} - \text{LDW} \tag{A4.1}$$

Or, be assumed as the intercept of the regression of the turgor loss region points, including the TLP, on the x-axis of Leaf Water Mass (LFW − LDW; g) when $\Psi_{\text{leaf}} = 0$ as the next figure shows:



Therefore, if the regression is expressed as

$$\Psi_{\text{leaf}}(\text{Leaf Water}) = a\text{Leaf Water} + b \tag{A4.2}$$

Saturated Water Content can be calculated as:

$$\mathrm{SWC} = -\frac{b}{a} \tag{A4.3}$$

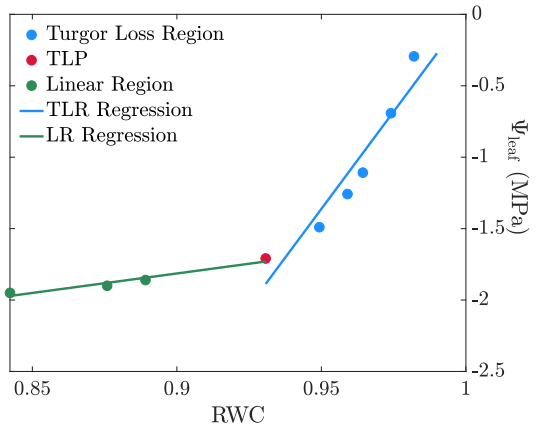
Following SWC determination, relative water content (RWC) of the leaf for each measurement t can be expressed as follows:

$$\mathrm{RWC}_t = \frac{\mathrm{LFW_t} - \mathrm{LDW}}{\mathrm{SWC}} \tag{A4.4}$$

Accordingly, RWC(%) is expressed as:

$$\mathrm{RWC\%}_t = \mathrm{RWC}_t \times 100 \tag{A4.5}$$

$\mathrm{C_{FT}}$, $\mathrm{C_{TLP}}$, and $\mathrm{C^*_{FT}}$ are determined by plotting Ψ_{leaf} against RWC:



$\mathrm{C_{FT}}$ is determined by the slope of the of all the points belonging to the turgor loss region, including the TLP, and $\mathrm{C_{TLP}}$ is given by the slope of the linear region, including the TLP. Accordingly, $\mathrm{C^*_{FT}}$ can be determined by following Eq. 4.3 in the main text.

The calculation for the total modulus of elasticity (ε) is described in Eq. 4.2. Π_o is derived from Fig. 4.1 by doing a linear regression of the points belonging to the Linear Region (including TLP) an calculating the intercept with the y-axis ($-\frac{1}{\Psi}$). If the regression is understood as follows:

$$-\frac{1}{\Psi}(\text{RWC}(\%)) = a \times \text{RWC}(\%) + b \tag{A4.6}$$

Since Π_o is the intercept with the y-axis, Π_o is calculated as:

$$\Pi_o = \frac{1}{b} \tag{A4.7}$$

Chapter5

Seasonal changes in leaf osmotic adjustment across a tropical drought gradient

Non-structural carbohydrates not only supply plants' metabolic and growth needs. NSC accumulation in the leaf provides for osmotic adjustment in order to maintain the soil-plant-atmosphere water continuum when soil water moisture is low. Osmotic adjustment is derived from differences in leaf osmotic potential throughout the season.

Here I present leaf osmotic adjustment throughout the wet and dry season across a tropical drought gradient in Southern Ghana. Osmotic potential can be derived from pressure-volume relationships. In this chapter I used the open-source tool presented in **Chapter 4** to analyse the pressure-volume curves measured in the field.

Furthermore I use the results from **Chapter 3** regarding key leaf traits that ensure rapid NSC translocation to correlate osmotic adjustment, as a proxy of NSC accumulation in the leaf, with the aforementioned traits. Finally, I study the relationship between leaf gas exchange throughout the seasons and leaf osmotic potential in order to understand if NSC are downregulating ecosystem productivity.

This manuscript is currently under review by co-authors to get their feedback. I did the analysis of the data and wrote the manuscript with help from YM. TP and AG collected the data in the field under the supervision of IO, SAB and YM. DB provided help with the statistical analysis. I would like to submit this article to *Tree Physiology*.

Seasonal changes in leaf osmotic adjustment across a tropical drought gradient

Nicolas Raab[1*], Imma Oliveras[1], Theresa Prepah[2], Agne Gvozdevaite[1], David Bauman[1,3], Stephen Adu-Bredu[2], Yadvinder Malhi[1]

[1]Environmental Change Institute, School of Geography and the Environment, University of Oxford, Oxford, OX1 3QY, UK. [2]Forestry Research Institute of Ghana, Council for Scientific and Industrial Research, Kumasi, PO Box UP 63 KNUST, Ghana. [3]Laboratoire d'Écologie Végétale et Biogéochimie (EvB), CP244, Faculté des Sciences, Université Libre de Bruxelles, 50 av. F.D. Roosevelt, Brussels 1050, Belgium.[*]Corresponding Author: nicolas.raab@ouce.ox.ac.uk

Abstract

The accumulation of solutes in the leaf allows plants to adjust their osmotic potential, thereby decreasing leaf water potential in order to maintain the soil-plant-water continuum during periods of soil moisture shortage. Osmotic adjustment in aerial organs is heavily dependent on the accumulation of non-structural carbohydrates (NSC) provided by photosynthesis. Nevertheless, NSC accumulation in the leaf has also been hypothesised as a consequence of lack of sink activity during periods of stress. This raises the question of whether leaf NSC concentration changes are an active strategy by plants in order to cope with drought or the result of a passive process given a lack of NSCs demand across the plant. By studying leaf osmotic potential *via* pressure-volume curves throughout the wet and dry season across a tropical drought gradient in Southern Ghana, we aim to identify if a decrease in leaf osmotic potential is an active strategy of plants' acclimation to drought or a consequence of lack of sink demand. We found that the driest (dry deciduous tropical forest) plot presented a higher degree of osmotic adjustment in comparison with the wettest plot (wet evergreen tropical forest). Osmotic adjustment correlated negatively with leaf traits that provide for fast NSC translocation from leaves. Furthermore, leaf osmotic potential at full turgor positively correlated with leaf gas exchange at light saturation. However, our data is inconclusive to support the hypothesis of leaf NSC accumulation because of a lack of sink activity. Thus, the accumulation of solutes in leaves remains an active strategy for plants' acclimation to water stress.

5.1 Introduction

In order to maintain the soil-plant-atmosphere water continuum, thus ensuring water transport across the plant, a water potential (Ψ_w) gradient along these three compartments must be maintained. This becomes particularly challenging when soil moisture is low, since soil water potential becomes more negative, thus jeopardizing the continuum. In response, plants need to lower their Ψ_w in order to ensure water absorption from an already low Ψ_w environment in the soil. At a cellular level, plants decrease their Ψ_w by adjusting cell's osmotic potential (Ψ_o) via solute accumulation. This allows for a decrease in Ψ_w without affecting other physiological functions such as cell turgor or volume.

Solutes that can be accumulated in the cell, allowing osmotic adjustment, range from inorganic ions, such as K^+, to organic compounds like carbohydrates, organic acids and amino acids (Taiz and Zeiger, 2006). Since high concentrations of some cations can interfere with enzymatic action, these compounds are preferably accumulated inside the cell's vacuole. In contrast, solutes compatible with cell functioning can be accumulated in the cytosol. These solutes are preferably rich in hydroxyl groups (-OH), and include sugars, cyclitols, proline and glycine betaine (Sanders and Arndt, 2012).

Plant osmotic adjustment can arise either as a passive phenomenon, given that the earliest response to water stress is a limitation on cell elongation, thus promoting solute accumulation (Meyer and Boyer, 1972), or as an active mechanism of acclimation to water stress, meaning plant cells actively accumulate solutes in order to reach a more negative Ψ_w than their surroundings. This ensures maintained cell turgor, cell elongation, and other cell physiological and metabolic processes (Sanders and Arndt, 2012).

Osmotic adjustment has been extensively reported in the literature (e.g., Kameli and Lösel, 1995; Patakas et al., 2002; Wang and Stutte, 1992). However, there is ambiguity as to whether the observed osmotic regulation in these studies is a result of cell dehydration, or is in fact the result of an active process of solute uptake and/or synthesis in the cell (Hsiao et al., 1976). At the root level, when soil Ψ_w is low, osmotic adjustment can be led by an accumulation of cations from the soil. In contrast, in aerial organs (shoots and leaves), osmotic adjustment is mostly associated with photoassimilates. Meyer and Boyer (1972) found that in soybean hypocotyls (the first true leaves after

germination), osmotic adjustment was highly dependent on the presence or absence of cotyledons. When cotyledons were removed, the hypocotyls showed less osmotic adjustment capacity, meaning that *a*) osmotic adjustment depends on the capacity of leaves to cleave starch reserves into simpler carbohydrates with a more negative osmotic potential, and/or *b*) osmotic adjustment ability depends directly on carbohydrate accumulation derived from photosynthesis (Eaton and Ergle, 1948; Iljin, 1957).

Non-structural carbohydrates (NSC) have been shown to play a major role in osmoregulation. Osmotic adjustment proved to be highly correlated with NSC mobilisation, usually when water soil moisture was depleted (Subbarao et al., 2000). In a Mediterranean savannah in California, Bowman and Roberts (1985) found adjustment in leaves in shrub species during the drought season. By adjusting leaf osmotic potential, cell turgor was maintained during hours of maximal radiation and vapour pressure deficit, thus avoiding turgor loss point, at which Ψ_w cell's wall collapses, and the cell can no longer be rehydrated. In tropical mountain forests in Venezuela, NSC accumulation also played a major role on leaf acclimation to abiotic stresses. Osmotic adjustment was observed together with an increase in leaf carbohydrate concentration in order to withstand sub-zero temperatures and avoid freezing of the tissue (Rada et al., 1985).

On the other hand, observed NSC accumulation during the drought season has also been associated with the lack of sink activity (Würth et al., 2005). When facing an abiotic stress such as drought, cell division and elongation across the plant are compromised. Thus, NSC translocation in the phloem is hampered (Fatichi et al., 2014; Hayat et al., 2017) forcing the accumulation of NSC in the leaf blade, which in turn triggers a cascade of chemical signals that downregulates the Calvin-Benson-Bassham (CBB) cycle (Azcón-Bieto, 1983; Franck et al., 2006; Paul and Foyer, 2001; Sharkey et al., 1986).

Key leaf traits, such as vein density and specific leaf area (SLA), have been shown to correlate well with NSC translocation in order to avoid photosynthetic feedback inhibition triggered by an excess of photoassimilates in the blade (Raab et al., submitted). Higher investment in vein infrastructure increases the phloem to mesophyll contact area and the leaf total density of plasmodesmata to allow channelling carbohydrates into the phloem sieve elements (Amiard et al., 2005). Moreover, higher vein density reduces leaf hydraulic resistance (Sack and Scoffoni, 2013), meaning that a less negative water potential in the xylem is needed for a determined transpiration rate from the leaf. If this is

the case, water movement from the xylem to the phloem should be enhanced, allowing to reach a higher turgor pressure in the phloem at a lower concentration of photoassimilates, thus facilitating NSC translocation (Hölttä et al., 2009). Accordingly, leaf within the fast spectrum of the leaf economic spectrum (LES) have evolved in order to coordinate leaf traits that ensure high photosynthetic rates (e.g., leaf nitrogen concentration) with fast translocation in order to recover the carbon investment in producing leaves with a shorter lifespan (Wright et al., 2004). On the other hand, species with leaves on the fast sprectrum present lower photosynthetic rate since they can recover carbon investment in a longer period of time. Phloem traits and anatomy have shown to also vary across species in order to minimise phloem resistance, a particular problem in trees where resistance increases with distance (Savage et al., 2017). The last shows the coordination between leaf traits for acquisition and later translocation.

We examine whether solute accumulation in leaves during a soil moisture shortage is mostly associated with a physiological coping mechanism to face drought (an active process resulting from photoassimilates and other solutes accumulation in the leaf), or if indeed NSC accumulation in the leaf is the result of a passive process triggered by a lack of sink activity in the plant during drought season by correlating leaf osmotic adjustment to leaf traits that have shown to relate to high photosynthetic feedback inhibition and low NSC translocation rates (Raab et al., submitted) by reporting on seasonal osmotic adjustment at species level along a tropical forest seasonal water stress gradient in Southern Ghana. In doing so we aim to:

a) Quantify the degree of osmotic adjustment across the gradient and along the wet-dry season.

b) Examine the consistency of the level of osmotic adjustment across species within a plot.

c) Investigate if the degree of osmotic adjustment across species is correlated to key leaf traits (leaf vein density and SLA) that have been shown to indicate the capability of rapid NSC translocation from the leaf to the rest of the plant, thus indicating that solute accumulation in the blade is a result of a passive process resulting from the restriction on sink activity and poor phloem translocation.

d) Determine if incorporating osmotic adjustment increases the predictability of photosynthetic capacity over considering leaf nutrient concentration alone, thus showing that osmotic adjustment is an active process that allow leaves to keep their metabolic activity despite shortage in soil moisture.

5.2 Materials and Methods

5.2.1 Sites description

Trees were sampled in three sites in southern Ghana across a drought gradient. The gradient encompasses three tropical biomes from North to South: a dry deciduous forest in Kogyae (KOG) Strict Nature Reserve (7°18′ N; 1°9′ W; mean annual precipitation (MAP): 1200 mm, and mean annual temperature (MAT): 26.4 °C; a moist semideciduous forest situated in Bobiri (BOB) Forest Reserve (6°41′ N; 1°20′ W; MAP: 1500 mm; MAT: 25.7 °C); and an evergreen forest in Ankasa (ANK) National Park (5°16′ N; 2°41′ W; MAP: 2050 mm; MAT: 25.0 °C). Table 5.1 shows other variables regarding soil texture and fertility and carbon stocks.

All trees were sampled from plots belonging to the Global Ecosystem Monitoring (GEM; `http://gem.tropicalforests.ox.ac.uk`). Plots are monitored monthly for carbon dynamics aiming to study the effect of climate change on natural ecosystem carbon storage (Marthews et al., 2014). Figure 5.1 shows MAP distribution along the year together with cumulative water deficit (CWD). Further information about these three sites can be found in Moore et al. (2017).

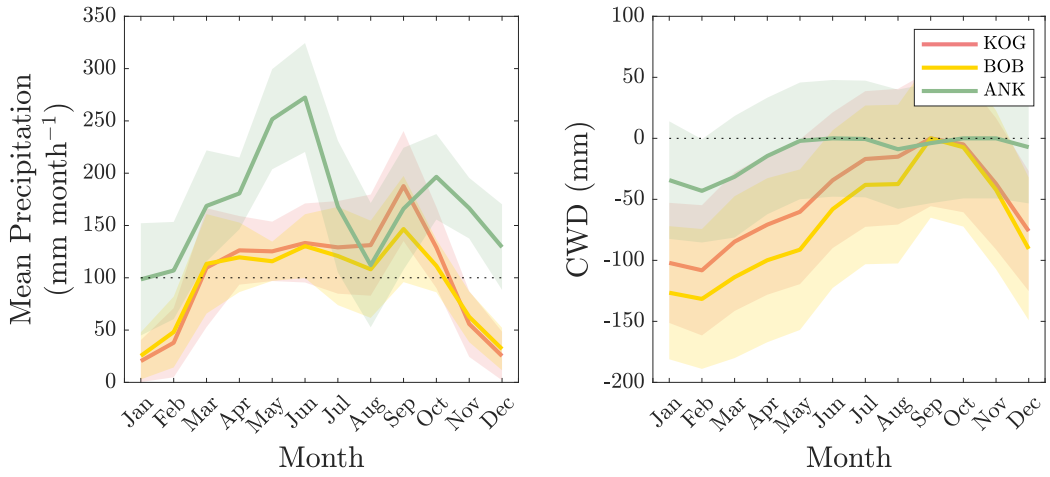


Figure 5.1: Mean annual precipitation and cumulative water deficit (CWD) distribution along the year for the three study sites from North to South (driest to wettest): Kogyae (KOG), Bobiri (BOB), and Ankasa (ANK).

Both Northern sites, KOG and BOB, present a similar precipitation regime (Fig. 5.1, left panel). However, the soil in KOG has a lower water retention capacity because of its sandy texture (83% sand) compared to the soil in BOB (47% sand) (Moore et al., 2017). These two sites present a rainy season from July to October, followed by a four-month dry season from November to February.

Table 5.1: Summary of main variables describing each site, from North to South: Kogyae (KOG), Bobiri (BOB) and Ankasa (ANK). First block describes geographical and climatic data, second block describes soil data and third block describes carbon stocks and residence times (averages shown ± standard error). ACW is aboveground coarse wood and LAI is leaf area index. All data but LAI was taken from Moore et al. (2017). LAI was obtained from Landsat images, images from KOG were not available.

	KOG	BOB	ANK
Vegetation Type	Dry Deciduous Forest	Moist Semideciduous Forest	Evergreen Forest
Latitude (°)	7°18′ N	6°41′ N	5°16′ N
Longitude (°)	1°9′ W	1°20′ W	2°41′ W
Elevation (m.a.s.l.)	229	235	114
Mean Annual Temperature (°C)	26.4	25.7	25.0
Mean Annual Precipitation (mm)	1200	1500	2050
Mean Annual Humidity (%)	79.2	83.9	91.0
Solar Radiation ($GJ\,m^{-2}\,yr^{-1}$)	2.4	2	1.7
pH	6.07	6.05	4.27
Soil N (%)	0.06	0.16	0.17
Soil C (%)	0.72	1.71	2.61
Soil C:N	11.35	10.18	14.57
P_{total} ($mg\,kg^{-1}$)	67	258	147
Base fraction	0.99	0.98	0.25
Sand (%)	83	47	63
Clay (%)	2	29	22
Silt (%)	15	24	15
ACW biomass ($Mg_C\,ha^{-2}$)	101.4 ± 20.3	111.8 ± 20.3	162.7 ± 32.5
ACW residence time (yr)	44.5 ± 9.94	47.3 ±10.6	99.0 ± 22.1
Leaf biomass ($Mg_C\,ha^{-2}$)	1.82 ± 0.15	1.75 ± 0.11	2.31 ± 0.10
Leaf residence time (months)	9.61 ±3.11	4.09 ± 0.42	9.22 ± 0.80
Fine root biomass ($Mg_C\,ha^{-2}$)	8.45 ± 1.69	22.87 ± 4.57	31.65 ± 6.33
Fine root residence time (months)	8.45 ±1.69	22.87 ± 4.57	31.65 ±6.33
LAI		3.41	3.5
LAI Coefficient of variation (%)		20.0	17.1

Ankasa presents a dual wet season (Fig. 5.1), encompassing the months of May and June, followed by a second peak in precipitation during September. Similar to the other two sites, ANK dry season occurs from November to February, although the magnitude of this event is not as intense as in KOG and BOB (Fig. 5.1, right panel).

5.2.2 Sampling campaigns

A main campaign for leaf functional traits and gas exchange was done in each of the sites abovementioned. KOG was sampled in November 2014, BOB was sampled in December 2014, and ANK was sampled in February 2015. Each campaign aimed to sample all the trees comprising 80% of the basal area. Nevertheless, for this research the main limiting facto was to obtain a successful pressure-volume curve in order to determine leaf osmotic potential. Table 5.2 summarises the number of species and individuals sampled in each plot.

Around 7 am, with the help of a tree climber, top of the canopy sun exposed branches were clipped. As soon as branches touched the ground, a wet-cut was done by doing a cut at 5 cm above the first cut with the bottom of the branch inside a plastic back filled with water. Branches were then covered with a big black plastic bags sprinkled with water in the inside in order to avoid leaf transpiration and ensure branch rehydration.

Covered branches were taken to a field station in the proximities of the plot. The bottom of one of the branches was put into a bucket filled with water and a second wet-cut was done. The branch was uncovered, and after 30 minutes (min) of acclimation to light, three healthy green leaves were selected for photosynthetic measurements.

Photosynthesis was measured with a leaf gas exchange analyser (Li-6400XT, LI-COR, Lincoln, NA, USA) in three leaves per branch. Leaf chamber temperature was set at 30 °C, and photosynthetic active radiation (PAR) at 2000 $\mu mol\, m^{-2}\, s^{-1}$, to avoid heat damage in tropical leaves (Doughty, 2011). This photosynthesis measurement is referred as net assimilation at light saturation (A_{sat}).

After A_{sat} was recorded, the three leaves were collected for specific leaf area (SLA; $m^2\, kg^{-1}$) measurement, and for determination of nitrogen (N) and phosphorus (P) concentrations. SLA was determined by scanning fresh leaves with an office scanner. Leaf area was derived from scan images using a custom Matlab R2015b (Natwick, MA, USA) script. Leaves were then oven-dried at 60 °C until weight difference was no longer observed and dried weight was recorded to finally calculate SLA. N and P were determined from pulverised dried leaves material digested in sulfuricsalicylic acid and selemium following colorimetric determination by a flow analyser (SKALAR SAN plus system, Breda, The Netherlands), yielding $g\, kg^{-1}$ of dry leaves. Individual's A_{sat},

Table 5.2: Trees and number of individuals sampled in each campaign on each site. From North to South: Kogyae (KOG), Bobiri (BOB) and Ankasa (ANK). Note that that the number of trees sampled is restricted by the number of successful pressure-volume curves obtained.

Site	Campaign	Date	N. Species sampled	N. Trees sampled
KOG	Main	October 2014	13	24
	Seasonal	April 2015	5	13
	Seasonal	July 2015	6	17
	Seasonal	October 2015	6	22
	Seasonal	December 2015	4	10
	Seasonal	September 2016	6	17
BOB	Main	December 2014	7	11
	Seasonal	May 2015	6	22
	Seasonal	August 2015	6	15
	Seasonal	November 2015	6	22
	Seasonal	March 2016	4	8
	Seasonal	July 2016	6	9
ANK	Main	January 2015	3	5
	Seasonal	June 2015	6	22
	Seasonal	September 2015	5	5
	Seasonal	January 2016	5	5
	Seasonal	March 2016	5	5
	Seasonal	August 2016	6	8

SLA and N and P leaf concentrations resulted from averaging these three measurements.

In addition to leaves collected after photosynthetic measurements, 5 healthy leaves were clipped from the branch and oven-dried following the abovementioned procedure to determine leaf vein density. One cm^2 sections from oven-dried leaves were used for analysis. Samples were chemically cleared with bleach and stained with saffranine following Pérez-Harguindeguy et al. (2013). Vein density was measured by photographing dyed slices using a trans-illumination microscope (Olympus SZX-12, Olympus, Tokyo, Japan). Veins of a region of interest were traced using a computer pen and pad, and the resulting paths were divided by the area of interest using an image processing algorithm (Blonder et al., 2017) to yield vein density ($mm\,mm^{-2}$).

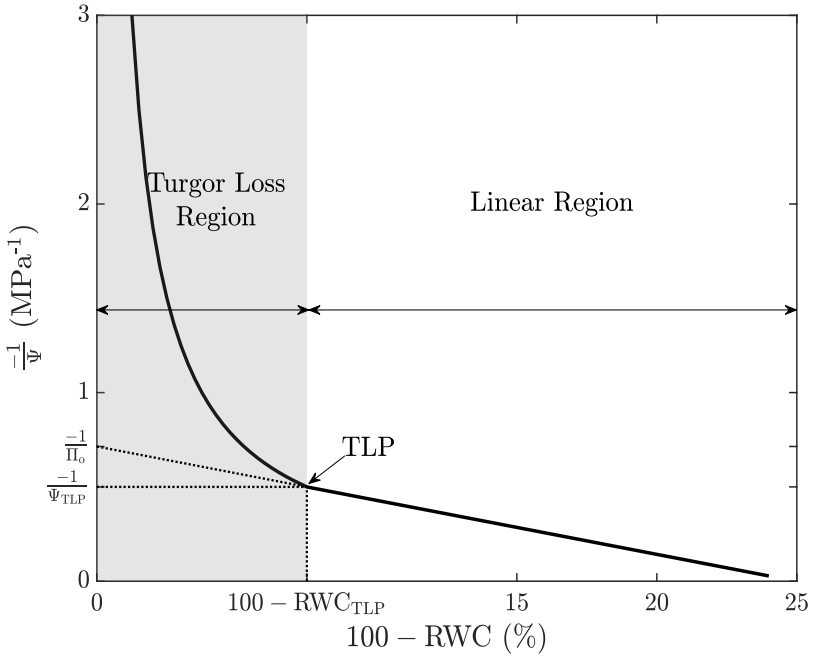


Figure 5.2: Diagram of an example leaf pressure-volume curve. The inverse of leaf water potential ($\frac{-1}{\Psi}$) is plotted against the complement to leaf relative water content (100 − RWC; %). Osmotic pressure at full turgor (Π_o) is derived from the extrapolation of the linear regression of points within the linear region of the curve (points defined after the turgor loss point (TLP)) to the Ψ_{leaf} axis. Figure taken from Raab et al., submitted *b*.

5.2.3 Pressure-volume curves

The second branch collected from the top of the canopy was kept in the shade, also covered with a black bag and another bag filled with water on the bottom of the branch. After photosynthesis measurements were completed, the branches were transported to a field laboratory. The bottom of the branch was dipped in a bucket full of water and a second underwater cut was done. The bucket was kept covered inside the facilities overnight (ca. 15 hours) in order to ensure full rehydration. The next morning, PV curves were generated by repeatedly making paired measurements of leaf water potential (Ψ_{leaf}) and leaf weight following intervals of bench drying ($n = 9 - 12$ points curve^{-1}). Leaves were scanned in order to obtain their area (cm^2) and then oven-dried for 3 days at 60 °C in order to obtain leaf dry weight.

Analysis of the curves was done using the open-source software described in Raab et al., submitted *b*. In summary, the inverse of Ψ_{leaf} was plotted against leaf relative water content, derived from leaf weight. Points belonging to the linear region of the curve (past the turgor loss point) were selected, and their regression was extrapolated to the Ψ_{leaf} axis ($\Psi_{\text{leaf}} = 0$; meaning leaf at full turgor), thus resulting in Π_{o}, rather than leaf osmotic potential (Ψ_{o}) (Fig. 5.2).

5.2.4 Seasonal campaigns

Further to the initial campaigns, several smaller campaigns were done in the same sites at different times during 2015 and 2016 with the goal of studying the seasonal variation of photosynthesis and hydraulic traits as determined through PV curves. Figure 5.3 shows a classification of the months according to their season for each site.

This time, only a sub-selection of trees was sampled based on their contribution to the basal area of the plot. Table 5.2 shows the number of species and individuals sampled each time and date of these campaigns.

5.2.5 Osmotic adjustment

Osmotic adjustment at a tree level was defined as the difference between the maximum (least negative) Π_{o} observed in that tree across the seasonal cycle (main and seasonal campaigns), minus Π_{o} observed in each of the campaigns (Sanders and Arndt, 2012), resulting in:

$$OA_i = max(\Pi_o) - \Pi_{oi} \tag{5.1}$$

Where OA is osmotic adjustment (MPa) at any sampling time i, $max(\Pi_o)$ is the highest Π_{o} (MPa) observed along the season, and Π_{oi} are individual Π_{o} observations along the different campaigns.

We then derived the maximum osmotic adjustment for each tree, $\Delta\Pi_o$, defined as the maximum calculated value of OA over the seasonal cycle, only when this difference occurred in contrasting seasons (e.g., dry and wet or dry and in between or wet and in between).

5.2.6 Species selection and statistical analysis

In order to ensure a minimum of repetitions for statistical purposes, only species that provided for three different individuals per plot were selected to analyse $\Delta\Pi_o$ differences at: *a*) species level, and *b*) plot level. Statistical differences were determined by T-test between pair of species. Statistical differences were given by α value below 0.05. Double level ANOVA (plot level and species level) were not possible to calculate given that very few species were present in the three sites.

We tested if $\Delta\Pi_o$ can be predicted from leaf traits that have proven to be good predictors of NSC translocation from the leaf (Raab et al., submitted) based on linear mixed models accounting for species nested into each plot as a random effect. We fitted different combination of these traits and model's goodness-of-fit was assessed based on the Akaike Information Criterion (AIC), and the adjusted coefficient of determination (R^2_{adj}). Models are presented based on their AIC ranking.

Similarly, in order to predict A_{sat} from Π_o and other traits associated with leaf gas exchange (mainly N and P concentrations), we tested several combinations of these traits accounting for plot and species as random effects. Model goodness-of-fit was assessed following their AIC ranking, shown together with R^2_{adj}.

5.3 Results

5.3.1 Osmotic adjustment and its along-gradient and seasonal variation

Climatological differences across plots (Fig. 5.1) affected tree level osmotic adjustment differently. The drier sites (KOG and BOB), with a marked dry season during the months of November to February, presented higher osmotic adjustment than the wet plot (ANK) (Fig. 5.3). Lowest osmotic adjustment at species level was generally found across all the plots in the months of June and July, very close to the wet season in KOG and BOB (August-October), and to the wet season in ANK (May-June).

The KOG site exhibited the largest average osmotic adjustment between sampled trees compared to the other two sites. Largest osmotic adjustment was achieved during the month of December, in the middle of the dry season (Fig. 5.3). In BOB, the highest average osmotic adjustment was reached in July, just before the onset of the wet season. In ANK, the largest osmotic adjustment occurred in between the two wet seasons. Average lowest osmotic adjustment occurred in the middle of the dry season (February); however, we only managed to produce three PV curve in order to determine Π_o that month. June (first wet season in ANK), presented the second lowest average osmotic adjustment determined from seven PV curves, which in turn is more representative than the low result for osmotic adjustment obtained on February.

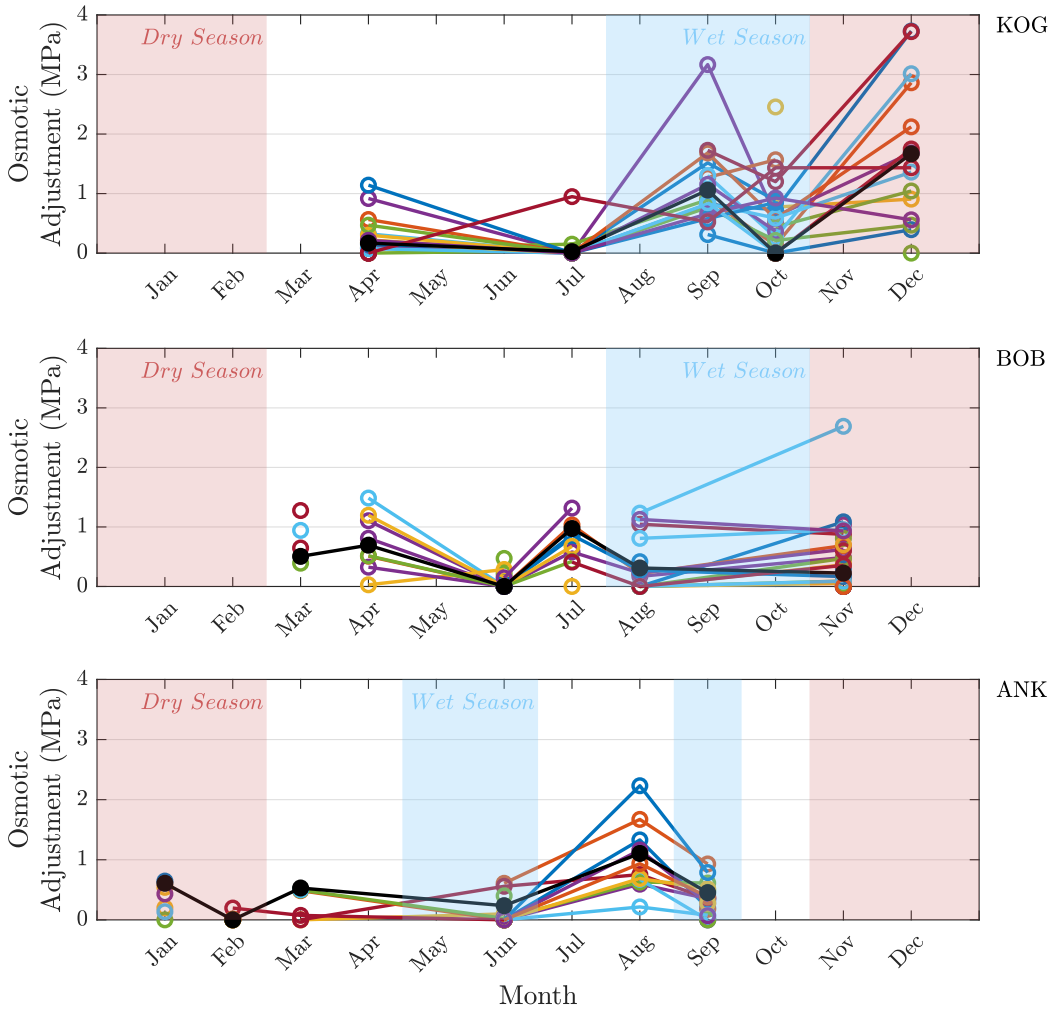


Figure 5.3: Osmotic Adjustment per tree in the three study sites. From North to South: Kogyae (KOG), Bobiri (BOB) and Ankasa (ANK). Osmotic adjustment along the season was defined as the most negative osmotic potential at full turgor (Π_o) observed at a tree level within the season ($max(\Pi_o)$), minus the Π_o obtained for each measurement. Coloured lines represent observations for the same tree throughout the year whilst the black line represents campaigns' osmotic adjustments averages.

5.3.2 Interspecific consistence in maximum osmotic potential at full turgor ($\Delta\Pi_o$)

We established statistical differences for $\Delta\Pi_o$ between species, and between sites (Table 5.3 and 5.4, respectively). At a species level, *Khaya tragacantha* from KOG, presented a degree of osmotic adjustment, quantified as $\Delta\Pi_o$, different to any other species sampled across the three sites. *Cola gigantean*, also from KOG, presented low P_{Value} when compared to other species, nonetheless $\Delta\Pi_o$ for *C. gigantean* was not statically different from any other species (α value < 0.05).

Table 5.3: P_{values} for T-test for osmotic adjustment between pair of species. Osmotic adjustment was defined as the difference of maximal osmotic potential at full turgor (Π_o), minus the minimal (Π_o) in contrasting seasons per individuals of the same species. P_{value} below 0.05 represent statistical differences between species.

	Ceiba pentandra	*Celtis wightii*	*Cola gigantea*	*Khaya tragacantha*	*Sterculia grandifoliola*	*Celtis mildbraedii*	*Celtis zenkeri*	*Triplochiton scleroxylon*	*Turraeanthus africanus*	*Lannea welwitschii*	*Sterculia rhinopetala*	*Bussea occidentalis*	*Dacryodes klaineana*	*Maranthes glabra*	*Strephonema pseudocola*
Ceiba pentandra															
Celtis wightii	0.551														
Cola gigantea	0.174	0.103													
Khaya grandifoliola	0.01	0.043	0.329												
Sterculia tragacantha	0.962	0.661	0.102	0.027											
Celtis mildbraedii	0.449	0.925	0.092	0.023	0.539										
Celtis zenkeri	0.730	0.658	0.282	0.095	0.724	0.602									
Triplochiton scleroxylon	0.915	0.707	0.082	0.025	0.986	0.569	0.671								
Turraeanthus africanus	0.301	0.569	0.104	0.026	0.384	0.541	0.434	0.302							
Lannea welwitschii	0.920	0.538	0.098	0.025	0.879	0.371	0.756	0.890	0.162						
Sterculia rhinopetala	0.327	0.622	0.053	0.033	0.407	0.713	0.463	0.305	0.896	0.262					
Bussea occidentalis	0.853	0.718	0.186	0.139	0.841	0.600	0.830	0.799	0.503	0.902	0.480				
Dacryodes klaineana	0.802	0.630	0.120	0.023	0.795	0.576	0.899	0.755	0.393	0.845	0.401	0.955			
Maranthes glabra	0.594	0.989	0.108	0.091	0.660	0.905	0.632	0.666	0.637	0.491	0.729	0.724	0.610		
Strephonema pseudocola	0.327	0.475	0.099	0.060	0.490	0.783	0.509	0.447	0.873	0.299	0.915	0.589	0.507	0.609	

At a site level, similar to Fig. 5.3, Table 5.4 shows that the only site that was statistically different from the rest was KOG. BOB and ANK presented similar levels of $\Delta\Pi_o$.

Table 5.4: P_{Values} for double entries ANOVA for osmotic adjustment at species level. Osmotic adjustment was defined as the difference of maximal osmotic potential at full turgor (Π_o), minus the minimal (Π_o) in contrasting seasons per individuals of the same plot. P_{Value} below 0.05 represent statistical differences between sites.

	KOG	BOB	ANK
KOG			
BOB	0.011		
ANK	0.027	0.714	

5.3.3 Maximum osmotic adjustment ($\Delta\Pi_o$) and leaf traits

Figure 5.4 shows the distribution of $\Delta\Pi_o$, and key leaf traits associated with fast NSC translocation from the leaf to the rest of the plant.

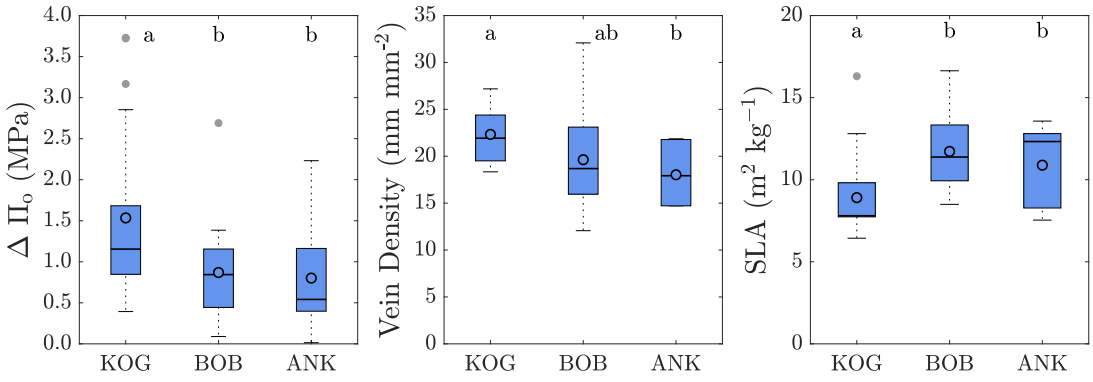


Figure 5.4: Per plot distribution of maximum osmotic potential difference per tree ($\Delta\Pi_o$) between different seasons, leaf vein density, and specific leaf area (SLA). Letters symbolise statistical difference given by a T-test at an α value of 0.05.

Kogyae, the driest site, presented the highest average $\Delta\Pi_o$ and statistically different from the other two sites, thus indicating a better acclimation to soil moisture short-

age. On the other hand, BOB and ANK (transition and wet forest sites, respectively) presented a similar distribution of $\Delta\Pi_o$, thus indicating a lower degree of sensitivity to drought reflected by osmotic adjustment. Vein density distribution across sites was rather similar, although KOG presented a slightly higher average.

Regarding SLA, KOG presents a lower average than BOB and ANK, showing that species in KOG were closer to the slow region of the leaf economic spectrum (LES) (Díaz et al., 2016; Wright et al., 2004).

We used leaf traits that proved to be relevant to NSC translocation to predict $\Delta\Pi_o$. The model that yielded the lowest AIC score was the one combining both leaf investment in vein infrastructure and SLA, together with an interaction between both terms (Table 5.5). However, the model only accounting for SLA (model 3) was within the same range of AIC score than model 1 and its R^2_{adj} was of 0.44. We also tested predicting $\Delta\Pi_o$ only using plot as explanatory variable (Model 4). AIC score was lower but R^2_{adj} (0.13) did not explain much of the observed variability.

Table 5.5: Model performance for different variable combination, aiming to predict osmotic adjustment. Model performance was asses using both the Akaike Information Criterion (AIC) and the adjusted coefficient of determination (R^2_{adj}). Models are sorted by their ranking determined by their AIC score. Furthermore, a model looking to predict osmotic adjustment solely based on a plot variable as a fixed effect, was also assessed.

	Model	ΔAIC	ΔR^2_{adj}
1	OsmoticAdjustment $\sim$ 1 + SLA + VeinDensity + SLA×VeinDensity + (1 + Species|Plot)	0 (335.98)	0 (0.18)
2	OsmoticAdjustment $\sim$ 1 + VeinDensity + (1 + Species | Plot)	+2.8	+0.05
3	OsmoticAdjustment $\sim$ 1 + SLA + (1 + Species | Plot)	+14.4	+0.25
4	OsmoticAdjustment $\sim$ 1 + Plot	0 (139.91)	0.13

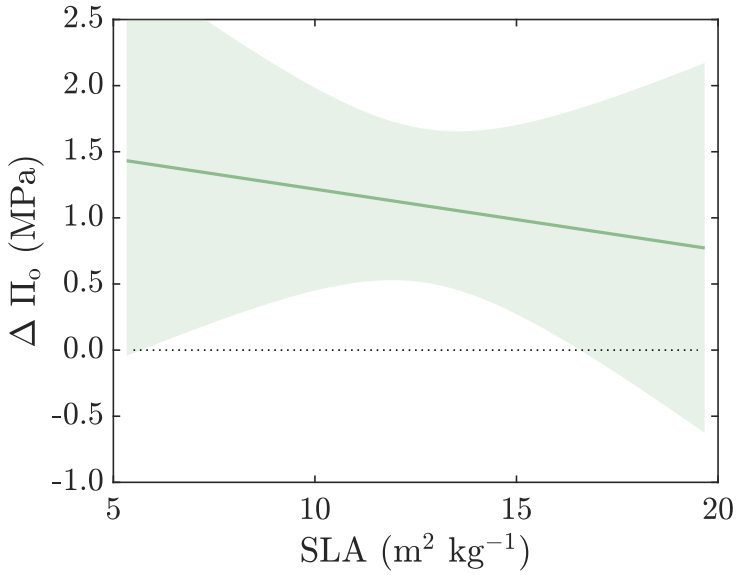


Figure 5.5: Specific leaf area (SLA) from the model explaining most of the observed variation (Table 5.5)when predicting maximum osmotic potential at full turgor between different seasons ($\Delta\Pi_o$) at a species level.

Model 3; Table 5.5 predicted a negative relationship between SLA and $\Delta\Pi_o$ (Fig. 5.5).

Table 5.6: P_{value} for fixed effect coefficients from model 2; Table 5.5. Model predicts leaf osmotic adjustment based on specific leaf area.

Fixed Effect Coefficient	P_{value}
Intercept	0.03
SLA	0.95

5.3.4 Predicting photosynthesis from osmotic leaf traits

We aimed to predict A_{sat} across the wet-dry seasons using a combination of leaf nutrient concentration (N and P), season (dry, between, wet) as a categorical variable and Π_o. The model that yielded the best result was the one using a combination of seasons and leaf N concentration (Model 1; Table 5.7), based on its AIC when compared to the other model where only a selection of variables was used. This model accounted for 30%

of the observed variability of A_{sat}. The model accounting only for Π_o as explanatory variable of A_{sat} (Model 5; Table 5.7), together with species nested into plots as random effects, explained 20% of the seasonal variability around A_{sat}.

Table 5.7: Models performance for different variable combination, aiming to predict photosynthesis at light saturation (A_{sat}). Variables used were osmotic potential at full turgor (Π_o), leaf nitrogen (N), and phosphorous (P) concentrations and seasons categorised as dry, wet and in between. Model performance was asses using both the Akaike Information Criterion (AIC) and the adjusted coefficient of determination (R^2_{adj}). Models are sorted by their ranking determined by their AIC score.

	Model	ΔAIC	ΔR^2_{adj}
1	$A_{sat} \sim$ Seasons + N + (1 + Species|Plot)	0 (110.16)	0 (0.30)
2	$A_{sat} \sim$ Seasons + (1 + Species|Plot)	+0.3	+0.04
3	$A_{sat} \sim$ N + (1 + Species|Plot)	+1.7	-0.14
4	$A_{sat} \sim \Pi_o$ + (1 + Species|Plot)	+0.6	+ 0.00
5	$A_{sat} \sim$ N + P + (1 + Species|Plot)	+0.7	−0.04
6	$A_{sat} \sim \Pi_o$ + N + (1 + Species|Plot)	+0.6	−0.01
7	$A_{sat} \sim \Pi_o$ + N + P + (1 + Species|Plot)	+1.3	−0.04

Figure 5.6 shows the effect of leaf nitrogen concentration (N) on A_{sat}. The higher the concentration of N in the leaf, the higher is the gas exchange at light saturation (A_{sat}). Table 5.8 shows the P_{values} for the fixed coefficients from Model 1; Table 5.7. Only coefficients for dry season and leaf N concentration were significant.

Table 5.8: P_{value} for fixed effect coefficients from model 1; Table 5.7. Model predicts leaf photosynthesis at light saturation based on seasonality (Wet, Dry, In Between) and leaf nitrogen concentration (N).

Fixed Effect Coefficient	P_{value}
Intercept	0.40
Season Wet	0.74
Season Dry	0.02
N	0.009

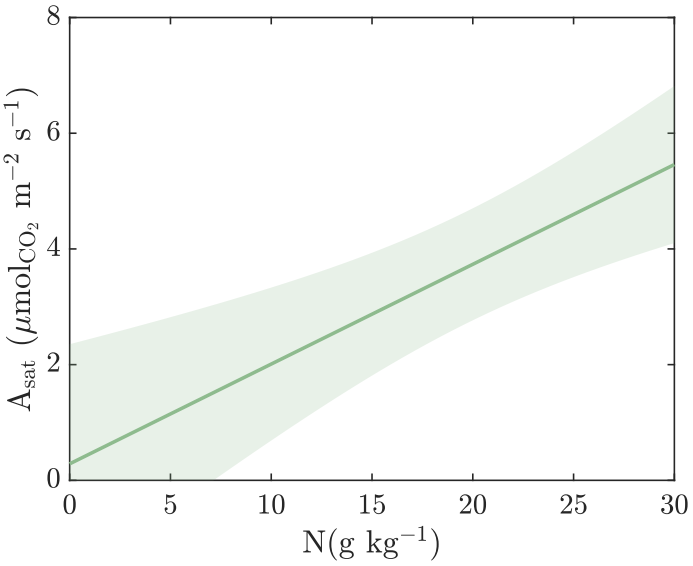


Figure 5.6: Effect of leaf nitrogen concentration (Π_o) on leaf net photosynthesis at light saturation (A_{sat}). Predictors were taken from the most parsimonious model (Model 1; Table 5.7).

5.4 Discussion

By measuring Π_o, rather than leaf osmotic potential (Ψ_o) through PV curves, and by rehydrating the branches overnight, we aimed to measure active osmotic adjustment to drought *via* the accumulation of solutes in the leaf, instead of just measuring the decrease in Ψ_o because of cell dehydration as a consequence of water stress.

5.4.1 Osmotic adjustment across the plots

As expected, KOG, the most water stressed site (Fig. 5.1), presented the highest degree of osmotic adjustment (Fig. 5.3). The campaign done during the early dry season (December) presented the highest average of osmotic adjustment, together with a large distribution, implying a large degree of acclimation at a tree level within the KOG site. The lowest degree of osmotic adjustment (values close to 0) occurred both in July and October, just before and during the wet season.

Even if BOB presented a very similar climatology to KOG (Fig. 5.1), and plants' acclimation mechanisms to drought were expected to be similar to the ones observed in KOG, the trees' osmotic adjustment was less variable and with a lower average. Highest average osmotic adjustment was observed in July, in between the dry and wet season, rather than in the dry season like in KOG. However, the BOB site was sampled only one time during the dry season (November), thus producing a bias. Lowest osmotic adjustment was observed in June, also in between the wet and dry seasons, rather than during the wet season as it would have been expected.

Differences in physiological responses between these two plots might arise because of soils water storage capacity. KOG has low soil water storage capacity given its sandy texture (83% sand), therefore species are better adapted to drought conditions than the ones in BOB, which has a higher capacity to retain water from the wet season (47% sand).

Ankasa, the wet tropical forest plot, exhibited a very low and steady osmotic adjustment along the year (Fig. 5.3). Species from these kinds of biomes, that show less pronounced differences along the year (Fig. 5.1), present lower acclimation to climatic variability along the year. The statistical analysis in Table 5.4 shows similar results. When $\Delta\Pi_o$ was compared across plots, the only plot that was statistically different from the rest was KOG because of its pronounced difference between wet and dry season, together with a low water retention capacity associated with the sandy texture of its soil.

5.4.2 Within plot species differences in acclimation to drought

All species across the three plots did not differ greatly according to their osmotic adjustment acclimation strategy (Table 5.3). Only *K. tragacantha*, presented a higher $\Delta\Pi_o$ compared to the other species. Nevertheless, we only used three individuals per species, thus reducing the statistical power of our analysis. We had expected a larger difference between species from different plots (given by the colour of the species in Table 5.3), however only one species from KOG was different from the whole sampling range.

When grouping all the species at a plot level, statistical differences were obtained. KOG was be statistically different from BOB and ANK given its marked drought season, together with its soil low capacity to retain moisture. Once again, the low number of repetitions per species might have affected the inter-species comparison. However, when species were grouped at a plot level, our analysis gained a higher number of repetitions, thus improving our results.

5.4.3 Osmotic adjustment during the drought season in tropical plots

It has been debated whether accumulation of carbohydrates in the leaf during the drought season results from the lack of sink activity across the plant because of abiotic stress (Würth et al., 2005), or is the result of an active strategy by the plant to lower Ψ_w without compromising cell turgor (Sanders and Arndt, 2012).

Our model accounting for SLA and leaf vein density only captured 7% of the observed variance on $\Delta\Pi_o$, indicating that other traits that we did not sample might contribute to a better explanation of $\Delta\Pi_o$ variability.

When predicating $\Delta\Pi_o$ using leaf traits, the most parsimonious model resulted from adding SLA, leaf investment in vein infrastructure, and their interaction. Similar to Raab et al., submitted, we found that higher vein density in leaves was correlated with the leaf capacity for translocating NSC *via* phloem, meaning that the individuals that presented low investment in vein infrastructure tended to present the largest difference between its highest and lowest $\Delta\Pi_o$ (Fig. 5.5). A high accumulation of solutes in the leaf during the drought season is dependant on a low capacity of the leaf to translocate these resources given their lack of investment in a vein network (Adams et al., 2018; Amiard et al., 2005). Nevertheless, the model that explained the most of the observed variability in $\Delta\Pi_o$ was Model 3; Table 5.5 ($R^2_{adj} = 0.44$) using only SLA fixed effect coefficient. Given the AIC score is similar to Model 1, we believe this is the best model we found to predict $\Delta\Pi_o$.

Species in the slow side of the LES (high SLA) accumulated a higher concentration of solutes (lower Π_o) than species on the fast end of the LES. Fast growing species tend to rapidly translocate photoassimilates across the plants in order to ensure that these

resources are rapidly ready to ensure high metabolic activity of heterotrophic organs, and to supply the building blocks for new growth (Díaz et al., 2016; Wright et al., 2005). The species we sampled followed this trend. We found that species with higher SLA tended to accumulate fewer solutes during the drought season, leading to lower $\Delta\Pi_o$.

Functional leaf traits, such as SLA, have demonstrated to have varying effects across climatic gradients. Greenwood et al. (2017) found that trees with a higher SLA (fast-growing strategy) were more susceptible to mortality triggered by drought that more conservative species (low SLA). KOG, the driest plot, presented lower SLA than BOB and ANK.

Our analysis indeed shows that the degree of osmotic adjustment across species and plots is partially explained by key leaf traits in terms of NSC translocation. The model yielded the expected results in terms of our physiological understanding of the plant. Leaf investment in vein infrastructure led to lower accumulation of solutes given by low $\Delta\Pi_o$. Likewise, high SLA (short leaf lifespan) tend to lower $\Delta\Pi_o$ because of rapid photoassimilate translocation from the leaf. However, these traits did not explain a high portion of the observed variability around $\Delta\Pi_o$. The fact that KOG, the driest plot, and the one where we found the largest $\Delta\Pi_o$, also presented a cluster of low SLA and high investment in vein infrastructure, might have influenced our model since these variables would be expected to be autocorrelated. Furthermore, only SLA explained most of the differences in $\Delta\Pi_o$Ṡince higher SLA is associated with higher photosynthetic rates, this could entail that osmotic adjustment is a result of an active strategy of NSC accumulation given higher photosynthetic rates in leaves.

5.4.4 Osmotic potential and leaf gas exchange at light saturation

When predicting A_{sat} using Π_o leaf N concentration and seasonality, our model explained a third of the seasonal variability in leaf gas exchange. Higher N concentration was associated to higher photosynthetic rates. When using N in combination with Π_o our model did not perform any better. Higher solutes concentrations in the leaf (more negative Π_o), are associated with a decrease in leaf gas exchange capacity. As previously shown, osmotic adjustment in aerial organs are highly dependent on the capacity of these to accumulate NSCs. However, high NSC concentrations also downregulated photosynthesis, thus affecting leaf gas exchange.

Altogether, our results do not allow to support the hypothesis that leaf NSC accumulation during the drought season is a passive process caused by a lack of sink activity across the plant, as Würth et al. (2005) claimed. Rather, it suggests that leaves keeping a portion of their photoassimilates is an active strategy to decrease Ψ_w, whilst maintaining cell turgor and other physiological activities.

5.5 Conclusions

In order to maintain the soil-water-continuum when facing water stress, plants need to lower their Ψ_w following a decrease in soil water potential. Osmotic adjustment has been described as an active mechanism in order to cope with low soil moisture during the months of drought (Sanders and Arndt, 2012). NSC accumulation in leaves has also been described as a passive process resulting from the lack of sink activity and carbon demand by the rest of the plant during water stress periods (Würth et al., 2005).

Our results show that leaves present osmotic adjustment in coordination with wet and dry seasons along the sampled tropical gradient. KOG, the driest plot, presented larger osmotic adjustment compared to BOB, the transition plot, given its low capacity to retain moisture by its soil. KOG also proved to be different from ANK, the wet forest plot, however statistical differences between ANK and BOB were not found. At a species level, our low level of repetition per species ($n = 3$) did not allow us to find statistical differences regarding $\Delta\Pi_o$. However, when observations were grouped at a plot level, KOG showed a higher degree of osmotic adjustment compared to the remaining two plots.

Using SLA and leaf vein density did not improve predictability of maximum osmotic adjustment. Even if these traits have been shown to be correlated with rapid NSC translocation, they did not explain much of the variance observed around $\Delta\Pi_o$. Similarly, Π_o had a very low power prediction over A_{sat} might be confounding the effect of NSC $_{\text{per se}}$ in photosynthesis with the inherent changes in Π_o in response to seasonal changes in soil moisture.

Leaf traits related to fast NSC translocation were found to have little power predicting NSC accumulation related to osmotic adjustment. Furthermore, the main variable explaining A_a was leaf N concentration, rather than NSC accumulation modulating photosynthetic feedback inhibition. Our results suggest that osmotic adjustment is indeed an active process by plants to regulate their Ψ_w at a leaf level. Consistent with these findings, this suggests that NSC accumulation in the leaf, derived from Π_o calculation *via* PV curves, is not the result of a passive process resulting from the lack of carbon demand caused water stress during the drought season, but rather an active strategy to acclimate to soil moisture shortage.

Acknowledgements

NR would like to thank the Chilean National Commission for Scientific and Technological Research (CONICYT) for his doctorate scholarship. The dataset used was funded with ERC GEM Traits (YM) and EU-Marie Curie Fellowship TipTropTrans (IO).

Chapter6

Are leaf non-structural carbohydrates (NSC) directly detectable with field spectroscopy?

Along this thesis, I have shown that non-structural carbohydrates play an important role in downregulating leaf photosynthesis. Nevertheless, there is a big gap in correlating leaf photosynthesis to leaf natural non-structural carbohydrates concentration. Whilst both are dynamic processes, only leaf photosynthesis can be tracked *in vivo*. In order to determine leaf non-structural carbohydrates concentration, leaves must be processed in the field to stop enzymatic activity, hence non-structural carbohydrates degradation. Only then, leaves can be taken to a facility to perform rather cumbersome chemical protocols for NSC determination.

In the last empirical chapter of this thesis I look at the use of leaf spectral footprint in determining leaf total, and fractions, non-structural carbohydrates concentrations. Even if leaf spectral signature has proven to be successful in determining key leaf chemical compounds, such as nitrogen and lignin, leaf non-structural carbohydrates determination remains an open question.

I did the fieldwork, collected the samples, did the chemical and statistical analysis and wrote the manuscript with the support of AS and YM. JMV and LG helped with the chemical analysis and provided comments on the manuscript. CD also provided

comments regarding the statistical analysis and the manuscript. This manuscript was submitted to *Journal of Geophysical Research - Biogeosciences*.

Are leaf non-structural carbohydrates (NSC) directly detectable with field spectroscopy?

Nicolas Raab[1*], Alexander Shenkin[1], Jordi Martínez-Vilalta[2,3], Christopher E. Doughty[4], Lucía Galiano[3], Yadvinder Malhi[1]

[1]Environmental Change Institute, School of Geography and the Environment, University of Oxford, Oxford, OX1 3QY, UK.[2]CREAF, Cerdanyola del Vallès, E-08193, Barcelona, Spain. [3]Universitat Autònoma de Barcelona, Cerdanyola del Vallès, E-08193, Barcelona, Spain. [4]School of Informatics, Computing and Cyber systems, Northern Arizona University, Flagstaff AZ, USA. [*]Corresponding Author: nicolas.raab@ouce.ox.ac.uk

Abstract

Non-structural carbohydrates (NSC) allow the exchange of energy from leaves to other organs and can be stored and spent during periods of stress. While NSC dynamics have garnered increased interest, direct NSC measurements are cumbersome and expensive. Field spectroscopy represents a quicker approach to quantify leaf NSC concentration *in vivo* and has been successfully applied across landscapes of tropical vegetation and crops. Whether spectroscopy can discern intraspecific differences in NSC concentrations within a site is an open question, given the decreased variation compared with multi-site studies. Here we assess if spectroscopy can measure leaf NSC concentrations across species within a single site with a limited cohort of species. We found that it is not possible to quantify NSC concentration within species using spectroscopy (soluble sugar fraction prediction ranged from 0.27 normalised root mean square error (NRMSE) for *Fagus sylvatica*, to 0.42 for *Acer pseudoplatanus*; for total NSC prediction ranged from 0.29 for *F. sylvatica* to 0.61 for *A. pseudoplatanus*). NSC predictability using spectroscopy improved when grouping all species, probably because of interspecific trait variation (for the soluble sugars fraction: NRMSE = 0.38 and 0.39 for total NSC). The visible spectrum (400-700 nm), associated with photosynthetic pigments, near-infrared (750-1400 nm), associated with specific leaf area, and short-wave infrared (2000-2500 nm), were the strongest predictors in our models. This study advises caution in regard to attempting to predict NSC from field reflectance spectra, as models may be confounded by NSC co-variation with other leaf traits that present a spectral footprint.

6.1 Introduction

Non-structural carbohydrates (NSC) in plants are synthesised in carbon source organs, mainly leaves, and then allocated to sinks in order to fulfil their respiration, growth, symbiont exchange, osmotic regulation, and storage needs (Hartmann and Trumbore, 2016). A plant's NSC pool is composed of two fractions: a soluble fraction comprised largely of glucose, fructose and sucrose. Whilst the two first ones arethe end product of the Calvin-Benson-Bassham cycle, sucrose is the most common carbohydrate translocated through the phloem; and a non-soluble fraction dominated by starch, which is employed for storage (Martínez-Vilalta et al., 2016). NSC are stored during periods when carbon supply *via* photosynthesis surpasses carbon demand. These reserves might be used in the long term to help the plant to cope with environmental stresses such as drought, shading, herbivory, pathogen attack, and fire (Cardoso et al., 2016; Chapin et al., 1990; Doughty et al., 2015; Martínez-Vilalta et al., 2016; O'Brien et al., 2014; Richardson et al., 2013). On a diurnal basis, NSC are accumulated in the leaf after their synthesis either to generate a sugar concentration gradient for long distance phloem transport (Dietze et al., 2014; Gamalei, 2007; Savage et al., 2017), or to sustain respiration and growth requirements overnight (Martínez-Vilalta et al., 2016; Smith and Stitt, 2007).

Understanding the changes in leaf NSC concentration is of paramount importance to better understand the dynamics of forest productivity (e.g., Cardoso et al., 2016; Doughty et al., 2015; O'Brien et al., 2014). To the extent that NSC concentrations in leaves tend to follow the same patterns that NSC concentrations in other organs such as stem and roots (O'Brien et al., 2014), foliage NSC detection could serve as a proxy of a plant's overall NSC status. In addition, leaf photosynthesis appears to be closely dependent on leaf NSC concentration (e.g., Franck et al., 2006; Lobo et al., 2015; Moore et al., 1999; Paul and Foyer, 2001), indicating that when leaves over-synthesise NSC, a sugar-induced photosynthetic feedback is triggered, thus restricting leaf carbon exchange and overall plant productivity (**Chapter 3**).

Measuring NSC concentration in plants is cumbersome and expensive, and impossible to do *via* chemical assays when *in vivo* measurements are required. Laboratory analyses require stopping enzymatic activity immediately after sample collection, thus entailing protein denaturation by field-based microwave processing or liquid nitrogen storage

(Richter et al., 2009). The labour and expense incurred in laboratory processing further hinders sample size (Quentin et al., 2015). Furthermore, NSC determination across different assays tends to yield different concentrations for the same sample, making absolute NSC concentration determination extremely challenging. These results also call for the use of NSC standards to facilitate inter-technique and inter-laboratory comparisons (Quentin et al., 2015; Richter et al., 2009).

Measuring NSC *via* spectral reflectance methods has been hailed as a potential solution to the challenges above. Laboratory infrared (IR) spectroscopy has been able to measure NSC concentration in dried and ground plant tissues (Batten et al., 1993; Curran, 1989; Quentin et al., 2017; Ramirez et al., 2015), indicating a predictable interaction between certain wavelengths and sugar molecules that constitute a plant's NSC pool. In particular, the bands between 500-700; 1400-1800 nm and 2000-2500 nm have proven to be highly correlated with NSC concentration in these studies.

Field spectroscopy has demonstrated its usefulness in determining leaf chemical properties and physical leaf traits (e.g., Asner et al., 2011; Doughty et al., 2017; Ourcival et al., 1999; Wu et al., 2017). Asner and Martin (2015) succeeded in correlating in-field leaf spectral signatures with NSC content in tropical trees distributed across different landscapes. The study focused on tropical and sub-tropical species, sampling leaves across a wide range of species and sites. A strong correlation between leaf spectra and soluble carbon concentration was found on both the 1300-1800 nm, and 2000-2450 nm bands, thus coinciding with wavelengths also associated with leaf NSC concentrations prediction in laboratory-based studies (e.g., Batten et al., 1993; Curran, 1989; Decruyenaere et al., 2012; Dreccer et al., 2014; Quentin et al., 2017; Ramirez et al., 2015; Yendrek et al., 2017). Furthermore, this predictive ability held when scaled up from the leaf to the tree-crown scale, thus paving the way to NSC detection with remote sensing (Asner et al., 2015).

The developments outlined above hold promise, yet some aspects of these techniques require closer examination. Firstly, Asner and Martin (2015) used neutral detergent fibre (NDF) and gravimetric difference *pre* and *post* washing in a fibre analyser to analyse leaf NSC content. This method allows users to process a large batch of leaf samples, but has not been documented in any other inter-methodology comparison for NSC determination (Quentin et al., 2015; Richter et al., 2009). Using a fibre analyser may miss non-soluble NSC fractions, and may include other soluble molecules such

as pigments, vitamins and proteins. Even if these molecules do not represent a large fraction of leaf's carbon soluble content, the contamination by pigments, and other soluble compounds, risks mistaken spectral correlation with NSC if those compounds present a spectral signature themselves (Curran, 1989). Secondly, when the focus is determining NSC across species, as is often the case in large-scale studies, purported NSC detection *via* leaf spectroscopy may in fact be due to detection of other leaf chemical and physical traits that co-vary with NSC synthesis and storage, such as leaf nitrogen concentration and specific leaf area (SLA). NSC detection in the visible spectrum is associated with leaf investment in photosynthetic pigments (Richardson et al., 2002), whilst the near and short-wave IR spectrum are usually correlated with SLA (Asner and Martin, 2015; Doughty et al., 2017; Ourcival et al., 1999). Correlating leaf spectral footprint at a landscape scale, thus accounting for a large variation of leaf traits, might be useful to assess the general NSC status of a particular site. However, if the goal is to measure daily, or seasonal, leaf NSC dynamics (therefore avoiding destructive leaf sampling), confounding NSC prediction with leaf trait determination via spectroscopy could lead to misleading results and interpretation. It is therefore important directly test whether the spectral signatures identified as being associated with NSC concentrations reflect real changes in NSC concentrations over time.

In this paper we explore the potential for direct detection of leaf NSC concentration *via in vivo* field spectroscopy, and the extent to which inter-specific variation in leaf traits may confound this potential. We focus on four temperate European species: *Acer pseudoplatanus* (sycamore), *Quercus robur* (European oak), *Fagus sylvatica* (beech), and *Fraxinus excelsior* (ash). By having 40-60 replicates per species, we aim to: *i*) test whether spectral signatures derived from field spectroscopy can predict total NSC content or specific NSC components (i.e., monosaccharides, sucrose, soluble sugars, and starch), *ii*) assess whether the most predictive spectral regions vary for different NSC components, and *iii*) identify the likely interferences due to other structural and biochemical traits that co-vary with NSC concentrations (e.g., chlorophyll concentration or SLA).

6.2 Materials and Methods

6.2.1 Site description and sample collection

Leaf samples were collected in Wytham Woods (51°46′ N; 1°20′ W), a mature woodland located in Oxfordshire, UK, at 160 m.a.s.l. At this site mean annual temperature is 10.1 °C with an average total annual precipitation of 730 mm (Thomas et al., 2010). Bud break starts at the end of March, whilst canopy full deployment is in late April-early May. Senescence (50% of canopy changing colour) occurs between mid and end of October. The woodland is dominated by temperate broadleaf species, mainly *A. pseudoplatanus*, *Betula pendula*, *Q. robur*, *F. sylvatica*, and *F. excelsior*.

Samples were collected over seven days, from early August to mid-September 2016, generally between 11:00 and 16:00 hours. Mature and healthy leaves of *A. pseudoplatanus*, *Q. robur*, *F. sylvatica* (60 leaves each), and *F. excelsior* (40 leaves) were harvested across five individuals of each species. Leaves were sampled at 1.8-2.2 m heights from trees bordering forest gaps, that at the time of collection were fully sunlit. Leaves were immediately transported to a field laboratory [within three minutes] for spectroscopy measurements to avoid leaf desiccation.

6.2.2 Spectral measurements

In vivo spectroscopy measurements were made with a field spectrometer (QualitySpec Trek, ASD, Boulder, CO, USA), using a magnetic leaf contact probe with an absorbing black target provided with the instrument to measure reflectance. The instrument automatically optimises measurements by calibrating itself with both white and black internal references every 20 measurements. Reflectance was measured across wavelengths from 350 to 2500 nm at a 1 nm resolution, however, only wavelengths from 400 nm onwards were used in the analysis. Measurements were always taken on the mid right side of the leaf, avoiding veins (primary veins in all cases, and secondary veins when the size of the leaf/leaflet allowed it). After measurements were completed, the leaves were placed in liquid nitrogen to stop NSC metabolism, and then transported to the laboratory and transferred from the field liquid nitrogen dewar to a laboratory freezer and stored at −20 °C prior to chemical analysis.

6.2.3 Non-structural carbohydrate measurements

Non-structural carbohydrate concentration was determined by enzymatic method adapted from (Hoch et al., 2002) on a microplate absorbance reader (Sunrise Absorbance Reader, Tecan, Männedorf, Switzerland) by accounting for the difference between NAD^+ and NADH absorbance at 340 nm. 10 mg of leaf ground powder was mixed with 1.6 ml of distilled water, vortexed for 10 s, and steamed for 1 hour. Vial content was mixed, and 700 µL was transferred to a new vial and set aside. Original vials were centrifuged for 15 minutes, from which 20 µL aliquots were extracted and mixed with isomerase (Phosphoglucose isomerase from baker's yeast (*S. cerevisiae*, Sigma-Aldrich)) for conversion from fructose to glucose, hexokinase (Glucose assay reagent, Sigma-Aldrich), and glucose-6-phosphate dehydrogenase (Glucose assay reagent, Sigma-Aldrich). Sucrose was measured by mixing aliquots with invertase (invertase from baker's yeast (*S. cerevisiae*, Sigma-Aldrich)) for sucrose hydrolysis, and following the beforementioned method for monosaccharides determination. Reserved vials were mixed with amyloglucosidase (Amyloglucosidase from *Aspergillus niger*, Sigma-Aldrich) and put in a water bath at 50 °C overnight for starch to break down into glucose. The next day, aliquots were mixed using glucose assay reagent kit (see above) and starch content was obtained by subtracting sample's original soluble sugar concentration.

In every assay, glucose, fructose, sucrose and starch standards (Sigma-Aldreich) were added to the microplate in order to ensure the effectiveness of the enzymatic reaction, and to test the quantitative recovery of these standards. All results are expressed as percentage of leaf dry matter content (%).

6.2.4 Data filtering, chemometrics, and statistical analysis

6.2.4.1 Partial least square regression

Partial least squares regression (PLSR) (Wold et al., 2001) was used to establish the relationship between leaf spectral reflectance and NSC concentration. PLSR analysis was performed with the *plsregress* function in Matlab R2015b (Natick, MA, USA). PLSR generates latent vectors (components) as predictors. In order to avoid model overfitting, we used full cross validation and selected the number of components to

include in the final model such that the predicted residual error sum of squares (PRESS) was minimal (Duckworth, 1998). We did so by calculating PRESS for each iteration forcing the *plsregress* function to use from 1 to 50 components, and then selecting the number of latent vectors which yielded the minimal PRESS, which was calculated as:

$$\text{PRESS} = \sum_{i=1}^{n} (Cp_{i,-i} - C_i)^2 \tag{6.1}$$

where n is the total number of samples, i is the observation removed and tested against during the i^{th} full cross-validation trial, Cp is PLSR's predicted concentration and C is the known NSC concentration.

To check for faulty field measurements, we compared Cp_i and C_i. If the difference between Cp_i and C_i was more than 100% and more than 60% of reflectance on the IR spectrum (700-2500 nm) fell outside ± 1 standard deviations from the species reflectance mean, the sample was excluded from the data set and the PLSR was re-run. IR reflectance has proven to be best correlated with NSC (Asner and Martin, 2015; Batten et al., 1993; Curran, 1989; Decruyenaere et al., 2012; Dreccer et al., 2014; Quentin et al., 2017; Ramirez et al., 2015; Yendrek et al., 2017).

In order to evaluate if leaf reflectance provides a direct estimate of NSC concentrations, and that NSC concentrations are not being indirectly derived from covariance with other leaf traits, we ran PLSR models at two levels: firstly, we ran a PLSR with all the collected data categorised per species, and secondly, we ran a separate PLSR for each species.

6.2.4.2 Assessing model performance

We assessed model performance using two similar methodologies, *i*) using a full cross validation derived from Eq. 6.1 (in each iteration taking one sample out), and *ii*) an independent validation by sub-sampling 70% of the data randomly to train the model, and then using the remaining 30% to determine model accuracy. In both cases model accuracy was calculated as the normalised root mean square error (NRMSE):

$$\text{NRMSE} = \frac{\sqrt{\frac{\sum_{i=1}^{m}(Cp_i - C_i)^2}{m}}}{\bar{C}} \tag{6.2}$$

where m is the number of samples of the validation set and $\bar{C}$ its average concentration. In the case of the independent validation, this procedure was repeated 50 times in order to determine PLSR weights and RMSE means, together with their corresponding uncertainties. Subsequently, we measured model performance at two levels, *i*) PLSR run with all the data (across species), and *ii*) PLSR run at species level.

6.3 Results

6.3.1 Leaf reflectance and non-structural carbohydrates across species

We found little variation of leaf reflectance within and between species in the visible spectrum Fig. 6.1. Larger variation between species was observed in the near IR region (NIR) (700-1400 nm). However, in the short-wavelength IR (SWIR) region (1400-2500 nm) all species showed similar reflectance except *F. sylvatica*, which had higher values than the remaining three species. Statistical difference between species reflectance is shown in Supplemental Material (6.6).

Overall, soluble sugar exhibited higher concentrations than starch across species (Fig. 6.2). The soluble sugar fraction was dominated by monosaccharides (glucose and fructose), whereas sucrose concentrations were small by comparison. All obtained NSC

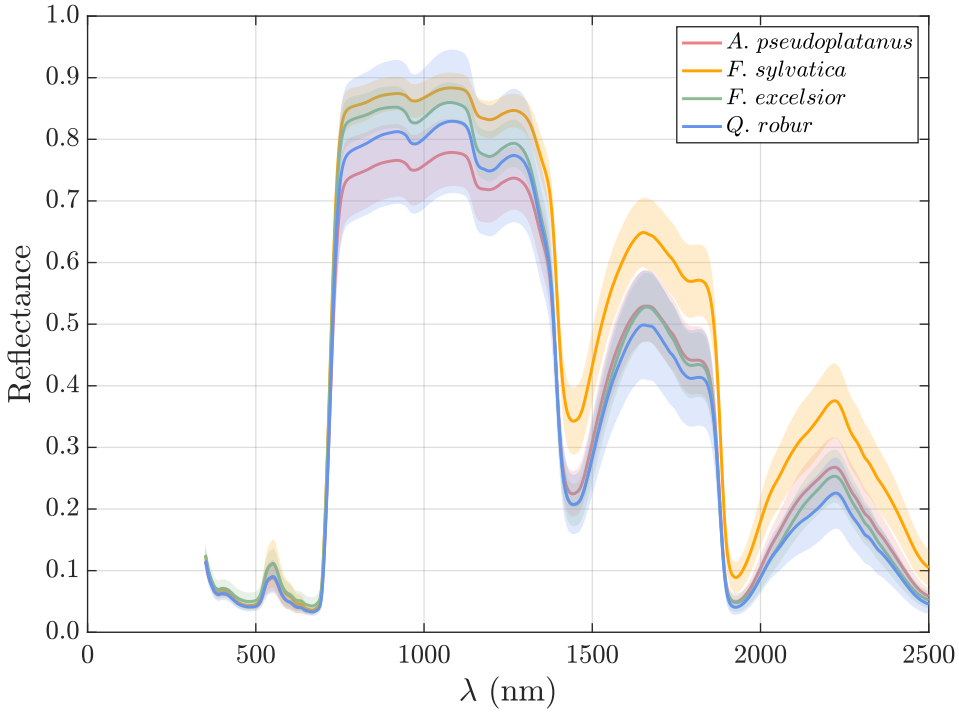


Figure 6.1: Leaf reflectance of *Acer pseudoplatanus*, *Fagus sylvatica*, *Quercus robur* ($n = 60$ each), and *Fraxinus excelsior* ($n = 40$) for each wavelength (λ). Solid lines represent the average reflectance of each species whilst the coloured area represents ± 1 standard deviation from the mean.

concentrations present wide distributions, indicating large variation of all NSC fractions, which is useful in order to improve PLSR given the broad range of concentrations available to train the model.

6.3.2 Predicting non-structural carbohydrates concentration across species

PLSR predicted total NSC concentration and its different fractions across species with different levels of accuracy (NRMSE), and precision (r^2 between predicted and observed concentrations) (Fig. 6.3). Although the relationship between a leaf's spectral signature and total NSC and NSC fractions proved to be significant ($P < 0.05$ in all cases), model predictability was only moderately good for the soluble sugars fraction (NRMSE = 0.38 and $r^2 = 0.46$), whereas accuracy and precision were low for total NSC (NRMSE = 0.45, $r^2 = 0.19$) (Fig. 6.3 and 6.5). Similarly, the independent validation (training the model with 70% of the data in order to predict the remaining 30%) indicated that

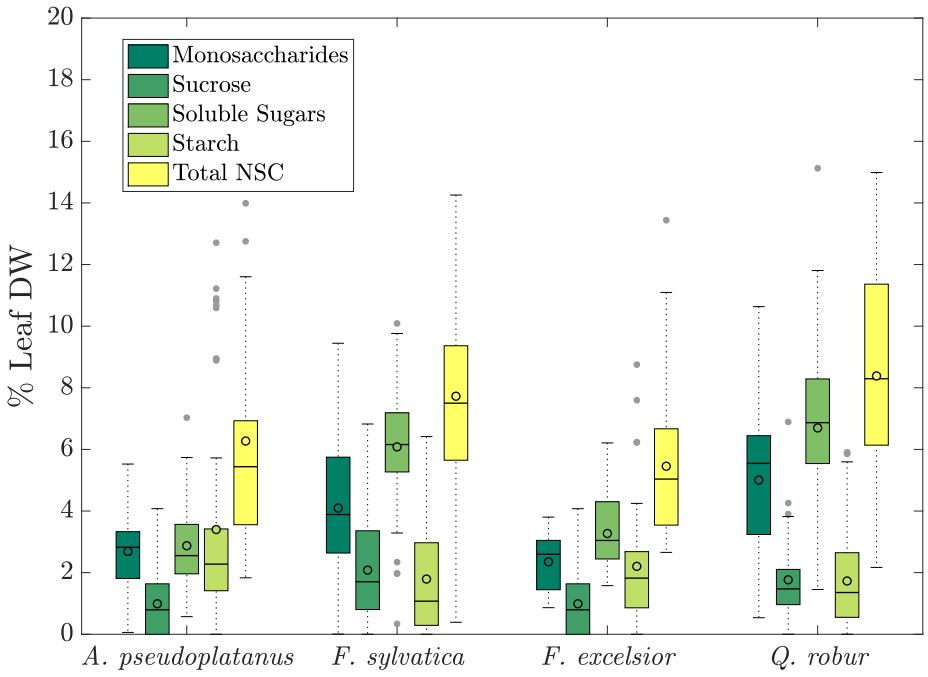


Figure 6.2: Box plot of leaf non-structural carbohydrates (NSC) partitioning for *Acer pseudoplatanus*, *Fagus sylvatica*, *Fraxinus excelsior* and *Quercus robur*. Monosaccharides correspond to both glucose and fructose, soluble sugars are both monosaccharides and sucrose concentrations. Total NSC correspond to the addition of soluble sugars and starch. Samples were collected between August and September 2016. Concentrations are expressed as % of leaf dry weight content.

the soluble sugars fraction was most accurately predicted (NRMSE = 0.39 with 10 components), followed by total NSC (NRMSE = 0.48 with 10 components) (Table 6.1). Secondly, the monosaccharides fraction, which dominates the soluble sugar fraction, presented a NRMSE of 0.49 (r^2 = 0.25); whilst model performance for sucrose and starch was clearly insufficient, with NRMSE values of 0.80 (r^2 = 0.26) and 0.98 (r^2 = 0.13), respectively (Supplemental Material 6.4), whilst for the independent validation the sucrose fraction achieved a NRMSE of 0.80 with 5 components (Table 6.1).

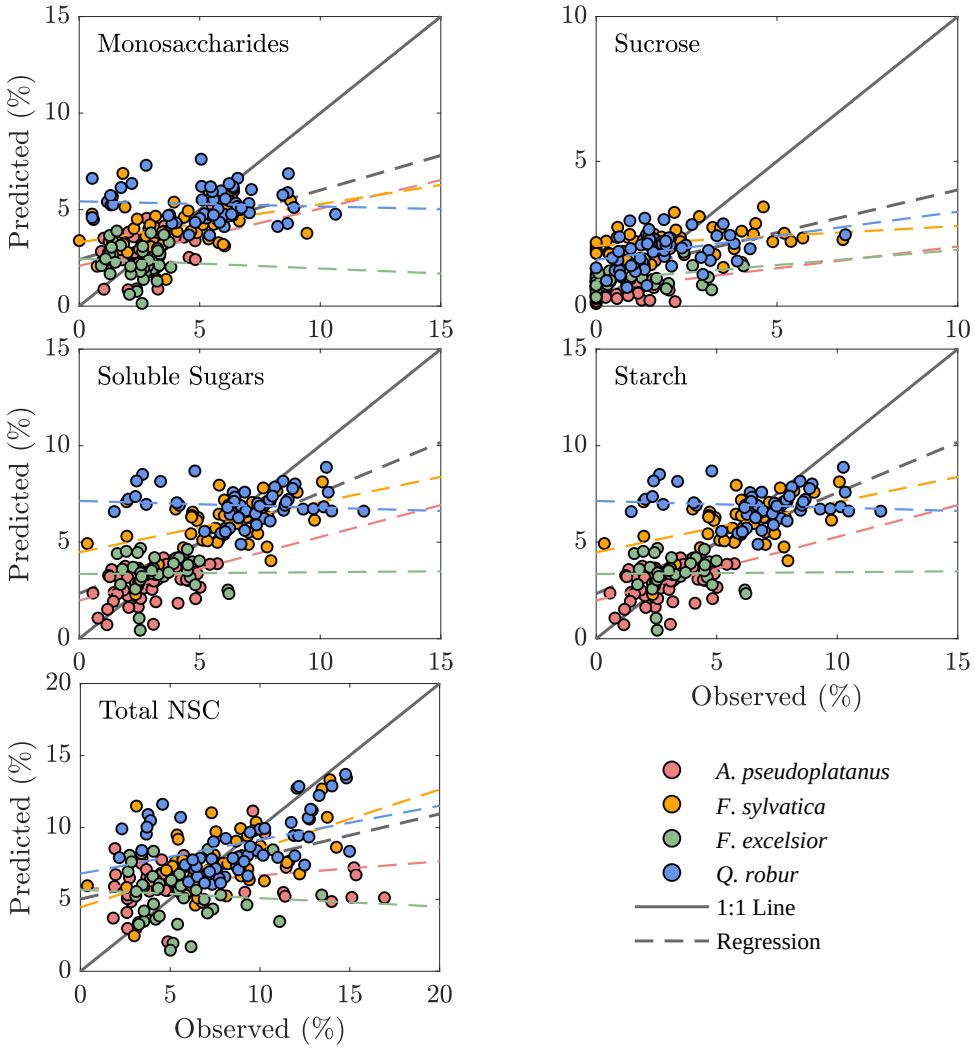


Figure 6.3: Observed and predicted values across *Acer pseudoplatanus*, *Fagus sylvatica*, *Fraxinus excelsior* and *Quercus robur* by partial least square regression using full cross validation procedure. Each panel represents a different fraction of the total non-structural carbohydrates fraction (NSC). The solid line represents a 1 to 1 relationship whilst dashed lines represent the regression for each species.

Table 6.1: General statistics of predicted values by partial least square regression (PLSR) trained with a random subset of 70% of the data and compared with the remaining 30% for 50 iterations. Mean parameters for each sugar fraction and total non-structural carbohydrates (NSC) are shown together with standard deviations, minimum and maximum values. NRMSE is the normalised root mean square error coefficient of variation, r^2 is the coefficient of determination between observed and predicted values by the model, and number of components corresponds to the number of vectors used for the PLSR.

	NRMSE				r^2				Number of Components			
	Mean	St. Dev.	Min	Max	Mean	St. Dev.	Min	Max	Mean	St. Dev.	Min	Max
Monosaccharides	0.50	0.05	0.35	0.64	0.26	0.09	0.08	0.41	10	1.9	5	19
Sucrose	0.81	0.09	0.62	1.05	0.27	0.08	0.08	0.41	5	1.0	5	10
Soluble Sugars	0.39	0.05	0.29	0.52	0.45	0.09	0.24	0.64	10	1.7	7	15
Starch	1.03	0.09	0.88	1.26	0.06	0.04	0.00	0.17	7	5.3	1	16
Total NSC	0.48	0.06	0.35	0.65	0.14	0.07	0.01	0.34	10	4.2	5	20

When predictions were grouped at a species level to assess if some species presented better model fits, only *F. sylvatica* soluble sugar fraction and total NSC concentrations presented relatively low NRMSE: 0.28 and 0.34; respectively, compared to the rest of the sampled species (Supplemental Material 6.4).

6.3.3 Inter-specific effects on non-structural carbohydrate prediction

When running PLSR at a species level, rather than aggregating all the species together and then categorising per species, results were mixed. PLSR predictions of all NSC fractions, except sucrose, were significant in *F. sylvatica*. Predictions of sucrose, starch, were significant in *Q. robur*. In *A. pseudoplatanus*, only monosaccharides and soluble sugars predictions were significant whilst in *F. excelsior* we failed to encounter any significant relationship between observed and predicted values for any of the NSC fractions. Notably, our models were insensitive to the substantial large variation in both soluble sugars and total NSC that was observed in *Q. robur* leaves (Fig. 6.4). Only *F. sylvatica* showed good correlations between observed and predicted concentrations for the non-soluble fraction and total NSC. Fig. 6.4 shows that lower NRMSE were obtained by monosaccharides in *A. pseudoplatanus* (0.32; $r^2 = 0.30$) (Supplemental Material 6.5), soluble sugar and total NSC in *F. sylvatica*, 0.27 ($r^2 = 0.27$) and 0.29 ($r^2 = 0.49$) respectively (Fig. 6.4; Supplemental Material 6.5). Although Fig. 6.4 shows a correct fitting for starch in *Q. robur*, NRMSE of the model is 0.73. Generally, all PLSR exhibit a low number of components, accompanied with poor model performance, except for *F. sylvatica* where the number of vectors used for the PLSR ranges from 4 to 9.

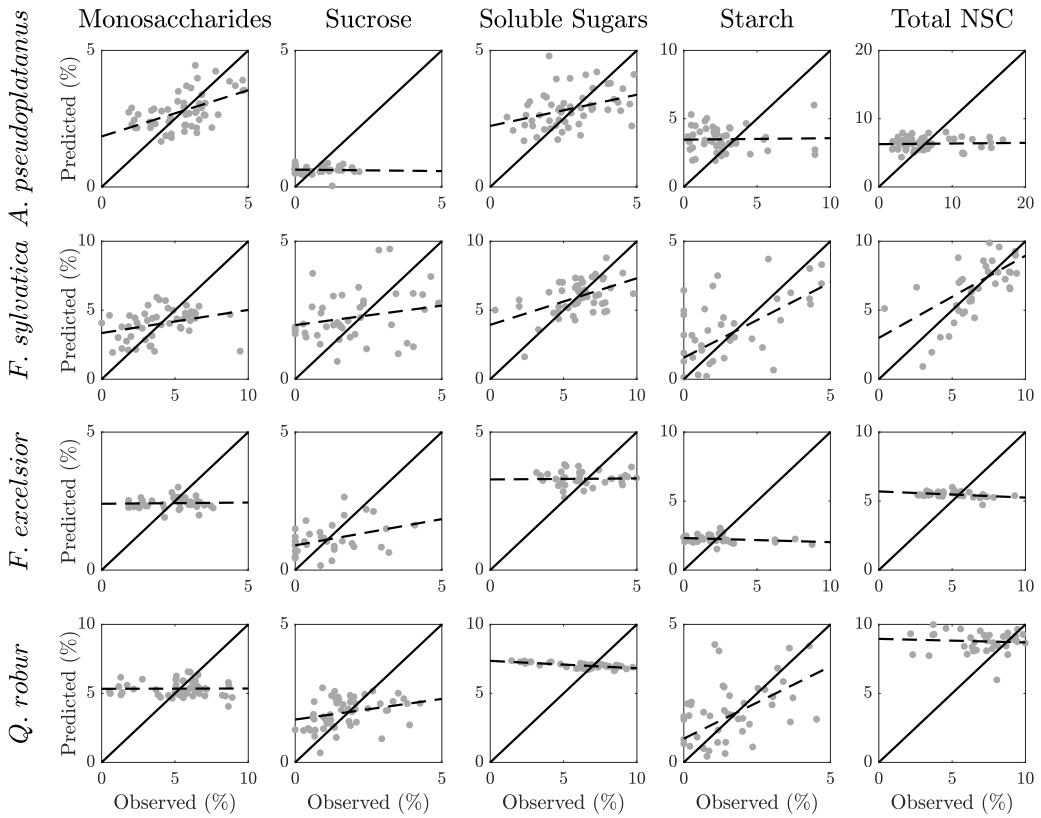


Figure 6.4: Observed against predicted concentrations, as percentage (%) of leaf dry matter content, by partial least square regression per species, using a full cross validation. Each panel represents a non-structural carbohydrates (NSC) fraction, or total NSC for each species sampled. Dashed lines correspond to the linear regression whilst solid lines represent a 1 to 1 relationship.

When validating the model at a species level using a random independent dataset (30% of the total number of samples per species), model performance was even poorer (Table 6.2). Every NSC fraction, in every species, presented poor agreement between observed and predicted data, with large variations between minimum and maximum NRMSE, r^2 and number of components within the ensemble of iterations. All mean NRMSE for NSC fractions across species were above 0.30, thus demonstrating a low capacity of leaf optical properties to predict total NSC and its different fractions.

Table 6.2: General statistics of predicted values by partial least square regression (PLSR) trained with a random subset of 70% of the data and compared with the remaining 30% for 50 iterations at a species level. Mean parameters for each sugar fraction and total non-structural carbohydrates (NSC) are shown together with standard deviations, minimum and maximum values. NRMSE is the normalised root mean square error, r^2 is the coefficient of determination between observed and predicted values by the model, and number of components corresponds to the number of vectors used for the PLSR.

	NRMSE				r^2				Number of Components			
	Mean	St. Dev.	Min	Max	Mean	St. Dev.	Min	Max	Mean	St. Dev.	Min	Max
A. pseudoplatanus												
Monosaccharides	0.34	0.06	0.21	0.54	0.26	0.17	0.00	0.69	4	4.0	3	18
Sucrose	1.18	0.29	0.73	2.15	0.07	0.11	0.00	0.53	3	2.7	1	10
Soluble Sugars	0.45	0.09	0.30	0.73	0.23	0.17	0.00	0.70	3	1.7	2	13
Starch	1.01	0.22	0.71	1.88	0.08	0.09	0.00	0.37	3	3.4	1	19
Total NSC	0.64	0.15	0.34	1.19	0.10	0.13	0.00	0.70	3	3.6	1	21
F. sylvatica												
Monosaccharides	0.57	0.15	0.32	0.87	0.13	0.12	0.00	0.43	5	3.9	1	19
Sucrose	0.91	0.22	0.54	1.48	0.06	0.10	0.00	0.62	4	3.6	1	16
Soluble Sugars	0.32	0.08	0.22	0.63	0.21	0.16	0.00	0.56	7	3.7	1	19
Starch	1.10	0.42	0.58	2.33	0.29	0.20	0.00	0.70	9	3.3	1	17
Total NSC	0.35	0.10	0.19	0.58	0.43	0.24	0.01	0.87	9	2.1	3	15
F. exelsior												
Monosaccharides	0.37	0.10	0.16	0.75	0.11	0.11	0.00	0.47	2	1.0	1	7
Sucrose	1.09	0.48	0.62	3.20	0.20	0.19	0.00	0.86	3	2.2	2	12
Soluble Sugars	0.39	0.09	0.22	0.75	0.11	0.14	0.00	0.60	2	1.4	1	9
Starch	0.96	0.27	0.56	2.22	0.08	0.13	0.00	0.75	1	1.1	1	8
Total NSC	0.46	0.10	0.26	0.66	0.09	0.14	0.00	0.58	1	0.2	1	2
Q. robur												
Monosaccharides	0.44	0.10	0.27	0.81	0.07	0.09	0.00	0.38	2	2.6	1	19
Sucrose	0.66	0.14	0.41	0.90	0.13	0.14	0.00	0.58	3	0.8	2	8
Soluble Sugars	0.38	0.10	0.20	0.74	0.09	0.11	0.00	0.43	1	1.4	1	9
Starch	0.92	0.22	0.62	1.71	0.24	0.15	0.00	0.52	8	4.2	1	20
Total NSC	0.43	0.10	0.28	0.81	0.05	0.10	0.00	0.64	3	3.0	1	11

6.3.4 Spectral Weights

Since the soluble sugar fraction and total NSC presented the highest agreement between observed and predicted concentrations, the respective spectral weights for each wavelength are shown in Fig. 5. The larger the deviation from zero, both negative and positive, the higher is the importance of a determined wavelength on predicting the variable of interest. Spectral weights for soluble sugar present high and low peaks in the visible spectrum (400 to 450 nm). Other peaks were registered in the NIR region (750-850 nm), near 1300 nm; 1700 nm; and in the 2300 to 2500 nm region. Total NSC, similarly to the soluble sugar fraction, presented peaks between the 400 and 450 nm, with notably high deviation from 0 nearby 1000 nm; 1300 nm; 1700 nm; and in the 1800 to 2500 nm region.

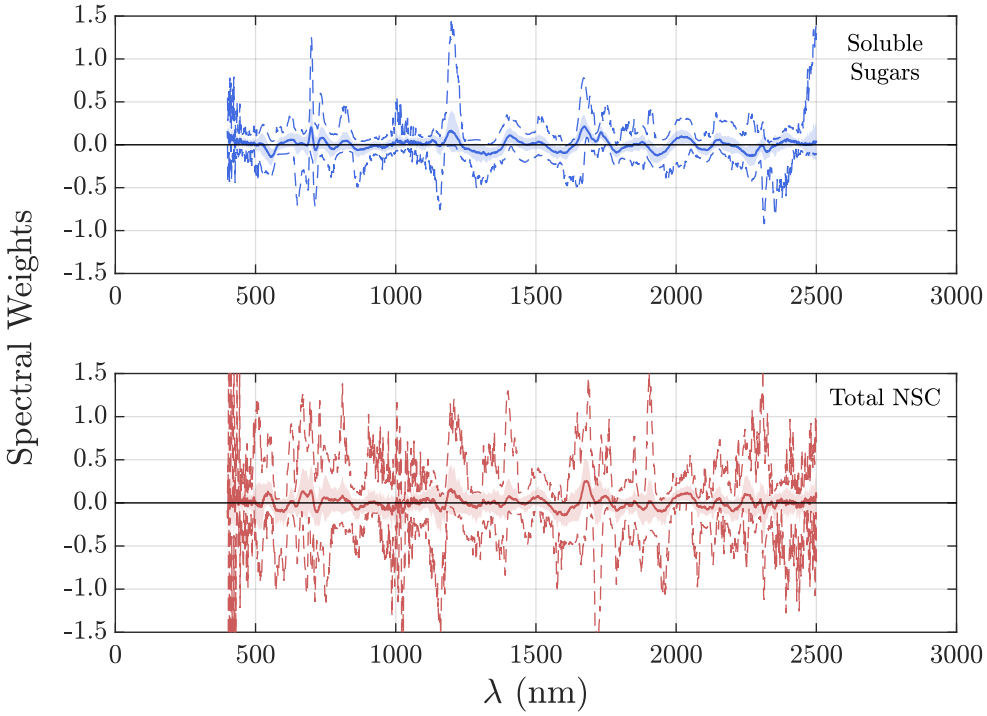


Figure 6.5: Spectral weights for the soluble sugars fraction and total NSC. The solid line represents the mean of 50 iterations with 70% of the data set, the coloured area represents ±1 standard deviation from the mean. The dashed lines represent maximum and minimum weights observed for the 50 iterations. The further the trend deviates from zero, the higher is the contribution of a specific spectral region to NSC prediction.

6.4 Discussion

6.4.1 Temperate woodland non-structural carbohydrates dynamics in leaves

Foliar fraction and total NSC concentrations in our study are representative of other NSC concentrations reported in leaves of temperate species in the literature. Measured NSC concentration in leaf tissues were similar to concentrations obtained by Hoch et al. (2003) for northern hemisphere temperate broadleaf species sampled in August - September. They found concentrations of total NSC of 10% in *Acer* whilst the bulk of our observations ranged from 2 to 12% with a mean of 6% for the same period (Fig. 6.2). Values of total NSC for *F. sylvatica* and *Q. robur* were somewhat lower than those reported by Hoch et al. (2003) for the same time window, as they found values close to 15% whilst the gross of our measurements ranged between 6 and 10%, with

a mean of total NSC concentration of 8% for both species (Fig. 6.2). Differences can be attributed to site-specific nutrient availability, together with genetic variations or year-specific abiotic conditions. In addition, the fact that Hoch et al. (2003) had access to the top of the canopy, while we collected leaves from the bottom that were fully sunlit at the time of collection, may also affect the comparison. Nutrient investment in photosynthetic machinery, hence NSC synthesis and possibly stock, has been shown to decrease with canopy height (Field and Mooney, 1986), thus possibly explaining our relatively lower values. Moreover, source to sink carbon imbalance has been shown to increase NSC concentrations in leaves in temperate ecosystems (Körner, 2003, 2006; Zotz et al., 2005). Furthermore, Quentin et al. (2015) warn about comparing NSC concentrations between different laboratories and techniques. Nevertheless, the NSC concentration distribution found in our samples falls within the observed range in NSC global compendia. Martínez-Vilalta et al. (2016) found that most of the soluble sugars concentrations in leaves for winter deciduous species range between 5 and 9%, whilst total NSC range from 5 to 12% with means around 7 and 10%, respectively. Bazot et al. (2013) found total NSC concentrations in *Quercus* in France averaged 7% for September, whilst Li et al. (2016) found similar total NSC concentrations in leaves of temperate forest in China.

6.4.2 Leaf chemometric determination through optical properties

Our analysis, both for the full cross validation and the independent validation set, showed that model performance differed among NSC fractions. When comparing observed against predicted concentrations by PLSR, only the soluble sugars fraction exhibited reasonably good agreement, with a NRMSE of 0.38. Curran (1989) describes that spectral regions between 1300 and 1800 nm, and especially the one between 2000 and 2450 nm, have proven to be of an especial interest given the stretching of O-H bonds, particularly abundant in carbohydrates, at these wavelengths. Our data shows that this effect is only true for the soluble sugar fraction, and does not hold for carbohydrate polymers, such as starch, which may interact with light in a different manner. Furthermore, Quentin et al. (2017) also found low predictability by spectroscopy when it comes to determine starch concentration in dried-ground leaves of *Eucalyptus globulus*.

Sucrose exhibited the second largest error, indicating that spectroscopy, at least in the range of wavelengths under consideration, cannot discriminate between the different

types of carbohydrates that compose the soluble sugars fraction. Nevertheless, Yendrek et al. (2017) succeeded in determining sucrose concentration in leaves of maize using field leaf spectroscopy. The soluble sugars fraction showed best agreement between measured and estimated concentrations for both the full cross validation and independent validation (Fig. 6.3 and Table 6.1). This is in concordance with Asner and Martin (2015), who found that leaf reflectance could be used to determine NSC concentration, although their NSC extraction method only accounts for soluble sugars and does not discriminate between the different fractions that comprise the leaf NSC pool.

When including all species, our model yielded substantial error for the soluble sugars fraction (NRMSE = 0.39) and even larger uncertainty for total NSC (NRMSE = 0.48) using the independent validation approach (Table 6.1). Asner and Martin (2015) found errors of 14% using field leaf spectroscopy to predict what they claim is total NSC, whilst Yendrek et al. (2017) found NRMSE of 0.2 to quantify sucrose in maize using the same technique, although their concentrations are expressed based on leaf area ($\mu mol_{suc}\, cm^{-2}$), thus already accounting for the effect of SLA detection by spectroscopy (Asner et al., 2009, 2011; Doughty et al., 2017; Ourcival et al., 1999). Dreccer et al. (2014) obtained similar errors (NRMSE = 0.15) when determining the soluble sugars fraction using canopy spectroscopy and only a limited range of wavelengths for their calibration. Nevertheless, Ramirez et al. (2015), similarly to our study, found errors of up to 37% when predicting total NSC in dried-ground leaves using laboratory spectroscopy.

When analysing PLSR at a species level, leaf optical properties had a low capacity to predict NSC concentrations, except for *F. sylvatica*, with a NRMSE of 0.27 obtained by full cross-validation. At the species level, poor predictability could mostly be associated with low number of observations to calibrate the PLSR; however, similar results were observed when calibrating PLSR with the whole dataset and then categorised per species (Supplemental Material 6.4). With 25 leaves samples, Ramirez et al. (2015) found errors closer to 40%. On the other hand, model accuracy was higher in Dreccer et al. (2014) ($n = 345$) and Asner and Martin (2015) ($n = 6136$) by measuring a larger number of samples. Nevertheless, with 61 samples Yendrek et al. (2017) succeeded at quantifying sucrose content in maize with relatively low error (NRMSE = 0.20).

6.4.3 Causes of relatively poor non-structural carbohydrates predictability from spectral measurements

Most studies aiming at correlating leaf optical properties with NSC concentration have found a high contribution of NIR (750-1400 nm) and SWIR (1400-2500 nm) (Table 6.3). Are these spectral regions specific to NSC or do they correlate with other leaf traits that might covary with leaf NSC concentration?

NSC concentrations correlate with leaf photosynthetic capacity (Dreccer et al., 2014), which present high collinearity with other traits such as nitrogen concentration and SLA, in accordance with the leaf economics spectrum (Díaz et al., 2016; Niinemets and Sack, 2006; Wright et al., 2004). Li et al. (2016) found that NSC concentration in plants have little correlation with spatial patterns along a large latitudinal gradient in China, but showed high dependency on plant functional types, thus suggesting that NSC dynamics are highly synchronised with plant traits that translate into photosynthetic capacity rather than environmental variables such as radiation, water stress and temperature. Batten et al. (1993) also found high correlation between nitrogen concentration, a leaf trait that is a good predictor of leaf's photosynthetic capacity, and starch in both rice and wheat shoots. Furthermore, Asner et al. (2015) found that leaf reflectance wavelengths associated to leaf NSC content were negatively correlated to other traits with optical properties, such as leaf cellulose and lignin content, thus indicating co-variation of leaf NSC concentration with other leaf traits that can be derived from leaf spectroscopy. When studying temperate vegetation in the Northern hemisphere, Ourcival et al. (1999) and Serbin et al. (2014) found that the 500-2500 nm region was a good predictor for SLA, a region that has shown a high NSC predictive power across all studies presented in Table 6.3. More specifically, Asner et al. (2011) and Doughty et al. (2017) found high contribution of the 700-1100 nm region for SLA determination, similar regions encountered by Curran (1989) and Asner and Martin (2015) when trying to predict leaf NSC with spectroscopy.

Table 6.3: Comparison of several studies aiming to predict tissue non-structural carbohydrates (NSC) from spectroscopy. The table shows spectral regions that have shown to be most relevant in NSC detection.

Reference	Vegetation	Spectral Method	Absorbance Vs Reflectance	NSC fraction	Spectral Region (nm)
Curran (1989)	Crop compendium by the United State Department of Agriculture (USDA)	Laboratory spectroscopy of dried and ground leaves	Absorbance	Starch	970 - 990 1200 1450 1530 - 1780 1900 - 1960 2000 2080 - 2100 2250 - 2280 2320
				Soluble Sugars	1450 1490 1580 1780 1960 2080 2270
Batten et al. (1993)	Rice	Laboratory spectroscopy of dried and ground shoots	Reflectance	Starch	1734 1778 2310 2348
	Wheat				1778 1818 2100 2310
Decruyenaere et al. (2012)	*Rumex obtusifolius*	Laboratory spectroscopy of dried and ground roots	Absorbance	Soluble Sugars	1174 1450 1720 2482
				Starch	1594 2134 2278 2310
Dreccer et al. (2014)	Wheat	Canopy Spectroscopy	Reflectance	Soluble Sugars	520 - 560 753 - 758 1960 926 - 928 1110 - 1150
Ramirez et al. (2015)	Temperate and tropical species	Laboratory spectroscopy of dried and ground tissues from different organs	Reflectance	Soluble Sugars	1740 - 1800
				Starch	1440 1740 - 1800 2000 - 2600
				Total NSC	1740 - 1800 2100 - 2300 2410 - 2490
Asner and Martin (2015)	Tropical and subtropical species	Leaf spectroscopy	Reflectance	Soluble Sugar	1300 - 1800 2000 - 2450
		Canopy Spectroscopy			700 - 720 1500 - 2300
Yendrek et al. (2017)	Maize	Leaf spectroscopy	Reflectance	Sucrose	500 - 780 1300 - 1500 2000 - 2400
Quentin et al. (2017)	*Eucalyptus globulus*	Laboratory spectroscopy of dried and ground leaves	Reflectance	Glucose	1898 - 2000 2257 - 2320
				Fructose	1895 - 1897 2257 - 2320
				Sucrose	1923 - 1930 2190 2257 - 2320

The studies presented in Table 6.3 might be confounding NSC detection with detection of other traits that covary with the former (Curran, 1989). Even if our total number of samples (200 paired leaf spectral and NSC measurements) is comparable to other studies, except for Asner and Martin (2015) (see above), variation regarding leaf traits in our study can be regarded as low as we sampled only four species. By sampling leaves across a canopy profile in a temperate forest, Serbin et al. (2014) found large SLA variation within individuals (hence nitrogen concentration on an area basis). Nevertheless, because we sampled at the same height and within a limited number of individuals per species, we expect that our dataset shows relatively low intra-specific variation in traits such as SLA or leaf nitrogen concentration. Since NSC have tight collinearity with other traits that exhibit optical properties (Batten et al., 1993; Yendrek et al., 2017), predicting species from a limited trait cohort can be challenging.

Researchers have succeeded in measuring NSC in single species of agricultural value, such as soluble sugars in wheat (Dreccer et al., 2014) and sucrose in maize (Yendrek et al., 2017), using both canopy and leaf reflectance. However, the contribution of the visible spectrum to the model is high in these cases. Dreccer et al. (2014) found high contribution of the 350 to 988 nm region, which is highly correlated with photosynthetic pigments. Similarly, Yendrek et al. (2017) found high contribution of the 450 to 1400 nm region, that was closely related to both leaf's chlorophyll content and carboxylation capacity. Moreover, Yendrek et al. (2017) found good predictability of sucrose content on the 1450 to 2400 nm region, that also proved to be highly correlated with SLA according to their study. Furthermore, Dreccer et al. (2014) sampled wheat leaves at different developmental stages. Sampling leaves at different ages has shown to change both leaf optical and physiochemical traits (Chavana-Bryant et al., 2017), therefore even by sampling only one species, Dreccer et al. (2014) might had access to a large cohort of leaf traits, thus improving leaf NSC predictability with spectrophotometry. Moreover, Dreccer et al. (2014) and Yendrek et al. (2017) studied spectroscopy in plants grown under low and high nitrogen, thus contributing to leaf trait, and hence spectral, variability.

Low intra-specific trait variation, and correspondingly low spectral variability likely explained why the number of PLSR components computed at species level was low for all species *A. pseudoplatanus*: 3; *F. excelsior*: 2; *Q. robur*: 1) except for*F. sylvatica* (7), which in turn exhibited the best agreement between observed and predicted data (Table 6.2). This is supported by the fact that *F. sylvatica*, which showed the largest

variation and difference from the other three species on the IR spectrum (Fig. 6.1; 6.6), yielded the best PLSR performance (Fig. 6.4). Asner and Martin (2015) success in measuring soluble sugars in wild vegetation might have been due to the high inter-specific variation (low ratio of repetitions per species to number of species sampled). They predicted soluble NSC by combining up to 24 components on their PLSR (ranging from 20 to 38 vectors), whilst we averaged 10 components (ranging from 7 to 15, sd: 1.7) when using our four-species dataset.

If variation in leaf reflectance in certain areas of the spectrum is only attributed to difference in NSC, species showing the largest span of NSC concentrations should exhibit larger spectral variation in regions of interest, hence higher agreement between observed and predicted concentration. Nevertheless, *Q. robur* soluble sugars concentration ranged from 2 to 16% (Fig. 6.2), yet intra-specific leaf reflectance variation was low (Fig. 6.1), and both model accuracy and precision, were poor (Tables 6.1 and 6.2).

Our analysis shows that both the soluble sugar fraction and total NSC concentration present high correlation with leaf reflectance in the visible spectrum (Fig. 6.5), suggesting high contribution of photosynthetic pigments and therefore photosynthetic capacity (Richardson et al., 2002) to the model. On the other hand, peaks between 800 and 1300 nm can be associated with SLA (Asner et al., 2009; Asner and Martin, 2015; Doughty et al., 2017; Ourcival et al., 1999; Serbin et al., 2014; Yendrek et al., 2017), which goes in tandem with leaf carboxylation capacity according to the leaf economic spectrum (Díaz et al., 2016; Wright et al., 2004). Low capacity to predict starch content by leaf reflectance in both our study and Quentin et al. (2017) might be related to the fact that leaf's photosynthesis partitioning between soluble sugars and starch is highly dependent of time of the day and plant phenological stage at the time of collection (Huber and Israel, 1982), instead of directly correlating with leaf photosynthetic capacity granted by certain leaf traits. Whilst both NSC concentration and partitioning is a dynamic process that changes throughout the day, leaf structural traits, such as SLA or chlorophyll concentration, hardly vary at a diurnal scale. Regrading photosynthetic levels, other optical techniques, such as leaf and canopy fluorescence might be more suitable to track photosynthesis and NSC photosynthetic feedback inhibition Campbell et al. (2019).

Finally, similar to Asner and Martin (2015) we found peaks within the NIR spectrum (2000 to 2500 nm) which could be better related to soluble sugar concentration *per*

se instead of others leaf traits that act as proxies of both leaf carbohydrate synthesis capacity, and its storage.

6.5 Conclusions

Field spectroscopy has been suggested to be a useful, non-destructive and low-cost tool to quantify NSC in both crops and wild vegetation. However, our results suggest that in forest ecosystems the apparent detection of NSC may be confounded by interspecific covariation with other leaf traits, while there is little evidence of detectability of the substantial NSC variation within species. We found that leaf optical properties correlate most strongly with the soluble fraction, and only secondarily with total NSC. Overall, our results suggest that prediction of NSC from spectral properties in wild vegetation requires a large variation of leaf traits (e.g., leaf SLA and nitrogen concentration) and leaf optical properties, which is normally obtained only when many species are combined in the same dataset. Further research is needed in order to better understand light and NSC interactions and give researchers an effective tool to allow quantification of plant NSC dynamics *in vivo*, particularly when NSC determinations aim at capturing intraspecific variability.

Acknowledgments

NR would like to thank the Chilean Science and Technology Commission (CONICyT) for providing a full scholarship for his doctoral studies. We are grateful to ASDinc for providing the field spectrophotometer throughout the Alexander Goetz Support Program for young researchers. YM is supported by the Jackson Foundation Grant. We are also thankful of Marta Ramirez Boixaderas for helping to run leaf NSC assays, to Teresa Rosas for helping to setup NSC assay protocol, and Emma McIntosh for assistance with editing the manuscript.

The data needed to run the analysis can be found in the Oxford Research Archive (`https://ora.ox.ac.uk/objects/uuid:d4983905-6649-47ff-9dc9-5c66e08a61d8`). For reviewers only: Data in ORA will be embargoed until final publication of the paper,

however you can access the data through the following link:
https://drive.google.com/drive/folders/1MgfEk7cW96cBZ3Heg6woAAUM-ofnCk4o?usp=sharing

6.6 Supplemental Material

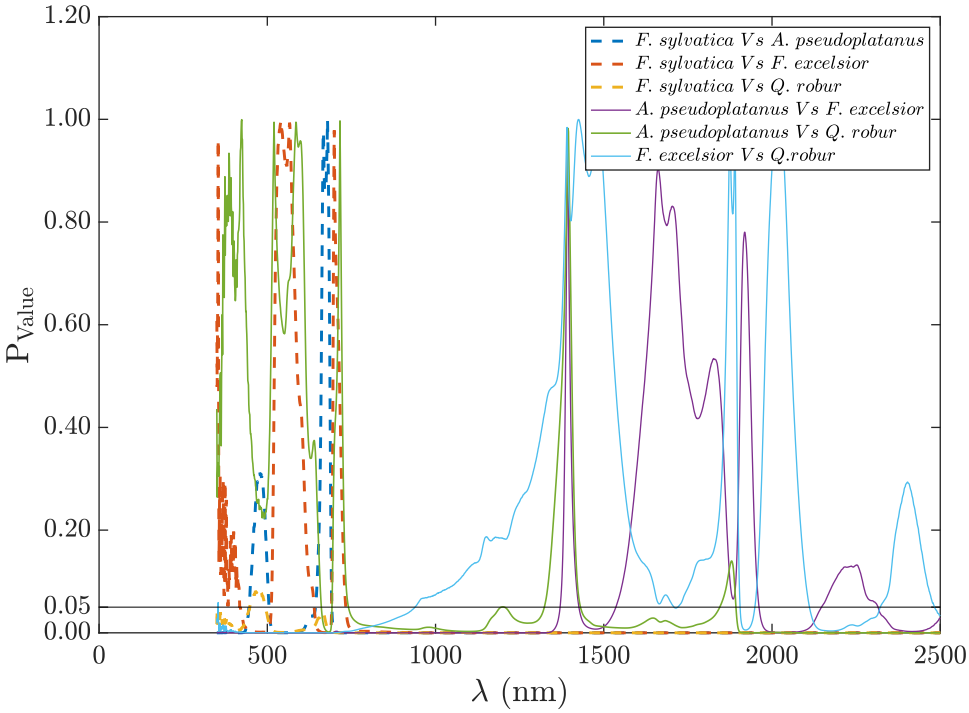


Figure 6.6: Pairwise comparison at wavelength level between different species reflectance. Comparison was done using two-sample T-test. P_{Value} shows the probability that both samples have the same mean. Probability below 0.05 (α Value) indicates that samples are statistically different at a given wavelength.

Table 6.4: Summary of the full cross validation across species, comparing observed and predicted non- structural carbohydrates (NSC). Variables a and b represent the slope and intercept of the linear regression between observed and predicted data. r^2 is the coefficient of determination of the regression and NRMSE is the normalised root mean square error of the model. Number of components corresponds to the number of vectors used for partial least square regression. Results using the whole dataset were then categorised at a species level.

Data Set	a	b	r^2	P value	n	NRMSE	Number of Components
All Species Together							
Monosaccharides	0.359	2.417	0.25	$\ll$0.001	201	0.49	13
Sucrose	0.295	1.066	0.26	$\ll$0.001	185	0.80	5
Soluble Sugars	0.522	2.336	0.46	$\ll$0.001	205	0.38	11
Starch	0.220	1.860	0.13	$\ll$0.001	195	0.99	15
Total NSC	0.296	5.012	0.19	$\ll$0.001	206	0.45	15
A. pseudoplatanus							
Monosaccharides	0.296	2.087	0.12	<0.050	56	0.41	13
Sucrose	0.150	0.557	0.05	0.136	46	1.14	5
Soluble Sugars	0.330	1.976	0.23	<0.001	58	0.42	11
Starch	0.075	3.088	0.04	0.119	56	0.92	15
Total NSC	0.098	5.686	0.05	0.091	58	0.60	15
F. sylvatica							
Monosaccharides	0.198	3.300	0.13	<0.050	52	0.49	13
Sucrose	0.068	2.084	0.07	0.070	48	0.75	5
Soluble Sugars	0.261	4.471	0.20	<0.001	52	0.28	11
Starch	0.382	1.138	0.21	<0.001	49	0.96	15
Total NSC	0.410	4.441	0.31	$\ll$0.001	52	0.34	15
F. excelsior							
Monosaccharides	−0.051	2.462	0.00	0.767	38	0.50	13
Sucrose	0.105	0.895	0.08	0.099	35	0.97	5
Soluble Sugars	0.009	3.351	0.00	0.940	39	0.43	11
Starch	−0.084	2.525	0.20	0.399	37	1.09	15
Total NSC	−0.059	5.670	0.01	0.626	40	0.57	15
Q. robur							
Monosaccharides	−0.026	5.427	0.01	0.616	55	0.47	13
Sucrose	0.166	1.600	0.12	<0.050	56	0.63	5
Soluble Sugars	−0.035	7.137	0.01	0.440	56	0.39	11
Starch	0.485	1.008	0.26	$\ll$0.001	53	0.84	15
Total NSC	0.236	6.779	0.15	<0.050	56	0.36	15

Table 6.5: Summary of the full cross validation at a species level for both fractions and total non-structural carbohydrates (NSC). Variables a and b represent the slope and intercept of the linear regression between observed and predicted concentrations. r^2 is the coefficient of determination of the regression and NRMSE is the normalised root mean square error of the model. Number of components is the number of vectors used for the partial least square regression.

Data Set	a	b	r^2	P value	n	NRMSE	Number of Components
A. pseudoplatanus							
Monosaccharides	0.339	1.849	0.30	$\ll$0.001	56	0.32	2
Sucrose	−0.011	0.635	0.00	0.739	46	1.09	1
Soluble Sugars	0.229	2.235	0.19	<0.001	58	0.42	2
Starch	0.011	3.465	0.00	0.765	56	0.95	2
Total NSC	0.010	6.268	0.00	0.745	58	0.61	1
F. sylvatica							
Monosaccharides	0.168	3.348	0.11	<0.050	52	0.49	4
Sucrose	0.141	1.963	0.08	0.057	48	0.74	4
Soluble Sugars	0.338	3.942	0.27	$\ll$0.001	52	0.27	5
Starch	0.545	0.782	0.43	$\ll$0.001	49	0.78	9
Total NSC	0.596	2.994	0.49	$\ll$0.001	52	0.29	9
F. excelsior							
Monosaccharides	0.009	2.403	0.00	0.829	38	0.35	1
Sucrose	0.190	0.896	0.13	<0.050	35	0.94	2
Soluble Sugars	0.007	3.285	0.00	0.849	39	0.35	1
Starch	−0.003	2.323	0.05	0.193	37	0.92	1
Total NSC	−0.045	5.700	0.26	<0.001	40	0.46	1
Q. robur							
Monosaccharides	0.002	5.333	0.00	0.945	55	0.44	1
Sucrose	0.149	1.552	0.12	<0.001	56	0.62	2
Soluble Sugars	−0.054	7.357	0.44	$\ll$0.001	56	0.38	1
Starch	0.523	0.861	0.37	$\ll$0.001	53	0.73	9
Total NSC	−0.026	8.952	0.01	0.389	56	0.39	2

Chapter7

Synthesis and conclusions

7.1 Summary and key findings

Increasing C_a due to anthropogenic emissions poses a problem for global vegetation models. On the one hand, an increase in C_a enables higher photosynthetic rates by decreasing photorespiration rates and by increasing photosynthesis main substrate, C_a. On the other hand, photoassimilates derived from photosynthesis must be translocated from the leaf to the rest of the plant in order to meet the metabolic demand of sink organs, support growth across the plant, and top up carbon storage reserves to endure abiotic stresses in the future. If these demands are limited by other factors, such as a plant's water status, soil nutrient limitations or temperature, phloem NSC downstream translocation is hampered. An accumulation of NSC in the leaf triggers a cascade of mechanisms that end up affecting the Calvin-Benson-Bassham cycle, hence leaf gas exchange. Therefore, plant productivity is not only subjected to the supply of carbon from the atmosphere, but also to the plant's carbon sink demand given by metabolic activity and growth. Empirical data are needed to understand the feedbacks between plant source and sink activity, and how NSCs interact with each one of these compartments within the plant in order to better predict ecosystem-atmosphere gas exchange under increasing C_a.

Throughout this thesis, I have tested the hypothesis of sink *versus* source activity leading plant productivity. I have demonstrated that when simulating an excess of photoasssimilates in leaves, photosynthetic rates are affected if NSCs are not rapidly translocated *via* the phloem. Furthermore, I have also examined the role of NSCs in

plant acclimation throughout the seasonal variation in soil moisture. Solute accumulation in leaves is an active strategy by plants to withstand water stress and lower leafΨ_w without affecting cell turgor and other leaf physiological process. Finally, the use of field leaf spectroscopy to monitor leaf NSC concentration *in vivo* remains a challenge. Results presented in the last empirical chapter of this thesis show that NSC detection through spectroscopy might be an artifact of cross-correlation with other leaf traits which do have a spectral footprint and correlate with leaf photosynthetic capacity.

Next, I will summarise the key findings of each empirical chapter by coming back to the main goals of the thesis shown in **Section 1.3**. Then, I will present the concluding remarks of the overall dissertation. Finally, I will address future challenges regarding leaf ecophysiology and NSC dynamics.

7.1.1 Photosynthetic downregulation mediated by non-structural carbohydrates

Question 1: Is there evidence that high NSC concentrations cause a downregulation of leaf photosynthesis?

This question was addressed in **Chapter 3** in the research article entitled *Photosynthetic downregulation in response to non-structural carbohydrates (NSC) in natural forest ecosystems.*

The key finding of this chapter is that species in contrasting ecotones (African tropical wet forest and temperate ancient European woodland) are sensitive to photosynthetic downregulation triggered by the addition of soluble NSC to the leaf. Nevertheless, the degree of photosynthetic downregulation observed in the cohort of the six species sampled relied on leaf traits associated with rapid photoassimilate translocation, such as specific leaf area (SLA), leaf investment in vein infrastructure, and petiole diameter. Species with high SLA (e.g., *F. sylvatica*) which are in the fast-growth region of the leaf economic spectrum, tended to exhibit lower photosynthetic downregulation compared to slow-growing species (e.g., *Q. robur*). Fast growing species not only present leaf traits that enable them to rapidly acquire photoassimilates, by allowing leaf high

photosynthetic rates, but also these traits are coordinated with other leaf traits that ensure fast translocation of these resources to be used throughout the plant (Reich, 2014).

Species that invested more in leaf vein infrastructure and presented larger petiole diameter tended to show a lower decrease in photosynthesis after sucrose addition. Leaf vein architecture proved not only to be important in providing water from the plant to the leaf in order to maintain leaf Ψ_w, and stomatal opening for photosynthesis purposes *via* the xylem, but also served as a collecting network that rapidly mobilises leaf NSC to the rest of the plant *via* phloem. This chapter casts light on the importance of integrating these traits when modelling the consequences of increasing C_a on terrestrial vegetation.

7.1.2 Non-structural carbohydrate dynamics throughout the wet-dry season

Question 2: Are seasonal changes in leaf NSC concentrations linked to seasonal changes in photosynthesis?

This hypothesis was explored in **Chapter 5**, *Seasonal changes in leaf osmotic adjustment across a tropical drought gradient.*

I found a strong seasonality in osmotic potential at full turgor (Π_o) following a decrease (more negative values) during the drought season, and an increase (less negative values) during, or close to, the wet season. Seasonal changes in Π_o, known as osmotic adjustment, were more pronounced in the driest plot in Ghana (dry deciduous tropical forest), compared to the wettest plot (wet tropical forest). I found evidence that leaf traits related to fast NSC translocation, such as SLA and leaf vein density, were negatively correlated to osmotic adjustment.

Furthermore, seasonal changes in Π_o were correlated with seasonal changes in leaf photosynthesis at light saturation. Nevertheless, since Π_o is dependent on changes in soil moisture, is hard to disentangle the effect of Π_o, as a proxy of leaf NSC concentration, on leaf gas exchange.

Altogether, even if I found that traits related to fast NSC translocation were negatively correlated to osmotic adjustment, and that leaf osmotic potential at full turgor was negatively correlated with leaf photosynthesis, I did not find enough evidence to support the hypothesis that seasonal differences in leaf photosynthesis depend on NSC leaf concentration. NSC accumulation in the blade appears primarily as an active acclimation strategy to cope with water stress, rather than a passive consequence of lack of sink activity resulting from water stress.

7.1.3 Leaf non-structural carbohydrates prediction with field leaf spectroscopy

Question 3: Is it possible to measure *in vivo* leaf NSC concentrations using field leaf spectrometry?

Probably not. In **Chapter 6** I used leaf field spectroscopy in leaves of four temperate European deciduous species to predict leaf total, and its fractions, NSC concentrations. Nevertheless, I found that perhaps other researchers succeeding at correlating leaf optical footprint with leaf NSC might have confounded interspecific covariation of NSC concentrations, with other traits that vary amongst species and do correlate with leaf photosynthetic capacity, and hence with NSC concentration. NSC concentration in the leaf is dynamic, varying along the day and throughout the season. Therefore, leaf traits that do not vary along the day are not good predictors of leaf NSC. Leaf gas exchange can be monitored *in vivo*, yet, live monitoring of NSC in the leaf remains a challenge when using field spectroscopy.

7.2 Concluding Remarks

Throughout this thesis I have proven that leaf NSC play a crucial role in leaf ecophysiology, regulating inner dynamics and leaf-atmosphere interactions. This thesis explored the hypothesis that plant productivity is not a result of a *"push"* by leaves into the plant, but rather that plant sinks *"pull"* carbon from leaves given their metabolic, growth and

storage carbon demand. A low capacity of leaves to rapidly translocate these photoassimilates *via* phloem would inevitably jeopardise photosynthesis, and thus affect overall forest productivity. Therefore, plant carbon assimilation does indeed rely on a tuned balance between source and sinks, where NSCs act as intermediary signals regulating both processes.

A novel finding in this thesis is that leaf investment in vein infrastructure does not only serve to ensure a supply of water to the leaf in order to satisfy water transpiration demand, thus keeping stomata opened and high photosynthetic rates, but also as a collecting network facilitating photoassimilate translocation. Even if these remarks have been observed in the laboratory in annual species, this is the first time that similar conclusions are obtained in tree species in natural conditions.

However, NSC accumulation in the leaf is not only a passive process resulting from slow translocation and/or lack of carbon sink demand in the plant. I have shown how the accumulation of solutes in the leaf is also an active strategy of plants to cope during periods of water stress.

As NSC have proven to downregulate photosynthesis when they reach a threshold in the leaf, their in vivo monitoring remains a challenge. Pairing leaf gas exchange measurements with leaf NSC diurnal dynamics is vital to better understand canopy-atmosphere fluxes and the fate of ecosystems under increasing C_a concentrations. NSC dynamics with plant productivity do need further research in order to be integrated with global vegetation models.

7.3 Further Work

Regarding the present thesis, in the future, I would like to deepen some issues left in two of the empirical chapters. Firstly, after **Chapter 5** I would like to pair Π_o with leaf NSC concentration to better understand what the main solutes are driving osmotic adjustment. A seasonal study of leaf, and plant, NSC concentration across a drought tropical gradient would shed light on how source activity under abiotic stress is regulated, thus triggering the aforementioned cascade of mechanisms that end up

accumulating NSC in source organs and regulating canopy's carbon water fluxes. Secondly, in **Chapter 6** we concluded that leaf spectroscopy might be confounding the prediction of leaf traits with an optical footprint and correlate with leaf photosynthesis, rather than directly measuring leaf NSCs. I would to measure these traits (i.e., leaf nitrogen concentration, SLA) and study how these correlate with leaf optical footprint and leaf NSC concentration. Furthermore, I would like to study diurnal variations of NSC, and learn how these traits explain leaf NSC concentration throughout the day.

Other line of work that I would like to explore in the future is the role of phloem in regulating photosynthesis. Novel tools, such as *"picogauges"* developed by Michael Knoblauch, allow to study phloem pressure in the field. I would be very interested to study how phloem pressure varies according to seasonal changes in sink activity and correlate these changes with photosynthesis and leaf water status, in order to disentangle the effects of abiotic stress in stomatal opening (source) *versus* the role of sinks and leaf NSC accumulation in leaf gas exchange.

If a plant's growth is not limited by C_a, what are the main restrictions for ecosystem biomass accumulation today and in the future? Since plant photosynthesis seems to be limited by a rapid translocation of NSC and the sink carbon demand, rather than by C_a, what other factors might be limiting leaf photosynthesis?

After spending time doing fieldwork in the top of the canopy in Wytham Woods, I came to realise that light is a major factor limiting individual leaf photosynthesis, and hence forest productivity. Leaves were never static, wind always changed their angle, they shaded one another, and only a very small fraction of the top of the canopy leaves were fully sun exposed for brief periods of time. According to Farquhar's photosynthesis model, leaf gas exchange is simulated as photosynthesis response to light curves. I think if light is becoming a factor limiting photosynthesis, we should focus on dynamic responses of photosynthesis to light. Simulated photosynthesis responses to light flickers, rather than steady levels of irradiance, should be integrated in the abovementioned framework. Also, it becomes important to better understand the effect of diffuse light in photosynthesis, rather than the response of photosynthesis to direct light, as studied with leaf gas exchange chambers.

Another area that has been poorly explored is the role of NSC reserves as a sink within the plant. NSC reserves play major role to overcome stresses such as fires,

drought, herbivory, *etc.* NSC reserves grant *"memory"* to the ecosystem. Research has shown that after severe drought forest biomass still increases because of these reserves (Doughty et al., 2015). Therefore, studying the availability and dynamics of these pools of carbon will improve the simulation of vegetation dynamics under a changing climate. Functional Structural Models look to merge the architectural representation of a tree in three dimensions, with process-based models, which look to model inputs, distribution and outputs of carbon to the system. Integrating NSC dynamics into these models would improve their performance by simulating NSC translocation and assigning NSCs the role of coordinating source and sink activities within the plant.

References

Adams, W. W., Cohu, C. M., Muller, O., and Demmig-Adams, B. (2013). Foliar phloem infrastructure in support of photosynthesis. *Frontiers in Plant Science*, 4(June):1–7.

Adams, W. W., Stewart, J. J., Polutchko, S. K., and Demmig-Adams, B. (2018). *Leaf Vasculature and the Upper Limit of Photosynthesis*. Advances in Photosynthesis and Respiration. Springer International Publishing, Cham, Switzerland, first edition.

Ainsworth, E. A., Davey, P. A., Hymus, G. J., Osborne, C. P., Rogers, A., Blum, H., Nösberger, J., and Long, S. P. (2003). Is stimulation of leaf photosynthesis by elevated carbon dioxide concentration maintained in the long term? A test with Lolium perenne grown for 10 years at two nitrogen fertilization levels under Free Air CO2 Enrichment (FACE). *Plant, Cell and Environment*, 26(5):705–714.

Ainsworth, E. A. and Lemonnier, P. (2018). Phloem function: a key to understanding and manipulating plant responses to rising atmospheric [CO2]? *Current Opinion in Plant Biology*, 43(September 2016):50–56.

Amiard, V., Mueh, K. E., Demmig-Adams, B., Ebbert, V., Turgeon, R., and Adams, W. W. (2005). Anatomical and photosynthetic acclimation to the light environment in species with differing mechanisms of phloem loading. *Proceedings of the National Academy of Sciences*, 102(36):12968–12973.

Arp, W. J. (1991). Effects of sourcesink relations on photosynthetic acclimation to elevated CO2. *Plant, Cell & Environment*, 14(8):869–875.

Asner, G. P. and Martin, R. E. (2015). Spectroscopic Remote Sensing of Non-Structural Carbohydrates in Forest Canopies. *Remote Sensing*, 7(4):3526–3547.

Asner, G. P., Martin, R. E., Anderson, C. B., and Knapp, D. E. (2015). Quantifying forest canopy traits: Imaging spectroscopy versus field survey. *Remote Sensing of Environment*, 158:15–27.

Asner, G. P., Martin, R. E., Ford, A. J., Metcalee, D. J., and Liddell, M. J. (2009). Leaf chemical and spectral diversity in Australian tropical forests. *Ecological Applications*, 19(1):236–253.

Asner, G. P., Martin, R. E., Tupayachi, R., Emerson, R., Martinez, P., Sinca, F., Powell, G. V., Wright, S. J., and Lugo, A. E. (2011). Taxonomy and remote sensing of leaf mass per area (LMA) in humid tropical forests. *Ecological Applications*, 21(1):85–98.

Azcón-Bieto, J. (1983). Inhibition of photosynthesis by carbohydrates in wheat leaves. *Plant physiology*, 73(3):681–6.

Bader, M. K. F., Leuzinger, S., Keel, S. G., Siegwolf, R. T. W., Hagedorn, F., Schleppi, P., and Körner, C. (2013). Central european hardwood trees in a high-CO2 future: Synthesis of an 8-year forest canopy CO2 enrichment project. *Journal of Ecology*, 101(6):1509–1519.

Ball, J., Woodrow, I., and Berry, J. A. (1987). A model predicting stomatal conductance and its contribution to the control of photosynthesis under different environmental conditions. In Biggins, J. and Nijhoff, M., editors, *Progress in Photosynthesis Research. Vol. 4. Proceedings of the 7th International Congress on Photosynthesis*, pages 221–224, Dordrecht, NE.

Baltzer, J. L., Davies, S. J., Bunyavejchewin, S., and Noor, N. S. (2008). The role of desiccation tolerance in determining tree species distributions along the Malay-Thai Peninsula. *Functional Ecology*, 22(2):221–231.

Bartlett, M. K., Scoffoni, C., and Sack, L. (2012). The determinants of leaf turgor loss point and prediction of drought tolerance of species and biomes: A global meta-analysis. *Ecology Letters*, 15(5):393–405.

Batten, G. D., Blakeney, A. B., McGrath, V. B., and Ciavarella, S. (1993). Non-structural Carbohydrate: Analysis by near infrared reflectance spectroscopy and its importance as an indicator of plant growth. *Plant And Soil*, 156:243–246.

Bazot, S., Barthes, L., Blanot, D., and Fresneau, C. (2013). Distribution of non-structural nitrogen and carbohydrate compounds in mature oak trees in a temperate forest at four key phenological stages. *Trees - Structure and Function*, 27(4):1023–1034.

Blonder, B., Salinas, N., Patrick Bentley, L., Shenkin, A., Chambi Porroa, P. O., Valdez Tejeira, Y., Violle, C., Fyllas, N. M., Goldsmith, G. R., Martin, R. E., Asner, G. P., Díaz, S., Enquist, B. J., and Malhi, Y. (2017). Predicting trait-environment relationships for venation networks along an Andes-Amazon elevation gradient. *Ecology*, 98(5):1239–1255.

Bowman, W. D. and Roberts, S. W. (1985). Seasonal and Diurnal Water Relations Adjustments in Three Evergreen Chaparral Shrubs Published. 66(3):738–742.

Brodribb, T. J., Feild, T. S., and Jordan, G. J. (2007). Leaf Maximum Photosynthetic Rate and Venation Are Linked by Hydraulics. *Plant Physiology*, 144(4):1890–1898.

Campbell, P. K., Huemmrich, K. F., Middleton, E. M., Ward, L. A., Julitta, T., Daughtry, C. S., Burkart, A., Russ, A. L., and Kustas, W. P. (2019). Diurnal and seasonal variations in chlorophyll fluorescence associated with photosynthesis at leaf and canopy scales. *Remote Sensing*, 11(5).

Cardoso, A. W., Medina-Vega, J. A., Malhi, Y., Adu-Bredu, S., Ametsitsi, G. K., Djagbletey, G., van Langevelde, F., Veenendaal, E., and Oliveras, I. (2016). Winners and losers: Tropical forest tree seedling survival across a West African forest-savanna transition. *Ecology and Evolution*, 6(10):3417–3429.

Chapin, F., Schulze, E., and Mooney, H. (1990). The ecology and economics of storage in plants. *Annual Review of Ecology and Systematics*, (21):423–447.

Chavana-Bryant, C., Malhi, Y., Wu, J., Asner, G. P., Anastasiou, A., Enquist, B. J., Cosio Caravasi, E. G., Doughty, C. E., Saleska, S. R., Martin, R. E., and Gerard, F. F. (2017). Leaf aging of Amazonian canopy trees as revealed by spectral and physiochemical measurements. *New Phytologist*, 214(3):1049–1063.

Collatz, G. J., Berry, J. A., Farquhar, G. D., and Pierce, J. (1990). The relationship between the Rubisco reaction mechanism and models of photosynthesis. *Plant, Cell and Environment*, 13(3):219–225.

Comtet, J., Jensen, K. H., Turgeon, R., Stroock, A. D., and Hosoi, A. E. (2017). Passive phloem loading and long-distance transport in a synthetic tree-on-a-chip. *Nature Plants*, 3(March):1–8.

Cortes, P. and Sinclair, T. (1907). No Title. *Agronomy Journal*, 77(5):798–802.

Cowan, I. R. and Farquhar, G. D. (1977). Stomatal function in relation to leaf metabolism and environment. *Symposia of the Society for Experimental Biology*, 31(February 1977):471–505.

Cramer, W., Bondeau, A., Woodward, F. I., Prentice, I. C., Betts, R. a., Brovkin, V., Cox, P. M., Fisher, V., Foley, J. a., Friend, A. D., Kucharik, C., Lomas, M. R., Ramankutty, N., Sitch, S., Smith, B., White, A., and Young-Molling, C. (2001). Global response of terrestrial ecosystem structure and function to CO2 and climate change: results from six dynamic global vegetation models. *Global Change Biology*, 7(4):357–373.

Curran, P. J. (1989). Remote sensing of foliar chemistry. *Remote Sensing of Environment*, 30(3):271–278.

Decruyenaere, V., Clément, C., Agneessens, R., Losseau, C., and Stilmant, D. (2012). Development of near-infrared spectroscopy calibrations to quantify starch and soluble sugar content in the roots of Rumex obtusifolius. *Weed Research*, 52(1):1–5.

Díaz, S., Grime, J. P., Harris, J., and McPherson, E. (1993). Evidence of a feedback mechanism limiting plant response to elevated carbon dioxide. *Nature*, 364(6438):616–617.

Díaz, S., Kattge, J., Cornelissen, J. H. C., Wright, I. J., Lavorel, S., Dray, S., Reu, B., Kleyer, M., Wirth, C., Colin Prentice, I., Garnier, E., Bönisch, G., Westoby, M., Poorter, H., Reich, P. B., Moles, A. T., Dickie, J., Gillison, A. N., Zanne, A. E., Chave, J., Joseph Wright, S., Sheremet'ev, S. N., Jactel, H., Baraloto, C., Cerabolini, B., Pierce, S., Shipley, B., Kirkup, D., Casanoves, F., Joswig, J. S., Günther, A., Falczuk, V., Rüger, N., Mahecha, M. D., and Gorné, L. D. (2016). The global spectrum of plant form and function. *Nature*, 529(7585):167–171.

Dietze, M. C., Sala, A., Carbone, M. S., Czimczik, C. I., Mantooth, J. A., Richardson, A. D., and Vargas, R. (2014). Nonstructural Carbon in Woody Plants. *Annual Review of Plant Biology*, 65(1):667–687.

Doughty, C. E. (2011). An In Situ Leaf and Branch Warming Experiment in the Amazon. *Biotropica*, 43(6):658–665.

Doughty, C. E., Metcalfe, D. B., Girardin, C. A. J., Amézquita, F. F., Cabrera, D. G., Huasco, W. H., Silva-Espejo, J. E., Araujo-Murakami, A., da Costa, M. C., Rocha, W., Feldpausch, T. R., Mendoza, A. L. M., da Costa, A. C. L., Meir, P., Phillips, O. L., and Malhi, Y. (2015). Drought impact on forest carbon dynamics and fluxes in Amazonia. *Nature*, 519(7541):78–82.

Doughty, C. E., Santos-Andrade, P. E., Goldsmith, G. R., Blonder, B., Shenkin, A., Bentley, L. P., Chavana-Bryant, C., Huaraca Huasco, W., Díaz, S., Salinas, N., Enquist, B., Martin, R., Asner, G. P., and Malhi, Y. (2017). Can leaf spectroscopy predict leaf and forest traits along a Peruvian tropical forest elevation gradient? *Journal of Geophysical Research: Biogeosciences*, 122(11):2952–2965.

Dreccer, M. F., Barnes, L. R., and Meder, R. (2014). Quantitative dynamics of stem water soluble carbohydrates in wheat can be monitored in the field using hyperspectral reflectance. *Field Crops Research*, 159:70–80.

Duckworth, J. H. (1998). Spectroscopic Quantitative Analysis. In Workman, J. and Springsteen, A., editors, *Applied spectroscopy: a compact reference for practitioners*, chapter 4, pages 93–163. Academic Press, San Diego, CA, USA, first edition.

Eaton, F. and Ergle, D. (1948). Carbohydrates accumulation in the cotton plant at low moisture levels. *Plant physiology*, 23(2):169–187.

Eckardt, N. A. (2005). Photorespiration Revisited. *The Plant cell*, 17(8):2139–2141.

Ellsworth, D. S., Anderson, I. C., Crous, K. Y., Cooke, J., Drake, J. E., Gherlenda, A. N., Gimeno, T. E., Macdonald, C. A., Medlyn, B. E., Powell, J. R., Tjoelker, M. G., and Reich, P. B. (2017). Elevated CO2 does not increase eucalypt forest productivity on a low-phosphorus soil. *Nature Climate Change*, 7(4):279–282.

Fang, Y., Michalak, A. M., Schwalm, C. R., Huntzinger, D. N., Berry, J. A., Ciais, P., Piao, S., Poulter, B., Fisher, J. B., Cook, R. B., Hayes, D., Huang, M., Ito, A., Jain, A., Lei, H., Lu, C., Mao, J., Parazoo, N. C., Peng, S., Ricciuto, D. M., Shi, X., Tao, B., Tian, H., Wang, W., Wei, Y., and Yang, J. (2017). Global land carbon sink response to temperature and precipitation varies with ENSO phase. *Environmental Research Letters*, 12(6).

Farquhar, G. D., von Caemmerer, S., and Berry, J. A. (1980). A Biochemical Model of Photosynthetic CO2 Assimilation in Leaves of C3 Species. *Planta*, 149:78–90.

Fatichi, S., Leuzinger, S., and Körner, C. (2014). Moving beyond photosynthesis: From carbon source to sink-driven vegetation modeling. *New Phytologist*, 201(4):1086–1095.

Field, C. B. and Mooney, H. (1986). The photosynthesis-nitrogen relationship in wild plants. In Givnish, T., editor, *On the Economy of Plant Form and Function*, chapter 1, pages 25–55. Cambridge University Press, Cambridge, UK, revised edition.

Fleischer, K., Rammig, A., De Kauwe, M. G., Walker, A. P., Domingues, T. F., Fuchslueger, L., Garcia, S., Goll, D. S., Grandis, A., Jiang, M., Haverd, V., Hofhansl, F., Holm, J. A., Kruijt, B., Leung, F., Medlyn, B. E., Mercado, L. M., Norby, R. J., Pak, B., von Randow, C., Quesada, C. A., Schaap, K. J., Valverde-Barrantes, O. J., Wang, Y.-P., Yang, X., Zaehle, S., Zhu, Q., and Lapola, D. M. (2019). Amazon forest response to CO2 fertilization dependent on plant phosphorus acquisition. *Nature Geoscience*, 12(September).

Flexas, J., Loreto, F., and Medrano, H. (2012). *Terrestrial Photosynthesis in a Changing Environment*. Cambridge University Press, Cambridge.

Franck, N., Vaast, P., Génard, M., and Dauzat, J. (2006). Soluble sugars mediate sink feedback down-regulation of leaf photosynthesis in field-grown Coffea arabica. *Tree physiology*, 26(4):517–25.

Galmés, J., Flexas, J., Savé, R., and Medrano, H. (2007). Water relations and stomatal characteristics of Mediterranean plants with different growth forms and leaf habits: responses to water stress and recovery. *Plant Soil*, 290:139–155.

Gamalei, Y. V. (2007). The role of mesophyll cell tonoplast in determining the route of phloem loading. Thirty years of the studies of phloem loading. *Russian Journal of Plant Physiology*, 54(1):1–9.

Giaquinta, R. (1978). Source and Sink Leaf Metabolism in Relation to Phloem Translocation. *Plant Physiology*, 61(3):380–385.

Girardin, M. P., Bouriaud, O., Hogg, E. H., Kurz, W., Zimmermann, N. E., Metsaranta, J. M., De Jong, R., Frank, D. C., Esper, J., Büntgen, U., Guo, X. J., and Bhatti, J. (2016). No growth stimulation of Canada's boreal forest under half-century of combined warming and CO2 fertilization. *Proceedings of the National Academy of Sciences of the United States of America*, 113(52):E8406–E8414.

Greenwood, S., Ruiz-Benito, P., Martínez-Vilalta, J., Lloret, F., Kitzberger, T., Allen, C. D., Fensham, R., Laughlin, D. C., Kattge, J., Bönisch, G., Kraft, N. J., and Jump, A. S. (2017). Tree mortality across biomes is promoted by drought intensity, lower wood density and higher specific leaf area. *Ecology Letters*, 20(4):539–553.

Griffiths, H. (2006). Designs on Rubisco. *Nature*, 44(June):940–941.

Hartmann, H. and Trumbore, S. (2016). Understanding the roles of nonstructural carbohydrates in forest trees - from what we can measure to what we want to know. *New Phytologist*, 211:836–403.

Hayat, A., Hacket-Pain, A. J., Pretzsch, H., Rademacher, T. T., and Friend, A. D. (2017). Modeling Tree Growth Taking into Account Carbon Source and Sink Limitations. *Frontiers in Plant Science*, 8(March):1–15.

Hoch, G., Popp, M., and Körner, C. (2002). Altitudinal increase of mobile carbon pools in Pinus cembra suggests sink limitation of growth at the Swiss treeline. *Oikos*, 98(3):361–374.

Hoch, G., Richter, A., and Körner, C. (2003). Non-structural carbon compounds in temperate forest trees. *Plant Cell and Environment*, 26:1067–1081.

Hölttä, T., Mencuccini, M., and Nikinmaa, E. (2009). Linking phloem function to structure: Analysis with a coupled xylem-phloem transport model. *Journal of Theoretical Biology*, 259(2):325–337.

Hölttä, T., Mencuccini, M., and Nikinmaa, E. (2014). Ecophysiological Aspectes of Phloem Transport in trees. In Tausz, M. and Grulke, N., editors, *Trees in a Changing Environment*, chapter 2, pages 25–37. Springer, Dordrecht, first edition.

Hsiao, T., Acevedo, E., Fereres, E., and Henderson, D. (1976). Stress Metabolism. Water strees, growth, and osmotic adjustment. *Philosophical Transactions of the Royal Society B: Biological Sciences*, 273:479–500.

Huang, C.-w., Domec, J.-C., Palmroth, S., Pockman, W. T., Litvak, M. E., and Katul, G. G. (2018). Advances in Water Resources Transport in a coordinated soil-root-xylem-phloem leaf system. *Advances in Water Resources*, 119(May):1–16.

Huber, S. C. and Israel, D. W. (1982). Biochemical Basis for Partitioning of Photosynthetically Fixed Carbon between Starch and Sucrose in Soybean (Glycine max Merr.) Leaves. *Plant physiology*, 69(3):691–696.

Huntingford, C., Zelazowski, P., Galbraith, D., Mercado, L. M., Sitch, S., Fisher, R., Lomas, M., Walker, A. P., Jones, C. D., Booth, B. B., Malhi, Y., Hemming, D., Kay, G., Good, P., Lewis, S. L., Phillips, O. L., Atkin, O. K., Lloyd, J., Gloor, E., Zaragoza-Castells, J., Meir, P., Betts, R., Harris, P. P., Nobre, C., Marengo, J., and Cox, P. M. (2013). Simulated resilience of tropical rainforests to CO2-induced climate change. *Nature Geoscience*, 6(4):268–273.

Iljin, W. S. (1957). Drought Resistance in Plants and Physiological Processes. *Annual Review of Plant Physiology*, 8(1):257–274.

Jones, P. G., Lloyd J. C., and Raines, C. A. (1996). Glucose feeding of intact wheat plants represses the expression of a number of Calvin cycle genes. *Plant, Cell and Environment*, 19(2):231–236.

Kallarackal, J. and Milburn, J. (1984). Specific Mass Transfer and Sink-Controlled Phloem Translocation in Castor Bean. *Functional Plant Biology*, 11:483–90.

Kameli, A. and Lösel, D. M. (1995). Contribution of Carbohydrates and other Solutes to Osmotic Adjustment in Wheat Leaves Under Water Stress. *Journal of Plant Physiology*, 145:363–366.

Kattge, J., Díaz, S., Lavorel, S., Prentice, I. C., Leadley, P., Bönisch, G., Garnier, E., Westoby, M., Reich, P. B., Wright, I. J., Cornelissen, J. H., Violle, C., Harrison, S. P., Van Bodegom, P. M., Reichstein, M., Enquist, B. J., Soudzilovskaia, N. A., Ackerly,

D. D., Anand, M., Atkin, O., Bahn, M., Baker, T. R., Baldocchi, D., Bekker, R., Blanco, C. C., Blonder, B., Bond, W. J., Bradstock, R., Bunker, D. E., Casanoves, F., Cavender-Bares, J., Chambers, J. Q., Chapin, F. S., Chave, J., Coomes, D., Cornwell, W. K., Craine, J. M., Dobrin, B. H., Duarte, L., Durka, W., Elser, J., Esser, G., Estiarte, M., Fagan, W. F., Fang, J., Fernández-Méndez, F., Fidelis, A., Finegan, B., Flores, O., Ford, H., Frank, D., Freschet, G. T., Fyllas, N. M., Gallagher, R. V., Green, W. A., Gutierrez, A. G., Hickler, T., Higgins, S. I., Hodgson, J. G., Jalili, A., Jansen, S., Joly, C. A., Kerkhoff, A. J., Kirkup, D., Kitajima, K., Kleyer, M., Klotz, S., Knops, J. M., Kramer, K., Kühn, I., Kurokawa, H., Laughlin, D., Lee, T. D., Leishman, M., Lens, F., Lenz, T., Lewis, S. L., Lloyd, J., Llusià, J., Louault, F., Ma, S., Mahecha, M. D., Manning, P., Massad, T., Medlyn, B. E., Messier, J., Moles, A. T., Müller, S. C., Nadrowski, K., Naeem, S., Niinemets, Ü., Nöllert, S., Nüske, A., Ogaya, R., Oleksyn, J., Onipchenko, V. G., Onoda, Y., Ordoñez, J., Overbeck, G., Ozinga, W. A., Patiño, S., Paula, S., Pausas, J. G., Peñuelas, J., Phillips, O. L., Pillar, V., Poorter, H., Poorter, L., Poschlod, P., Prinzing, A., Proulx, R., Rammig, A., Reinsch, S., Reu, B., Sack, L., Salgado-Negret, B., Sardans, J., Shiodera, S., Shipley, B., Siefert, A., Sosinski, E., Soussana, J. F., Swaine, E., Swenson, N., Thompson, K., Thornton, P., Waldram, M., Weiher, E., White, M., White, S., Wright, S. J., Yguel, B., Zaehle, S., Zanne, A. E., and Wirth, C. (2011). TRY - a global database of plant traits. *Global Change Biology*, 17(9):2905–2935.

Keel, S. G., Siegwolf, R. T. W., Jäggi, M., and Körner, C. (2007). Rapid mixing between old and new C pools in the canopy of mature forest trees. *Plant, Cell and Environment*, 30(8):963–972.

Keenan, T. F., Hollinger, D. Y., Bohrer, G., Dragoni, D., Munger, J. W., Schmid, H. P., and Richardson, A. D. (2013). Increase in forest water-use efficiency as atmospheric carbon dioxide concentrations rise. *Nature*, 499(7458):324–7.

Kokaly, R. F., Despain, D. G., Clark, R. N., and Livo, K. E. (2003). Mapping vegetation in Yellowstone National Park using spectral feature analysis of AVIRIS data. *Remote Sensing of Environment*, 84(3):437–456.

Körner, C. (2003). Carbon limitation in trees. *Journal of Ecology*, 91(1):4–17.

Körner, C. (2006). Plant CO2 responses: An issue of definition, time and resource supply. *New Phytologist*, 172(3):393–411.

Körner, C. (2013). Growth Controls Photosynthesis - Mostly. *Nova Acta Leopoldina*, 114(391):273–283.

Körner, C., Pelaez-Riedl, S., and Van Bel, A. J. E. (1995). CO2 responsiveness of plants: a possible link to phloem loading. *Plant, Cell and Environment*, 18(5):595–600.

Kozaki, A. and Takeba, G. (1996). Photorespiration protects C3 plants from photooxidation. *Nature*, 384:557–560.

Kramer, P. J. and Boyer, J. S. (1995). *Water Relations of Plant Soils*. Number JANUARY 2011. Academic Press, San Diego, CA, USA, first edition.

Lawson, T., Kramer, D. M., and Raines, C. A. (2012). Improving yield by exploiting mechanisms underlying natural variation of photosynthesis. *Current Opinion in Biotechnology*, 23(2):215–220.

Li, N., He, N., Yu, G., Wang, Q., and Sun, J. (2016). Leaf non-structural carbohydrates regulated by plant functional groups and climate: Evidences from a tropical to cold-temperate forest transect. *Ecological Indicators*, 62:22–31.

Lobo, A. K. M., de Oliveira Martins, M., Lima Neto, M. C., Machado, E. C., Ribeiro, R. V., and Silveira, J. A. G. (2015). Exogenous sucrose supply changes sugar metabolism and reduces photosynthesis of sugarcane through the down-regulation of Rubisco abundance and activity. *Journal of Plant Physiology*, 179:113–121.

Long, S. P., Ainsworth, E. A., Leakey, A. D., Nösberger, J., and Ort, D. R. (2006). Food for Thought: Lower-Than-Expected Crop Yield Stimulation with Rising CO2 Concentrations. *Science*, 312(June):91–95.

Lotka, A. J. (1922). Contribution to the Energetics of Evolution. *Proceedings of the National Academy of Sciences*, 8(6):147–151.

Malhi, Y., Aragão, L. E. O. C., Metcalfe, D. B., Paiva, R., Quesada, C. a., Almeida, S., Anderson, L., Brando, P., Chambers, J. Q., da Costa, A. C. L., Hutyra, L. R., Oliveira, P., Patiño, S., Pyle, E. H., Robertson, A. L., and Teixeira, L. M. (2009). Comprehensive assessment of carbon productivity, allocation and storage in three Amazonian forests. *Global Change Biology*, 15(5):1255–1274.

Malhi, Y., Doughty, C., and Galbraith, D. (2011). The allocation of ecosystem net primary productivity in tropical forests. *Philosophical transactions of the Royal Society of London. Series B, Biological sciences*, 366(1582):3225–45.

Marthews, T., Riutta, T., Oliveras Menos, I., Urrutia, R., Moore, S., Metalcafe, D., Malhi, Y., Phillips, O., Huaraca-Huasco, W., Ruiz-Jaen, M. C., Girardin, C., Butt, N., and Cain, R. (2014). *Measuring Tropical Forest Carbon Allocation and Cycling: A RAINFOR-GEM Field Manual for Intensive Census Plots (v3.0)*. Oxford, UK, third edition.

Martínez-Vilalta, J., Sala, A., Asensio, D., Galiano, L., Hoch, G., Palacio, S., Piper, F., and Lloret, F. (2016). Dynamics of non-structural carbohydrates in terrestrial plants: a global synthesis. *Ecological Monographs*, 86(4):495–516.

Matthews, J. S., Vialet-Chabrand, S. R., and Lawson, T. (2017). Diurnal variation in gas exchange: the balance between carbon fixation and water loss. *Plant Physiology*, 174(June):614–623.

Medlyn, B. E., Duursma, R. a., Eamus, D., Ellsworth, D. S., Prentice, I. C., Barton, C. V. M., Crous, K. Y., De Angelis, P., Freeman, M., and Wingate, L. (2011). Reconciling the optimal and empirical approaches to modelling stomatal conductance. *Global Change Biology*, 17(6):2134–2144.

Mencuccini, M. and Christoffersen, B. (2019). Tansley review Modelling water fluxes in plants : from tissues to biosphere. *New Phytologist*, (1991):1207–1222.

Mencuccini, M. and Hölttä, T. (2010). The significance of phloem transport for the speed with which canopy photosynthesis and belowground respiration are linked. *New Phytologist*, 185(1):189–203.

Meyer, R. F. and Boyer, J. S. (1972). Sensitivity of cell division and cell elongation to low water potentials in soybean hypocotyls. *Planta*, 108(1):77–87.

Minchin, P. E. H. and Lacointe, A. (2005). New understanding on phloem physiology and possible consequences for modelling long-distance carbon transport. *The New phytologist*, 166(3):771–9.

Miziorko, H. M. and Lorimer, G. H. (1983). Ribulose-1,5-Biphosphate Carboxylase-Oxygenase. *Annual Review of Biochemestry*, 52:507–535.

Moore, B. D., Cheng, S.-H., Sims, D., and Seemann, J. R. (1999). The biochemical and molecular basis for photosynthetic acclimation to elevated atmospheric CO2. *Plant, Cell and Environment*, 22(6):567–582.

Moore, S., Adu-Bredu, S., Duah-Gyamfi, A., Addo-Danso, S. D., Ibrahim, F., Mbou, A. T., de Grandcourt, A., Valentini, R., Nicolini, G., Djagbletey, G., Owusu-Afriyie, K., Gvozdevaite, A., Oliveras, I., Ruiz-Jaen, M. C., and Malhi, Y. (2017). Forest biomass, productivity and carbon cycling along a rainfall gradient in West Africa. *Global Change Biology*, 24(2):496–510.

Morecroft, M. D. and Roberts, J. M. (1999). Photosynthesis and stomatal conductance of mature canopy Oak (Quercus robur) and Sycamore (Acer pseudoplatanus) trees throughout the growing season. *Functional Ecology*, 13(3):332–342.

Muller, O., Cohu, C. M., Stewart, J. J., Protheroe, J. A., Demmig-Adams, B., and Adams, W. W. (2014a). Association between photosynthesis and contrasting features of minor veins in leaves of summer annuals loading phloem via symplastic versus apoplastic routes. *Physiologia Plantarum*, 152(1):174–183.

Muller, O., Stewart, J. J., Cohu, C. M., Polutchko, S. K., Demmig-Adams, B., and Adams, W. W. (2014b). Leaf architectural, vascular and photosynthetic acclimation to temperature in two biennials. *Physiologia Plantarum*, 152(4):763–772.

Münch, E. (1930). *Die Stoffbewegungen in der Pflanze*. Fischer, Gustav, Jena, Germany, first edition.

Niinemets, U. and Sack, L. (2006). Structural determinants of leaf light-harvesting capacity and photosynthetic potentials. *Progress in Botany*, 67:383–419.

NOAA (2019). Trends in Atmospheric Carbon Dioxide.

Norby, R. J., Warren, J. M., Iversen, C. M., Medlyn, B. E., and McMurtrie, R. E. (2010). CO2 enhancement of forest productivity constrained by limited nitrogen availability. *Proceedings of the National Academy of Sciences*, 107(45):19368–19373.

Nowak, R. S., Ellsworth, D. S., and Smith, S. D. (2004). Functional responses of plants to elevated atmospheric CO2 - Do photosynthetic and productivity data from FACE experiments support early predictions? *New Phytologist*, 162(2):253–280.

O'Brien, M. J., Leuzinger, S., Philipson, C. D., Tay, J., and Hector, A. (2014). Drought survival of tropical tree seedlings enhanced by non-structural carbohydrate levels. *Nature Climate Change*, 4(June):710–714.

Osnas, J. L. D., Katabuchi, M., Kitajima, K., Wright, S. J., Reich, P. B., Van Bael, S. A., Kraft, N. J. B., Samaniego, M. J., Pacala, S. W., and Lichstein, J. W. (2018). Divergent drivers of leaf trait variation within species, among species, and among functional groups. *Proceedings of the National Academy of Sciences*, 115(21):5480–5485.

Ourcival, J. M., Joffre, R., and Rambal, S. (1999). Exploring the relationships between reectance and anatomical and biochemical properties in Quercus ilex leaves. *New Phytologist*, 143(2):351–364.

Palacio, S., Hoch, G., Sala, A., Körner, C., and Millard, P. (2014). Does carbon storage limit tree growth? *New Phytologist*, 201(4):1096–1100.

Patakas, A., Nikolaou, N., Zioziou, E., Radoglou, K., and Noitsakis, B. (2002). The role of organic solute and ion accumulation in osmotic adjustment in drought-stressed grapevines. *Plant Science*, 163(2):361–367.

Paul, M. J. and Foyer, C. H. (2001). Sink regulation of photosynthesis. *Journal of experimental botany*, 52(360):1383–1400.

Paul, M. J. and Pellny, T. K. (2003). Carbon metabolite feedback regulation of leaf photosynthesis and development. *Journal of Experimental Botany*, 54(382):539–547.

Pérez-Harguindeguy, N., Diaz, S., Garnier, E., Lavorel, S., Poorter, H., Jaureguiberry, P., Bret-Harte, M. S., Cornwell, W. K., Craine, J. M., Gurvich, D. E., Urcelay, C., Veneklaas, E. J., Reich, P. B., Poorter, L., Wright, I. J., Ray, P., Enrico, L., Pausas, J. G., de Vos, A. C., Buchmann, N., Funes, G., Quétier, F., Hodgson, J. G., Thompson, K., Morgan, H. D., ter Steege, H., van der Heijden, M. G. A., Sack, L., Blonder, B., Poschlod, P., Vaieretti, M. V., Conti, G., Staver, A. C., Aquino, S., and Cornelissen, J. H. C. (2013). New handbook for standardised measurment of plant functional traits worldwide. *Australian Journal of Botany*, 61(34):167–234.

Peuke, A. D., Rokitta, M., Zimmermann, U., Schreiber, L., and Haase, A. (2001). Simultaneous measurement of water flow velocity and solute transport in xylem and phloem of adult plants of Ricinus communis over a daily time course by nuclear magnetic resonance spectrometry. *Plant, Cell and Environment*, 24(5):491–503.

Pieters, A. J., Paul, M. J., and Lawlor, D. W. (2001). Low sink demand limits photosynthesis under Pi deficiency. *Journal of experimental botany*, 52(358):1083–91.

Polutchko, S. K., Stewart, J. J., Demmig-Adams, B., and Adams, W. W. (2018). Evaluating the link between photosynthetic capacity and leaf vascular organization with principal component analysis. *Photosynthetica*, 56(1):392–403.

Poorter, L. and Kitajima, K. (2007). Carbohydrate storage and light requirements of tropical moist and dry forest tree species. *Ecology*, 88(4):1000–1011.

Quentin, A. G., Pinkard, E. A., Ryan, M. G., Tissue, D. T., Baggett, L. S., Adams, H. D., Maillard, P., Marchand, J., Landhäusser, S. M., Lacointe, A., Gibon, Y., Anderegg, W. R., Asao, S., Atkin, O. K., Bonhomme, M., Claye, C., Chow, P. S., Clément-Vidal, A., Davies, N. W., Dickman, L. T., Dumbur, R., Ellsworth, D. S., Falk, K., Galiano, L., Grünzweig, J. M., Hartmann, H., Hoch, G., Hood, S., Jones, J. E., Koike, T., Kuhlmann, I., Lloret, F., Maestro, M., Mansfield, S. D., Martínez-Vilalta, J., Maucourt, M., McDowell, N. G., Moing, A., Muller, B., Nebauer, S. G., Niinemets, Ü., Palacio, S., Piper, F., Raveh, E., Richter, A., Rolland, G., Rosas, T., Joanis, B. S., Sala, A., Smith, R. A., Sterck, F., Stinziano, J. R., Tobias, M., Unda, F., Watanabe, M., Way, D. A., Weerasinghe, L. K., Wild, B., Wiley, E., and Woodruff, D. R. (2015). Non-structural carbohydrates in woody plants compared among laboratories. *Tree Physiology*, 35(11):1146–1165.

Quentin, A. G., Rodemann, T., Doutreleau, M. F., Moreau, M., and Davies, N. W. (2017). Application of near-infrared spectroscopy for estimation of non-structural carbohydrates in foliar samples of Eucalyptus globulus Labilladière. *Tree Physiology*, 37(1):131–141.

Quéré, C., Andrew, R., Friedlingstein, P., Sitch, S., Hauck, J., Pongratz, J., Pickers, P., Ivar Korsbakken, J., Peters, G., Canadell, J., Arneth, A., Arora, V., Barbero, L., Bastos, A., Bopp, L., Ciais, P., Chini, L., Ciais, P., Doney, S., Gkritzalis, T., Goll, D., Harris, I., Haverd, V., Hoffman, F., Hoppema, M., Houghton, R., Hurtt, G., Ilyina, T., Jain, A., Johannessen, T., Jones, C., Kato, E., Keeling, R., Klein Goldewijk, K., Landschützer, P., Lefèvre, N., Lienert, S., Liu, Z., Lombardozzi, D., Metzl, N., Munro, D., Nabel, J., Nakaoka, S. I., Neill, C., Olsen, A., Ono, T., Patra, P., Peregon, A., Peters, W., Peylin, P., Pfeil, B., Pierrot, D., Poulter, B., Rehder, G., Resplandy, L., Robertson, E., Rocher, M., Rödenbeck, C., Schuster, U., Skjelvan, I., Séférian, R., Skjelvan, I., Steinhoff, T., Sutton, A., Tans, P., Tian, H., Tilbrook, B., Tubiello, F., Van Der Laan-Luijkx, I., Van Der Werf, G., Viovy, N., Walker, A., Wiltshire, A., Wright, R., Zaehle, S., and Zheng, B. (2018). Global Carbon Budget 2018. *Earth System Science Data*, 10(4):2141–2194.

Rada, F., Goldstein, G., Azocar, A., and Meinzer, F. (1985). Daily and seasonal osmotic changes in a tropical treeline species. *Journal of Experimental Botany*, 36(6):989–1000.

Ramirez, J. A., Posada, J. M., Handa, I. T., Hoch, G., Vohland, M., Messier, C., and Reu, B. (2015). Near-infrared spectroscopy (NIRS) predicts non-structural carbohydrate concentrations in different tissue types of a broad range of tree species. *Methods in Ecology and Evolution*, 6(9):1018–1025.

Reich, P. B. (2014). The world-wide 'fast-slow' plant economics spectrum: a traits manifesto. *Journal of Ecology*, 102(2):275–301.

Richardson, A. D., Carbone, M. S., Keenan, T. F., Czimczik, C. I., Hollinger, D. Y., Murakami, P., Schaberg, P. G., and Xu, X. (2013). Seasonal dynamics and age of stemwood nonstructural carbohydrates in temperate forest trees. *New Phytologist*, 197(3):850–61.

Richardson, A. D., Duigan, S. P., and Berlyn, G. P. (2002). An evaluation of noninvasive methods to estimate foliar chlorophyll content. *New Phytologist*, 153(1):185–194.

Richter, A., Wanek, W., Werner, R. A., Ghashghaie, J., Jäggi, M., Gessler, A., Brugnoli, E., Hettmann, E., Göttlicher, S. G., Salmon, Y., Bathellier, C., Kodama, N., Nogués, S., Søe, A., Volders, F., Sörgel, K., Blöchl, A., Siegwolf, R. T. W., Buchmann, N., and Gleixner, G. (2009). Preparation of starch and soluble sugars of plant material for the analysis of carbon isotope composition: a comparison of methods. *Rapid Communications in Mass Spectrometry*, 23(16):2476–2488.

Richter, H. (1978). A diagram for the description of water relations in plant cells and organs. *Journal of Experimental Botany*, 29(112):1197–1203.

Sack, L. and Holbrook, N. M. (2006). Leaf Hydraulics. *Annual Review of Plant Biology*, 57(1):361–381.

Sack, L. and Pasquet-Kok, J. (2011). Leaf pressure-volume curve parameters. *PrometheusWiki (http://prometheuswiki.publish.csiro.au/tiki-index.php?page=Leaf%20pressure-volume%20curve%20parameters)*.

Sack, L. and Scoffoni, C. (2013). Leaf venation: Structure, function, development, evolution, ecology and applications in the past, present and future. *New Phytologist*, 198(4):983–1000.

Sala, A., Woodruff, D. R., and Meinzer, F. C. (2012). Carbon dynamics in trees: Feast or famine? *Tree Physiology*, 32(6):764–775.

Sanders, G. and Arndt, S. (2012). Osmotic Adjustment under Drought Conditions. In Aroca, R., editor, *Plant Responses to Drought Stress*, chapter 8, pages 199–230. Springer Heidelberg, London, UK, first edition.

Santelia, D. and Lawson, T. (2016). Rethinking guard cell metabolism. *Plant Physiology*, 172(3):1371–1392.

Sarmiento, J. L., Gloor, M., Gruber, N., Beaulieu, C., Jacobson, A. R., Fletcher, S. E., Pacala, S., and Rodgers, K. (2010). Trends and regional distributions of land and ocean carbon sinks. *Biogeosciences*, 7(8):2351–2367.

Savage, J. A., Beecher, S. D., Clerx, L., Gersony, J. T., Knoblauch, J., Losada, J. M., Jensen, K. H., Knoblauch, M., and Michele Holbrook, N. (2017). Maintenance of carbohydrate transport in tall trees. *Nature Plants*, 3(December).

Savage, J. A., Clearwater, M. J., Haines, D. F., Klein, T., Mencuccini, M., Sevanto, S., Turgeon, R., and Zhang, C. (2016). Allocation, stress tolerance and carbon transport in plants: how does phloem physiology affect plant ecology? *Plant, Cell & Environment*, 39(4):709–725.

Schulte, P. J., Hinckley, T. M., and Resources, F. (1985). A Comparison of Pressure-Volume Curve Data Analysis Techniques. *Journal of experimental botany*, 36(171):1590–1602.

Scoffoni, C., Chatelet, D. S., Pasquet-Kok, J., Rawls, M., Donoghue, M. J., Edwards, E. J., and Sack, L. (2016). Hydraulic basis for the evolution of photosynthetic productivity. *Nature Plants*, 2(May).

Sendall, K. M., Reich, P. B., Zhao, C., Jihua, H., and Wei, X. O. (2014). Acclimation of photosynthetic temperature optima of temperate and boreal tree species in response to experimental forest warming. *Global Change Biology*, September:1–16.

Serbin, S. P., Singh, A., McNeil, B. E., Kingdon, C. C., and Townsend, P. A. (2014). Spectroscopic determination of leaf morphological and biochemical traits for northern temperate andboreal tree species. *Ecological Applications*, 24(7):1651–1669.

Sharkey, T. D., Stitt, M., Heineke, D., Gerhardt, R., Raschke, K., and Heldt, H. W. (1986). Limitation of Photosynthesis by Carbon Metabolism. *Plant physiology*, 81:1123–1129.

Sholtis, J. D., Gunderson, C. A., Norby, R. J., and Tissue, D. T. (2004). Persistent stimulation of photosynthesis by elevated CO2 in a sweetgum (Liquidambar styraciflua) forest stand. *New Phytologist*, 162(2):343–354.

Sinclair, T. and Venables, W. N. (1983). An alternative method for analysing pressurevolume curves produced with the pressure chamber. *Plant, Cell & Environment*, 6(3):211–217.

Smith, A. M. and Stitt, M. (2007). Coordination of carbon supply and plant growth. *Plant, Cell and Environment*, 30(9):1126–1149.

Somerville, C. R. and Ogren, W. L. (1982). Mutants of the cruciferous plant Arabidopsis thaliana lacking glycine decarboxylase activity. *The Biochemical journal*, 202:373–380.

Subbarao, G. V., Nam, N. H., Chauhan, Y. S., and Johansen, C. (2000). Osmotic adjustment, water relations and carbohydrate remobilization in pigeonpea under water deficits. *Journal of Plant Physiology*, 157(6):651–659.

Taiz, L. and Zeiger, E. (2006). *Plant Physiology*. Sinauer Associates, Inc, Sunderland, MA, USA, fourth ed. edition.

Terrer, C., Prentice, I., Jackson, R., Keenan, T., Kaiser, C., Vicca, S., Fisher, J., Reich, P., Stocker, B., Hungate, B., Penuelos, J., McCallum, I., Soudzilovskala, N., Cernusak, L., Talhelm, A., Van, S. K., Piao, S., Newton, P., Hovenden, M., Blumenthal, D., Liu, Y., Muller, C., Winter, K., Field, C., Viechtbauer, W., Van, L. C.,

Hoosbeek, M., Watanabe, M., Koike, T., Leshyk, V., Polley, W., and Franklin, O. (2019). Nitrogen and phosphorus constrain the CO2 fertilization of global plant biomas. *Nature Climate Change*, 9(September).

Thomas, M. V., Malhi, Y., Fenn, K. M., Fisher, J. B., Morecroft, M. D., Lloyd, C. R., Taylor, M. E., and McNeil, D. D. (2010). Carbon dioxide fluxes over an ancient broadleaved deciduous woodland in southern England. *Biogeosciences Discussions*, 7(3):3765–3814.

Tixier, A., Orozco, J., Roxas, A. A., Earles, J. M., and Zwieniecki, M. A. (2018). Diurnal variation in nonstructural carbohydrate storage in trees: Remobilization and vertical mixing. *Plant Physiology*, 178(4):1602–1613.

Townsend, A. R., Asner, G. P., and Cleveland, C. C. (2008). The biogeochemical heterogeneity of tropical forests. *Trends in ecology & evolution*, 23(8):424–31.

Turgeon, R. (2010). The Role of Phloem Loading Reconsidered. *Plant Physiology*, 152(4):1817–1823.

Turgeon, R. and Wolf, S. (2009). Phloem Transport: Cellular Pathways and Molecular Trafficking. *Annual Review of Plant Biology*, 60(1):207–221.

Tyree, M. T. and Hammel, H. T. (1972). The Measurement of the Turgor Pressure and the Water Relations of Plants by the Pressure-bomb Technique. *Journal of experimental botany*, 23(74):267–282.

Tyree, M. T. and Richter, H. (1981). Alternative methods of analysing water potential isotherms: Some cautions and clarifications: I. The impact of non-ideality and of some experimental errors. *Journal of Experimental Botany*, 32(3):643–653.

Urban, L., Jaffrin, A., and Chraibi, A. (1993). Analysis of pressure-volume curves of leaves of Rosa hybrida cv. sonia. *Journal of Experimental Botany*, 44(3):605–613.

Van Bel, A. J. E. (2003). The phloem, a miracle of ingenuity. *Plant, Cell and Environment*, 26:125–149.

Verryckt, L. T., Van Langenhove, L., Ciais, P., Courtois, E. A., Vicca, S., Peñuelas, J., Stahl, C., Coste, S., Ellsworth, D. S., Posada, J. M., Obersteiner, M., Chave, J., and Janssens, I. A. (2020). Coping with branch excision when measuring leaf net photosynthetic rates in a lowland tropical forest. *Biotropica*, 00(December 2019):1–8.

Violle, C., Navas, M.-L., Vile, D., Kazakou, E., Fortunel, C., Hummel, I., and Garnier, E. (2007). Let the concept of trait be functional! *Oikos*, 116(5):882–892.

Wang, Z. and Stutte, G. W. (1992). The Role of Carbohydrates in Active Osmotic Adjustment in Apple under Water Stress. *Journal of the American Society for Horticultural Science*, 117(5):816–823.

Wardlaw, I. F. (2005). Consideration of apoplastic water in plant organs: a reminder. *Functional Plant Biology*, 32(6):561–569.

Willis, K. J. and McElwain, J. (2002). *The Evolution of Plants*. Oxford University Press, Oxford, UK, first edition.

Wold, S., Sjöström, M., and Eriksson, L. (2001). PLS-regression: A basic tool of chemometrics. *Chemometrics and Intelligent Laboratory Systems*, 58(2):109–130.

Wong, S., Cowan, I., and Farquhar, G. (1979). Stomatal conductance correlates with photosynthetic capacity. *Nature*, 282:424–426.

Wright, I. J., Reich, P. B., Cornelissen, J. H. C., Falster, D. S., Groom, P. K., Hikosaka, K., Lee, W., Lusk, C. H., Niinemets, Ü., Oleksyn, J., Osada, N., Poorter, H., Warton, D. I., and Westoby, M. (2005). Modulation of leaf economic traits and trait relationships by climate. *Global Ecology and Biogeography*, 14(5):411–421.

Wright, I. J., Reich, P. B., Westoby, M., Ackerly, D. D., Baruch, Z., Bongers, F., Cavender-Bares, J., Chapin, T., Cornelissen, J. H. C., Diemer, M., Flexas, J., Garnier, E., Groom, P. K., Gulias, J., Hikosaka, K., Lamont, B. B., Lee, T., Lee, W., Lusk, C., Midgley, J. J., Navas, M.-L., Niinemets, U., Oleksyn, J., Osada, N., Poorter, H., Poot, P., Prior, L., Pyankov, V. I., Roumet, C., Thomas, S. C., Tjoelker, M. G., Veneklaas, E. J., and Villar, R. (2004). The worldwide leaf economics spectrum. *Nature*, 428(6985):821–827.

Wu, J., Chavana-Bryant, C., Prohaska, N., Serbin, S. P., Guan, K., Albert, L. P., Yang, X., van Leeuwen, W. J., Garnello, A. J., Martins, G., Malhi, Y., Gerard, F., Oliviera, R. C., and Saleska, S. R. (2017). Convergence in relationships between leaf traits, spectra and age across diverse canopy environments and two contrasting tropical forests. *New Phytologist*, 214(3):1033–1048.

Würth, M. K., Peláez-Riedl, S., Wright, S. J., and Körner, C. (2005). Non-structural carbohydrate pools in a tropical forest. *Oecologia*, 143(1):11–24.

Yendrek, C. R., Tomaz, T., Montes, C. M., Cao, Y., Morse, A. M., Brown, P. J., McIntyre, L. M., Leakey, A. D., and Ainsworth, E. A. (2017). High-Throughput Phenotyping of Maize Leaf Physiological and Biochemical Traits Using Hyperspectral Reflectance. *Plant Physiology*, 173(1):614–626.

Zotz, G., Pepin, S., and Körner, C. (2005). No down-regulation of leaf photosynthesis in mature forest trees after three years of exposure to elevated CO2. *Plant Biology*, 7(4):369–374.